

January 2016

STRUCTURAL ELUCIDATION OF DEPROTONATED ANALYTES VIA TANDEM MASS SPECTROMETRY BASED ON ION- MOLECULE REACTIONS AND COLLISION- ACTIVATED DISSOCIATION

Hanyu Zhu
Purdue University

Follow this and additional works at: https://docs.lib.purdue.edu/open_access_dissertations

Recommended Citation

Zhu, Hanyu, "STRUCTURAL ELUCIDATION OF DEPROTONATED ANALYTES VIA TANDEM MASS SPECTROMETRY BASED ON ION-MOLECULE REACTIONS AND COLLISION-ACTIVATED DISSOCIATION" (2016). *Open Access Dissertations*. 1239.
https://docs.lib.purdue.edu/open_access_dissertations/1239

This document has been made available through Purdue e-Pubs, a service of the Purdue University Libraries. Please contact epubs@purdue.edu for additional information.

PURDUE UNIVERSITY
GRADUATE SCHOOL
Thesis/Dissertation Acceptance

This is to certify that the thesis/dissertation prepared

By Hanyu Zhu

Entitled STRUCTURAL ELUCIDATION OF DEPROTONATED ANALYTES VIA TANDEM
MASS SPECTROMETRY BASED ON ION-MOLECULE REACTIONS AND
COLLISION-ACTIVATED DISSOCIATION

For the degree of Doctor of Philosophy

Is approved by the final examining committee:

Hilkka I. Kenttämäa

Garth J. Simpson

Mary J. Wirth

Shelley Claridge

To the best of my knowledge and as understood by the student in the Thesis/Dissertation Agreement, Publication Delay, and Certification/Disclaimer (Graduate School Form 32), this thesis/dissertation adheres to the provisions of Purdue University's "Policy on Integrity in Research" and the use of copyrighted material.

Hilkka I. Kenttämäa

Approved by Major Professor(s): _____

Approved by: Timothy Zwier

11/16/2016

Head of the Department Graduate Program

Date

STRUCTURAL ELUCIDATION OF DEPROTONATED ANALYTES VIA TANDEM
MASS SPECTROMETRY BASED ON ION-MOLECULE REACTIONS AND
COLLISION-ACTIVATED DISSOCIATION

A Dissertation

Submitted to the Faculty

of

Purdue University

by

Hanyu Zhu

In Partial Fulfillment of the

Requirements of the Degree

of

Doctor of Philosophy

December 2016

Purdue University

West Lafayette, Indiana

To my parents, for your unconditional love and support.

To Ximo, the luckiest finding of my life.

ACKNOWLEDGMENTS

First and foremost, I would like to express my deepest gratitude for my advisor, Dr. Hilka Kenttämä. She brought me into mass spectrometry, a field where I felt rewarded to have worked in during the past four years and would be excited to work for in the future. Working under her guidance has been a pleasing experience. I learned to think, talk, and write like a scientist, and most importantly, work independently as problem solver. I would also like to thank the past and present members of the Kenttämä group. Thank Dr. Tiffany Jarrell, Dr. Christopher Marcum, Dr. Huaming Sheng, Dr. Weijuan Tang, Dr. James Riedeman, Dr. Matt Hurt, Dr. Alex Dow, Chunfen Jin, Priya Murria, Joann Max, John Kong, Xin Ma and Xueming Dong for the discussions and supports on my research projects. It was my great pleasure to work with such talented and friendly individuals. Thank the Amy facility, especially Mark Carlson, for the technical supports on various instrumentations. Last but not least, thank my family and friends for their love and accompany to help me through the past four years.

TABLE OF CONTENTS

	Page
LIST OF TABLES	viii
LIST OF FIGURES	ix
ABSTRACT	xv
CHAPTER 1. INTRODUCTION AND OVERVIEW	1
1.1 Introduction	1
1.2 Thesis Overview	2
1.3 References	4
CHAPTER 2. INSTRUMENTATION AND EXPERIMENTAL PRINCIPLES	5
2.1 Introduction	5
2.2 Ionization Techniques	6
2.2.1 Electrospray Ionization (ESI)	6
2.3 Linear Quadrupole Ion Trap Mass Spectrometer (LQIT)	10
2.3.1 Instrumentation Setup	11
2.3.2 Ion Motion Inside Linear Quadrupole Ion-Trap	15
2.3.2.1 Ion Trapping in the X- and Y- Plane	15
2.3.2.2 Ion Trapping in the Z Direction	18
2.3.3 Ion Ejection and Detection	21
2.4 Tandem Mass Spectrometry in LQIT	24
2.4.1 Ion Isolation	25
2.4.2 Collision-activated Dissociation	27
2.4.3 Ion-molecule Reaction	29
2.5 Orbitrap Mass Spectrometer	32
2.5.1 Instrument Setup	33
2.5.2 Ion Motion Inside Orbitrap Mass Analyzer	34
2.6 References	36

CHAPTER 3. FUNCTIONAL GROUP IDENTIFICATION IN DEPROTONATED ANALYTES VIA ION-MOLECULE REACTIONS WITH DEMB AND WATER.....39

3.1 Introduction.....	39
3.2 Experimental.....	41
3.2.1 Chemicals.....	41
3.2.2 Mass Spectrometry.....	43
3.2.3 Ion-molecule Reactions.....	44
3.2.4 High-performance Liquid Chromatography.....	44
3.2.5 Computational Details.....	45
3.3 Results and Discussion.....	46
3.3.1 Ion-molecule Reactions with DEMB and H ₂ O.....	46
3.3.2 Reactions Between DEMB and Deprotonated Analytes.....	48
3.3.2.1 Reactions Between DEMB and Phenoxide Containing Ions.....	48
3.3.2.2 Reactions Between Carboxylate, Sulfonate or Phosphate Containing Ions and DEMB.....	58
3.3.2.3 DEMB Ion-molecule Reactions Coupled with HPLC.....	61
3.3.3 Reactions Between Deprotonated Analytes and DEHB/H ₂ O.....	62
3.3.3.1 Reactions Between Carboxylate Containing Analyte Ions and DEHB/H ₂ O.....	63
3.3.3.2 Reactions Between Phenoxide Containing Analyte Ions and DEHB/H ₂ O.....	67
3.3.3.3 Reactions Between Phosphate Containing Analyte Ions and DEHB/H ₂ O.....	72
3.3.3.4 DEMB/H ₂ O Ion-molecule Reactions Coupled with HPLC.....	74
3.4 Conclusions.....	76
3.5 References.....	77

CHAPTER 4. DIFFERENTIATION OF REGIOISOMERIC BENZENEDIOLS VIA ION-MOLECULE REACTIONS WITH THIONYL CHLORIDE79

4.1 Introduction.....	79
4.2 Experimental.....	80
4.2.1 Chemicals.....	80
4.2.2 Mass Spectrometry.....	80
4.2.3 Ion-molecule Reactions.....	81
4.2.4 Density Functional Theory Calculations.....	82
4.3 Results and Discussions.....	82

	Page
4.3.1 Ion-molecule Reactions with the Pulsed Valve System	82
4.3.2 Reaction Between Deprotonated Catechol and SOCl ₂	84
4.3.3 Reaction Between Deprotonated Resorinol and SOCl ₂	86
4.3.4 Reaction Between Deprotonated Hydroquinone and SOCl ₂	89
4.4 Conclusions	91
4.5 References	92
CHAPTER 5. IDENTIFICATION OF MICROBIAL LIGNIL DEGRADATION PRODUCTS VIA HIGH PERFORMANCE LIQUID CHROMATOGRAPHY COUPLED WITH TANDEM MASS SPECTROMETRY	94
5.1 Introduction	94
5.2 Experimental	96
5.2.1 Chemicals	96
5.2.2 Sample Preparation	97
5.2.2 High-performance Liquid Chromatography	98
5.2.3 Mass Spectrometry	98
5.3 Results and Discussions	99
5.3.1 Preparative HPLC Separation of Cordgrass Degradation Samples	99
5.3.2 HPLC-MS Analysis of Cordgrass Degradation Samples	101
5.3.3 Vanillin Quantification in Cordgrass Time Series Samples	107
5.3.4 HPLC-MS Analysis of Mimivirus Lignin Degradation Samples	110
5.4 Conclusions	113
5.5 References	114
CHAPTER 6. ANALYSIS OF ORGANOSOLV LIGNIN VIA HIGH PERFORMANCE LIQUID CHROMATOGRAPHY COUPLED WITH TANDEM MASS SPECTROMETRY	116
6.1 Introduction	116
6.2 Experimental	118
6.2.1 Materials	118
6.2.2 Mass Spectrometry	118
6.2.3 High-performance Liquid Chromatography	119
6.3 Results and Discussions	119
6.3.1 HPLC Data Visualization	119
6.3.2 Elemental Composition Determination via High Resolution Mass Spectrometry	121
6.3.3 Structural Elucidation via CAD	123
6.4 Conclusions	128
6.5 References	129

Page

VITA.....	130
PUBLICATION.....	131

LIST OF TABLES

Table	Page
3.1 Ionic products formed upon reactions of deprotonated model compounds with diethylmethoxyborane (DEMB) for 200 ms.....	49
3.2 Ionic products formed upon reactions of deprotonated model compounds containing a phenol and a carboxylic acid functional group with DEMB for 200 ms.....	52
3.3 Ionic products formed upon reactions of deprotonated phenol and its derivatives containing electron-withdrawing substituents with DEMB for 200 ms, calculated NBO charges of the deprotonated phenols, and calculated energy differences between the reactants and their products.....	57
3.4 Ionic products formed upon reactions of deprotonated model compounds with diethylmethoxyborane (DEMB) for 200 ms.....	60
3.5 Product ions observed upon reactions between diethylhydroxyborane (DEHB) and water (H ₂ O) with analyte ions containing carboxylate functionality for 200 ms.....	64
3.6 Product ions observed after 200 ms reactions of analyte ions containing a phenoxide, phosphate, or sulfate functionality with diethylhydroxyborane (DEHB) and water.....	69
5.1 m/z value of the deprotonated major components in CGSS sample, their MS ² and MS ³ fragmentation ions and proposed structures.....	104
6.1 Elemental composition obtained for the major components in organosolv lignin via high resolution mass measurement.....	122
6.2 Proposed structure for the major components present in organosolv lignin based on CAD fragmentation data of the ionized compounds.....	124

LIST OF FIGURES

Figure	Page
2.1 Schematic representation of the ESI ion source	8
2.2 Illustration of the three mechanisms proposed for the formation of gas phase ions in ESI: the ion evaporation model (IEM), the charged residue model (CRM), and the chain ejection model (CEM). Reproduced from reference 14.....	9
2.3 Schematic representation of the Thermo Scientific LTQ linear quadrupole ion trap (LQIT) mass spectrometer with operational pressures shown for each differentially pumped region of the instrument	12
2.4 Representation of the DC voltage gradient applied for the transfer of positive ions. Gate lens voltages colored in red and black correspond to the closed (red) and open (black) states, respectively.....	13
2.5 Schematic representation of the linear quadrupole ion trap used in Thermo scientific LTQ mass spectrometers.....	14
2.6 Illustration of the Mathieu stability diagram	18
2.7 Representation of the DC potential well created during (a) ion injection, (b) ion trapping, and (c) ion ejection Notice how the ions are focused into a much tighter packet during ion ejection by the sharper DC potential gradient	20
2.8 (a) Representation of ions trapped inside the ion trap in the Mathieu stability diagram. (b) Ion ejection by ramping the amplitude of the main RF voltage. (c) Resonance ion ejection using the supplementary resonance ejection ac voltage.....	23
2.9 Schematic representation of the ion detection system. Ions were radially ejected through the exit rods and converted to secondary particles in the conversion dynode that were detected by the electron multiplier. Note that the electric field direction and the secondary particles generated correspond to positive ion detection.	24

Figure	Page
2.10 Position of the ions on the Mathieu stability diagram during (a) ion trapping, (b) RF ramp to increase the q value of ion of interest to 0.830, (c) application of resonance ejection waveform to remove all unwanted ions	26
2.11 Position of the ions on the Mathieu stability diagram during (a) ion trapping, (b) ion excitation at q value of 0.250 (c) production of fragment ions	28
2.12 Position of the ions on the Mathieu stability diagram during (a) ion trapping, (b) RF ramp to increase the q value of ion of interest to 0.830, (c) application of resonance ejection waveform to remove all unwanted ions	31
2.13 An example representation of the Braumann double well potential energy surface	32
2.14 Schematic representation of the coupling between linear quadrupole ion trap and orbitrap in Thermo Scientific LTQ Orbitrap XL mass spectrometer. Parts in front of the linear quadrupole ion trap are identical with Thermo Scientific LTQ mass spectrometer (Fig 2.4). Ions are concentrated in the C-trap before being ejected off center into the orbitrap (red arrow)	33
2.15 Schematic representation of an orbitrap mass analyzer. The ions are injected off center to induced a harmonic axial oscillation (blue arrows).....	35
3.1 Reactions of deprotonated catechol (m/z 109) with DEMB and DEHB/H ₂ O. (a) Extracted ion current of the reactant ion (m/z 109), DEMB product ion (m/z 177), and DEHB/H ₂ O product ion (m/z 165) over time. (b) Averaged mass spectra measured (top) before and (bottom) after one pulsed introduction of H ₂ O	47
3.2 (A) Proposed mechanism and (B) calculated potential energy surface (enthalpy in kcal/mol) for the formation of a DEMB adduct that has lost methanol upon reactions between deprotonated catechol and DEMB (M06-2X/6-31+G(d,p) level of theory).....	50
3.3 MS ² CAD spectra measured for deprotonated 4-hydroxybenzoic acid (m/z 137) generated using ESI with (A) acetonitrile solution and (B) NaOH doped water solution.....	53
3.4 Calculated potential energy surface for the loss of CO ₂ upon CAD of deprotonated 4-hydroxybenzoic acid carboxylate form (A) and phenoxide form (B) (M06-2X/6-31+G(d,p) level of theory).	54

Figure	Page
3.5 (A) Logarithm of the abundances of deprotonated 4-hydroxybenzoic acid (black symbols) and DEMB adduct-CH ₃ OH product ion (blue symbols) plotted as a function of reaction time for the reaction between DEMB and deprotonated 4-hydroxybenzoic acid generated using NaOH doped water solution (left) and acetonitrile solution (right). (B) Mechanism proposed for the formation of DEMB adduct that has lost methanol. (C) Calculated potential energy surface (enthalpies in kcal/mol) for the formation of DEMB adduct-CH ₃ OH (M06-2X/6-31+G(d,p) level of theory).....	55
3.6 Proposed mechanism for the formation of DEMB adduct-CH ₃ OH product ion upon reactions between deprotonated glucuronides and DEMB.....	59
3.7 (A) (top) Total ion current HPLC chromatogram for a mixture obtained via catalytic conversion of <i>miscanthus</i> biomass. (bottom) Selected ion HPLC chromatogram for all ions that form a DEMB adduct. (B) Structures of the four major phenols that were identified in the mixture. (C) MS ² spectrum measured after isolation of ion 4 (m/z 165) and reaction with DEMB for 200 ms.....	62
3.8 (a) Mass spectrum measured after 200 ms reaction of deprotonated benzoic acid (m/z 121) with (left) H ₂ O/DEHB, (middle) D ₂ O/DEHB, and (right) H ₂ ¹⁸ O/DEHB. (b) Proposed mechanism for the formation of DEHB adduct+H ₂ O-CH ₃ CH ₃ product ion (m/z 195) upon reaction of deprotonated benzoic acid with DEHB/H ₂ O. Hydrogen and oxygen atoms that originate from the H ₂ O reagent are colored in blue and red, respectively. (c) Calculated potential energy surface (enthalpy in kcal/mol) for the mechanism shown in (b) (M06-2X/6-31G+(d,p) level of theory).....	66
3.9 (Top) Mass spectrum measured after the reaction between deprotonated 4-ethoxyphenol (m/z 137) with H ₂ O/DEHB, D ₂ O/DEHB, and H ₂ ¹⁸ O/DEHB for 200 ms. (bottom) Proposed mechanism for the formation of DEHB+H ₂ O-CH ₃ CH ₃ product ion upon reaction between deprotonated phenol and DEHB/H ₂ O.....	68
3.10 CAD mass spectrum obtained at 20 (arbitrary units) collision energy for product ion of (top) reaction between deprotonated catechol with DEMB and (bottom) reaction between deprotonated catechol with DEHB/H ₂ O.....	70

Figure	Page
3.11 (a) Mass spectrum measured after 200 ms reactions of deprotonated catechol (m/z 109) with (left) H ₂ O/DEHB, (middle) D ₂ O/DEHB, and (right) H ₂ ¹⁸ O/DEHB. (b) Proposed mechanism for the formation of DEHB adduct-CH ₃ CH ₃ product ion upon reactions between deprotonated catechol and DEHB/H ₂ O. Hydrogen and oxygen atoms that originate from the H ₂ O reactant are colored in blue and red, respectively. (c) Calculated potential energy surface (enthalpy in kcal/mol) for the mechanism shown in (b) (M06-2X/6-31G+(d,p) level of theory).	71
3.12 (top) Mass spectra measured after 200 ms reactions of deprotonated phenylphosphonic acid (m/z 157) with H ₂ O/DEHB, D ₂ O/DEHB, and H ₂ ¹⁸ O/DEHB. (Bottom) Proposed mechanism for the formation of DEHB-CH ₃ CH ₃ product ion upon reaction between deprotonated phenylphosphonic acid and DEHB/H ₂ O.	73
3.13 (a) HPLC chromatogram measured for an artificial mixture of 4-methylumbelliferyl phosphate (1), 4-methylumbelliferyl β-D-glucuronide (2), 4-methylumbelliferyl sulfate (3), and 4-methylumbelliferone (4). The total ion current is plotted in black. Selected ion current for ion-molecule reaction product ions with DEHB/H ₂ O are plotted in red (DEHB adduct-CH ₃ CH ₃) and green (DEHB adduct+H ₂ O-CH ₃ CH ₃). (b) Mass spectra measured after reactions between the deprotonated HPLC eluents (4-methylumbelliferyl phosphate (1), 4-methylumbelliferyl β-D-glucuronide (2), 4-methylumbelliferyl sulfate (3), and 4-methylumbelliferone) with DEHB/H ₂ O for 200 ms	75
4.1 Reaction between deprotonated resorcinol (m/z 109) and SOCl ₂ introduced via the pulsed valve system. (Top) Extracted ion current of the reactant ion (m/z 109) and product ion (m/z 155) over time. (Bottom) Averaged mass spectra measured during one pulsed introduction of SOCl ₂ .	83
4.2 Mass spectrum measured for (top) deprotonated resorcinol, (middle) deprotonated resorcinol, and (bottom) deprotonated hydroquinone after reaction with SOCl ₂ for 30 ms.	84
4.3 (Top) proposed mechanism and (bottom) calculated potential energy surface (enthalpy in kcal/mol) for the formation of SOCl ₃ ⁻ product ion upon reaction between deprotonated catechol and SOCl ₂ (M06-2X/6-31+G(d,p) level of theory).	86
4.4 Mass spectrum measured for the reaction between deprotonated 2-methylresorcinol and SOCl ₂ .	88

Figure	Page
4.5 (Top) Proposed mechanism and (bottom) calculated potential energy surface (enthalpy in kcal/mol) for the formation of SOCl_2 adduct-2HCl product ion upon reaction between deprotonated resorcinol and SOCl_2 (M06-2X/6-31+G(d,p) level of theory).....	89
4.6 Mass spectrum measured for the reaction between SOCl_2 and (top) deprotonated 3,4,5-trimethylhydroquinone and (middle) deprotonated hydroquinone. (Bottom) CAD mass spectrum measured for the $[\text{M-H+Cl}]^{\bullet-}$ product ion at 20 (arbitrary unit) collision energy.....	90
4.7 (Top) proposed mechanism and (bottom) calculated potential energy surface (enthalpy in kcal/mol) for the formation of Cl adduct ion upon reaction between deprotonated hydroquinone and SOCl_2 (M06-2X/6-31+G(d,p) level of theory).....	91
5.1 Preparative HPLC separations of the cordgrass samples. (A) Culture medium that contains both cordgrass and fungus (CGSS samples). (B) Culture medium that only contains fungus GSS. (C) Culture medium that only contains cordgrass (Fungal-free). UV signals were detected at 254 nm.....	100
5.2 (Top) Total ion current chromatogram and (bottom) UV absorbance chromatogram at 254 nm for CGSS water fraction.....	102
5.3 Total ion current chromatogram (top) and UV absorbance chromatogram (bottom) at 254 nm for (A) GSS water fraction and (B) fungal free water fraction.....	103
5.4 (Top) Total ion current chromatogram and (bottom) UV absorbance chromatogram at 254 nm for CGSS acetonitrile fraction.....	105
5.5 Preparative HPLC separations of the (top) artificial mixture and (bottom) CGSS samples. UV signal were detected at 254 nm.....	106
5.6 Total ion current chromatogram and UV absorbance chromatogram at 254 nm for (A) water fraction of the artificial mixture and (B) acetonitrile fraction of the artificial mixture.....	106
5.7 Analysis of the T_0 time series sample using (top) mass spectrometry detection by monitoring extracted ion current and (bottom) UV detection at 254 nm.....	108
5.8 Selected ion current chromatogram of deprotonated vanillin (m/z 151) measured for a vanillin sample with a concentration of 25 nmol.....	108

Figure	Page
5.9 Calibration curve for vanillin concentration vs peak area ratio (vanillin / internal standard)	109
5.10 Vanillin concentration measured in samples T ₀ -T ₆	110
5.11 HPLC-MS analysis of an artificial mixture of vanillin and guaiacyl glycerol- β -guaiacyl ether after SPE.	111
5.12 Selected ion chromatogram of the (A) experimental sample, (B) control sample with wildtype mimivirus, and (C) control sample with no added mimivirus.	112
6.1 (Top) Comparison between HPLC chromatograms obtained by plotting base peak ion current versus time and total ion current versus time. (Bottom) Mass spectra measured at time A and time B.	120
6.2 14 major components identified in organosolv lignin via base peak ion current chromatogram.	122
6.3 (Top) Base peak ion current chromatogram and (bottom) selected ion current chromatogram of the identified compounds for the organosolv lignin sample.	127

ABSTRACT

Zhu, Hanyu. Ph.D., Purdue University, December 2016. Structural Elucidation of Deprotonated Analytes via Tandem Mass Spectrometry Based on Ion-Molecule Reactions and Collision-Activated Dissociation. Major Professor: Hilikka I. Kenttämäa.

Mass Spectrometry has emerged as a powerful analytical tool for the characterization of unknown molecules. Molecular weight information and chemical formulas of the unknowns can be derived by measuring the m/z value of the ionized analyte. In addition, structural information can be obtained via tandem mass spectrometry methods such as collision-activated dissociation (CAD). However, CAD does not always guarantee unambiguously assignment of chemical structures, therefore, additional tandem mass spectrometric methods such as ion-molecule reactions were developed.

In this dissertation, both CAD and ion-molecule reactions were used to elucidate the structure of deprotonated analytes. Currently, most existing neutral reagents are designed to react with protonated analytes, making them suboptimal for the acidic analytes that are more sensitive when detected under negative ion mode. The identification of analyte ions containing phenoxide, carboxylate, and phosphate functionality was achieved by using a novel ion-molecule reaction setup that allowed two neutral reagents, diethylmethoxyborane (DEMB) and water, to be introduced into the ion trap. Using DEMB as the sole reagent, reactions between phenoxide, carboxylate, sulfate, and phosphate containing analytes and DEMB were studied. By pulsing in water, a new

reagent, diethylhydroxyborane (DEHB), was generated inside the ion trap, allowing the reactions between phenoxide, carboxylate, sulfate, and phosphate containing analytes and DEHB/H₂O to be studied as well. Reaction mechanisms were explored via isotope labeling experiments and quantum chemical calculations. The above mass spectrometry method allowed the differentiation of phenoxide, carboxylate, phosphate, and sulfate containing analyte and was successfully coupled with high-performance liquid chromatography for the analyses of a biomass conversion product mixture and drug metabolite mixture. In addition, ion-molecule reactions with thionyl chloride were explored as a mean to differentiate deprotonated benzendiol isomers that were not discernable via CAD. Finally, HPLC-MS_n with CAD were used to analyze complex mixtures related to lignin, including organosolv lignin and microbial converted biomass.

CHAPTER 1. INTRODUCTION AND OVERVIEW

1.1 Introduction

Mass spectrometry has grown into one of the most widely used analytical techniques since its invention almost a century ago.¹ Over these years, multiple types of mass spectrometers utilizing different scientific theories have been designed and developed, each with unique capabilities.² This diverse collection of instruments made mass spectrometry a versatile and powerful technique capable of solving scientific problems across different fields of studies.

Despite the differences in designs and capabilities, the fundamental of mass spectrometers remained the same: the ability to measure the mass to charge ratio (m/z) of gas-phase ions. In order to do this, most mass spectrometry experiments involves four steps. The first step is to evaporate analytes into the gas phase. This is followed by the second step, ionization of the gas-phase analyte. The generated ions then undergo mass analysis to be separated either in time or in space according to their m/z values. Finally, the separated ions are detected, producing a mass spectrum.

The m/z value of ionized analyte can provide multiple importance information. The most straightforward information is the molecular weight of the analyte, which is closely related to the m/z of its ionized form. If the m/z value can be measured ultra-high

accuracy, elemental composition of the analyte molecule can be derived.³ At the same time, isobaric ions with the same nominal mass can be differentiated.

Structural information of the analyte ions can be obtained via tandem mass spectrometry experiments. During these experiments, the ion of interest is isolated and subjected to reactions, producing product ions that are characteristic of the structural motifs present in the parent ion. The m/z of the reaction product ions are then measured. Currently, the most widely used ion reaction method in tandem mass spectrometry is collision-activated dissociation (CAD), where the parent ion is given enough energy to fragment into smaller pieces.^{4,5}

However, not all structural motifs can be revealed via CAD. This led to the development of additional ion reaction methods. One of these methods is ion-molecule reaction.^{6,7} Here, the ion of interest is isolated and subjected to reactions with a neutral reagent introduced into the mass spectrometer. If the analyte ion contains a structural motif that is reactive towards the neutral reagent, characteristic product ions are formed. This approach allows additional structural information to be obtained.

1.2 Thesis Overview

This thesis discusses the advancement in structural elucidation of deprotonated molecules via ion-molecule reactions and high-performance liquid chromatography coupled with collision-activated dissociation tandem mass spectrometry. Chapter 2 discusses the principle and theory behind the instruments and techniques used in this study. Chapter 3 and 4 discuss the development of novel ion-molecule reactions for the functional group identification and isomer differentiation in deprotonated molecules. In

chapter 3, diethylmethoxyborane (DEMB) and water are being explored as neutral reagents used for the identification of phenoxide, phosphate, and carboxylate ions via ion-molecule reaction. Results shown in this chapter demonstrated that the DEMB/H₂O ion-molecule reaction system can be used to analyze complex mixtures such as catalytically converted biomass and drug metabolite mixtures. Chapter 4 discusses the application of ion-molecule reactions with thionyl chloride in isomer differentiation of benzenediols, which is not possible with CAD. These two chapters demonstrate the potential of ion-molecule reactions in structural elucidation of deprotonated analytes.

Chapter 5 and 6 discuss the analysis of lignin related complex mixtures via high-performance liquid chromatography coupled with collision-activated dissociation tandem mass spectrometry. Chapter 5 discusses the analysis of microbial converted lignin product mixtures while chapter 6 discusses the analysis of swithgrass organosolv lignin. The samples analyzed in these two chapters are of great importance in utilizing biomass to produce biofuels and valuable aromatic compounds. The results show that mass spectrometry can play an important role in the field of renewable energy and resources.

1.3 References

- (1) Cooks, R. G.; Busch, K. L.; Glish, G. L. *Science* **1983**, 222 (4621), 273–291.
- (2) Makarov, A.; Denisov, E.; Kholomeev, A.; Balschun, W.; Lange, O.; Strupat, K.; Horning, S. *Anal. Chem.* **2006**, 78 (7), 2113–2120.
- (3) Hernández, F.; Sancho, J. V.; Ibáñez, M.; Abad, E.; Portolés, T.; Mattioli, L. *Anal. Bioanal. Chem.* **2012**, 403 (5), 1251–1264.
- (4) Cooks, R. G. *J. Mass Spectrom.* **1995**, 30 (9), 1215–1221.
- (5) Mitchell Wells, J.; McLuckey, S. A. Enzymology, B.-M. in, Ed.; Biological Mass Spectrometry; Academic Press, 2005; 402, 148–185.
- (6) Brodbelt, J. S. *Mass Spectrom. Rev.* **1997**, 16 (2), 91–110.
- (7) Gronert, S. *Chem. Rev.* **2001**, 101 (2), 329–360.

CHAPTER 2. INSTRUMENTATION AND EXPERIMENTAL PRINCIPLES

2.1 Introduction

Since its invention nearly a century ago, mass spectrometry has grown into a versatile and powerful analytical tool widely used in both academia and industry.^{1,2} Its applications include but are not limited to studying gas-phase reaction chemistry,³ fuel analysis,⁴ environmental monitoring,⁵ and drug discovery.⁶ All applications of mass spectrometry are based on the ability to measure the mass to charge ratio (m/z) of ions. In order to do this, a mass spectrometry experiment generally involves three steps: 1) analyte evaporation and ionization, 2) mass analysis that separates ions based on their m/z values, and 3) ion detection. The experiments discussed in this dissertation utilized electrospray ionization (ESI) technique to evaporate and ionize analytes. Mass analysis and ion detection were performed using linear quadrupole ion trap (LQIT) mass spectrometers or linear quadrupole ion trap mass spectrometers coupled with an orbitrap detector (LQIT-Orbitrap).

In addition to molecular weight information, mass spectrometry also provides structural information for the ionized analytes. This was achieved via performing tandem mass spectrometry experiments. Such experiments generally involve the isolation of the ion of interest inside the ion trap, followed by subsequent dissociation or bimolecular reaction experiments. In this dissertation, tandem mass spectrometry experiments based

on collision-activated dissociation (CAD) and ion-molecule reactions were performed for the structural elucidation of analyte ions.

2.2 Ionization Techniques

Evaporation and ionization of analytes is the first step in mass spectrometry experiments. The evaporation and ionization are achieved separately for earlier ionization methods, such as electron ionization⁷ (EI) and chemical ionization (CI).⁸ These two steps are coupled in most ionization methods developed later, such as matrix assisted laser desorption ionization (MALDI),⁹ electrospray ionization (ESI),¹⁰ atmospheric pressure chemical ionization (APCI),¹¹ atmospheric pressure photoionization (APPI),¹² and desorption electrospray ionization (DESI).¹³ Each ionization method has its advantages and drawbacks, and proper selection of the ionization method is necessary for a successful mass spectrometry experiment. ESI is used for all experiments discussed in this dissertation and thus will be discussed in detail.

2.2.1 Electrospray Ionization (ESI)

ESI was invented in 1989 by Fenn and coworkers.¹⁰ It was a revolutionary technique as it allowed the evaporation and ionization of thermally labile and non-volatile biomolecules, such as proteins, oligonucleotides, and large lipids, without fragmentation, making it possible to study these molecules of great biological importance via mass spectrometry. For large biomolecules such as proteins, ESI generally generates multiple charged analyte ions. This gives it potential advantages over MALDI, another soft ionization technique that generally produce singly charged biomolecule ions, as multiple

charged ions 1) have lower m/z value which can fall into the mass ranges of all common mass analyzers and 2) are easier to dissociate during tandem mass spectrometry experiments.¹⁴

Figure 2.1 shows a schematic representation of an ESI ion source. Generally, analyte solution is pumped continuously through a capillary needle that has a high voltage (3-5 kV) applied at the tip. A Taylor cone is formed at the tip of the capillary due to the high voltage applied, resulting in the dispersion of the analyte solution into a fine aerosol consisting of charged droplets.¹⁵ The polarity of the charge on the droplets is consistent with the polarity of the applied voltage. Dry nitrogen gas (sheath gas) introduced through openings that are coaxial with the capillary facilitates aerosol formation by nebulizing the analyte solution. Sheath gas also directs the spray towards the inlet of the mass spectrometer. Certain ESI sources introduce another stream of dry nitrogen gas (auxiliary gas) to further help solvent evaporation by dehumidifying the environment around the charged droplets.

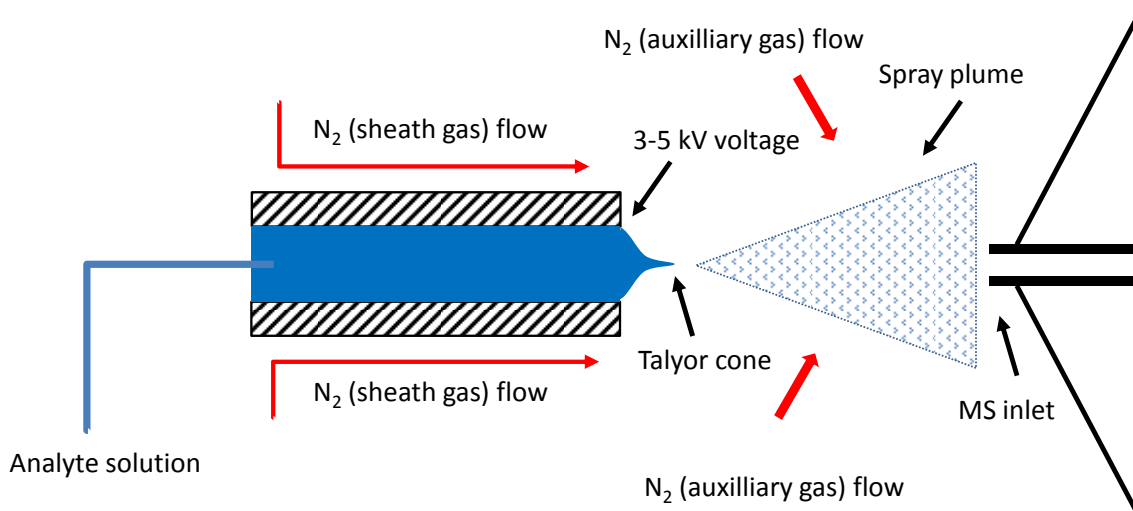


Figure 2.1 Schematic representation of the ESI ion source

The charges in the droplets are distributed along its surface. The coulombic repulsion among these charges increases as the droplet evaporates. When the size of a droplet decreases to a point where the coulombic repulsion overcomes its surface tension (Rayleigh limit),¹⁶ the droplet explodes into smaller progeny droplets that typically carry larger charge density than the parent droplet. This process, known as “Coulomb explosion” or “Coulomb fission”,¹⁷ occurs repeatedly for the progeny droplets, eventually converting them into highly charged nanodroplets that release analyte ions into the gas phase. Multiple theories have been proposed to explain the production of gas-phase ions from the highly charged nanodroplets, including the ion evaporation model (IEM),¹⁸ the charged residue model (CRM),¹⁹ and the chain ejection model (CEM) (Figure 2.2).¹⁴

According to the ion evaporation model (IEM), small ions in a droplet can be directly ejected into the gas phase. As charged nanodroplets shrink in size, the electric field emanating from the surface of the droplet keeps increasing. When this electric field

is strong enough, it can push the charged analyte molecule away, forming gas-phase analyte ions.

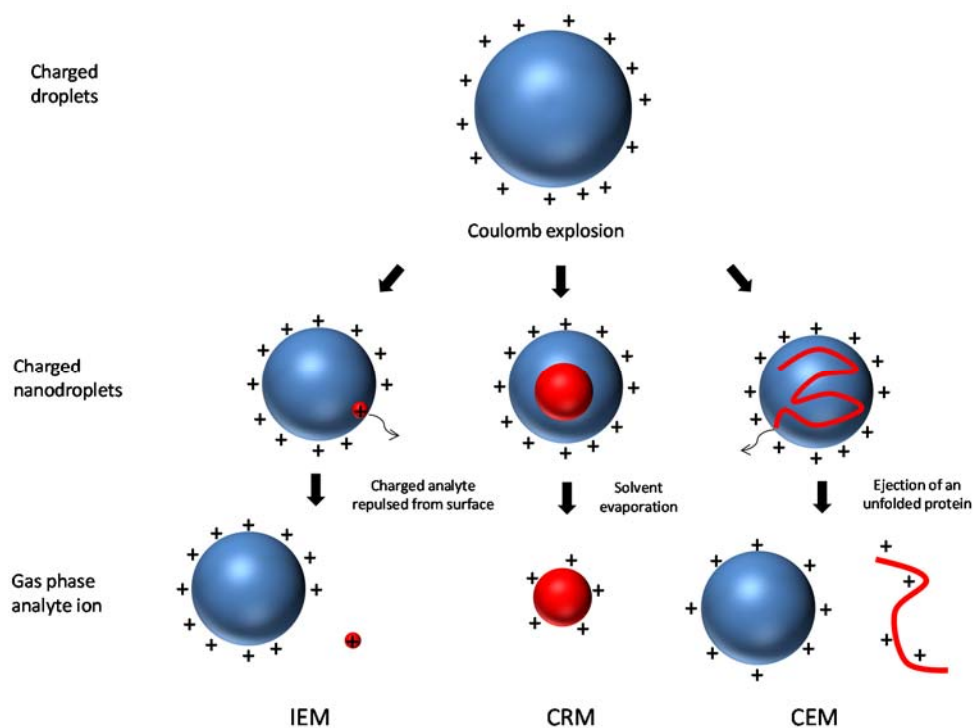


Figure 2.2 Illustration of the three mechanisms proposed for the formation of gas phase ions in ESI: the ion evaporation model (IEM), the charged residue model (CRM), and the chain ejection model (CEM). Reproduced from reference 14.

The charged residue model mainly applies to large globular molecules such as folded proteins. This model proposes that consecutive Coulomb explosions would eventually result in the formation of nanodroplets containing only one analyte ion. These nanodroplets continue to evaporate until all solvent molecules are gone and the charges have been transferred from the surface of the droplet to the analyte ion, creating multiply charged gas-phase ions.

The chain ejection model (CEM) was proposed for partially hydrophobic polymer chains such as unfolded proteins. According to this model, when the charged droplet shrinks to a size small enough, its electric field can expel one terminus of the polymer chain from the surface. This is followed by the sequential ejection of the rest of the polymer. As the polymer is ejected from the droplet, part of the charge carried in the droplet equilibrates to the polymer, resulting in the formation of multiply charged polymer ion.

ESI can also generate adduct ions such as Most analytes studied in this dissertation contain small molecules. In most cases, they form protonated molecules ($[M+H]^+$) under positive ion mode ESI or deprotonated molecules ($[M-H]^-$) under negative ion mode ESI.

2.3 Linear Quadrupole Ion Trap Mass Spectrometer (LQIT)

LQIT mass spectrometers were first introduced in 2002.^{20,21} Compared with traditional 3D quadrupole ion trap (QIT) mass spectrometers, the LQIT has a better ion trapping efficiency and capacity, resulting in higher sensitivity, lower detection limit, and better overall performance.²² As with all trapping instrument, LQIT has the capability to perform multiple stages of tandem mass spectrometry experiments (MS^n), making it a powerful instrument for the structural elucidation of ionized analytes.

2.3.1 Instrumentation Setup

All LQITs used in this dissertation were Thermo scientific LTQ XL mass spectrometers.²³ According to the schematic representation shown in Figure 2.3, the instrument can be divided into three regions: atmospheric pressure ionization (API) stack region, ion optics region, and ion trap region. Different regions of the instrument operate under different pressure provided by differential pumping using two rough pumps and a triple ported turbomolecular pump. The API stack region was pumped by two Edwards E2M30 rotary-vane mechanical pumps to a pressure of ~ 1 Torr. The ion optics region and the ion trap region were pumped by a Leybold Tw220/15r0/15S triple ported turbomolecular pump. The region immediate after the API stack (between skimmer and lens L0) was connected to the first inlet of the turbomolecular pump and was pumped to a pressure of ~ 50 mTorr. The next turbomolecular pump inlet was used to pump the region between lenses L0 and L1 to a pressure of ~ 1 mTorr. The third inlet was used to maintain the pressure of the ion trap region at $\sim 1 \times 10^{-5}$ Torr.

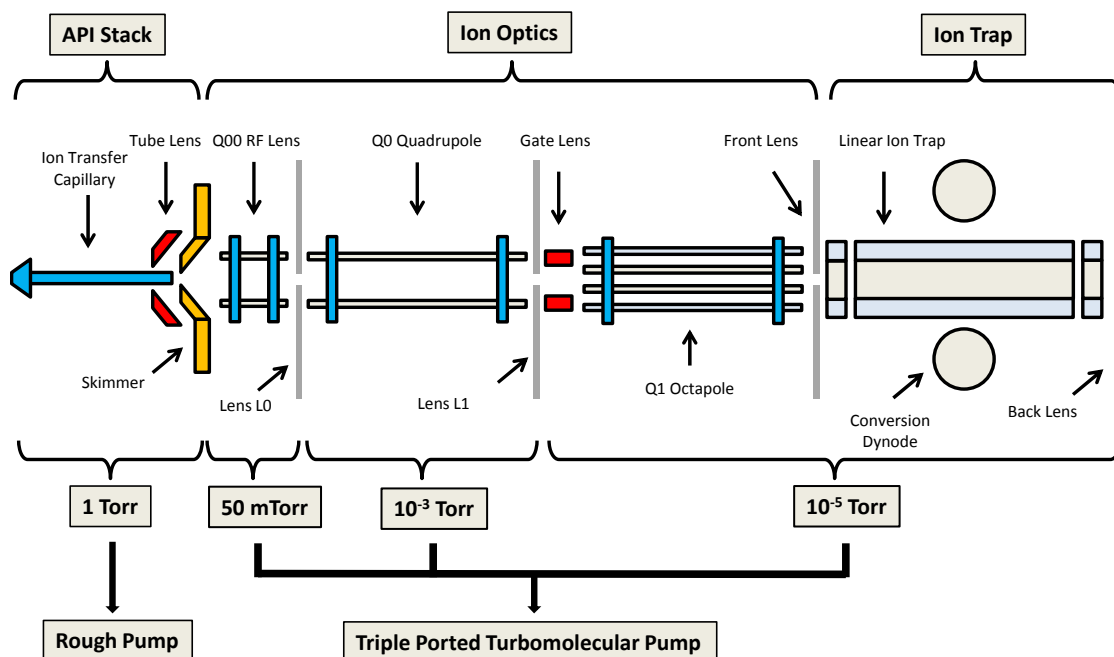


Figure 2.3 Schematic representation of the Thermo Scientific LTQ linear quadrupole ion trap (LQIT) mass spectrometer with operational pressures shown for each differentially pumped region of the instrument.

Ions generated in the ion source were drawn into the API stack region because this region had a lower pressure and a lower DC voltage potential applied to it. The ions first passed through a heated ion transfer capillary (200-300 °C), which facilitated ion desolvation. A DC potential with the same polarity as the ions being transferred was applied to the capillary to prevent ions from hitting the capillary wall. After passing through the transfer capillary, ions were directed through the skimmer via a DC potential applied on the tube lens. The outlet of the transfer capillary was misaligned with the opening on the skimmer in order to prevent neutral molecules from entering the mass spectrometer.

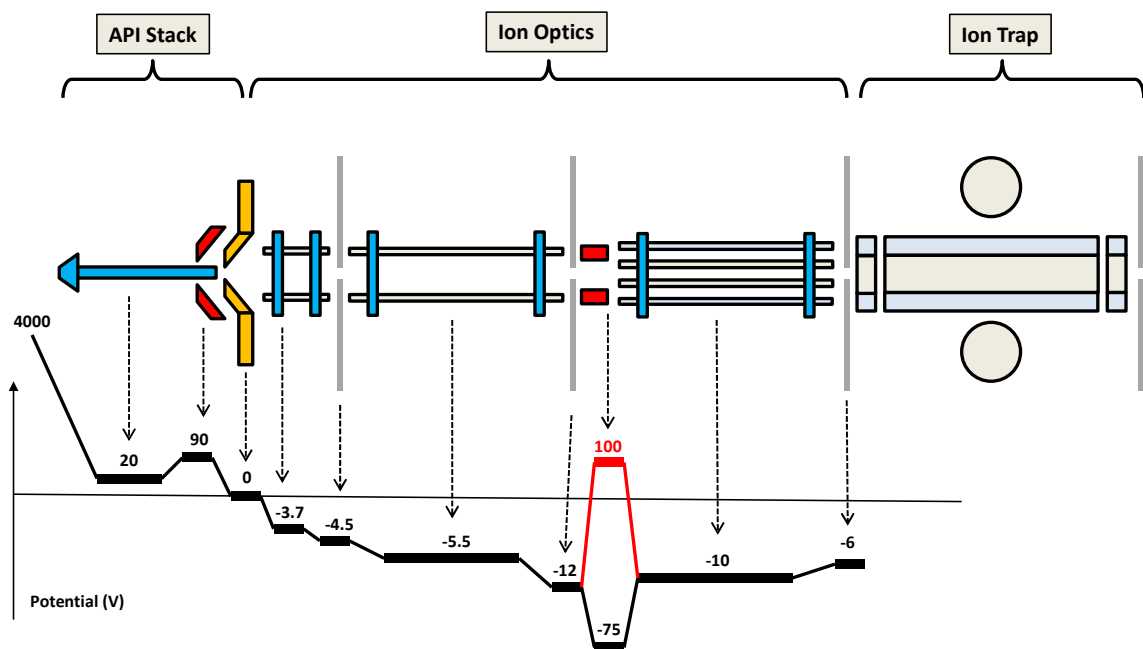


Figure 2.4 Representation of the DC voltage gradient applied for the transfer of positive ions. Gate lens voltages colored in red and black correspond to the closed (red) and open (black) states, respectively.

After passing through the skimmer, the ions were guided by a series of multipole ion guides (Q00 rf lens, Q0 quadrupole, and Q1 octapole). These multipole ion guides confine ions in the x and y direction by applying radio frequency (RF) voltages to the multipole rods. RF voltages applied to adjacent multipole rods had the same amplitude but were 180 degrees out of phase. Every set of opposing multipole rods had the exact same RF voltages applied to them. These RF voltages created an alternating electric field that confined ions into a circular oscillating movement in the x and y plane. In order to guide ions in the z direction, additional DC potentials were applied to each element of the ion optics. These DC potentials formed a DC gradient that dropped as ions traveled further into the mass spectrometer (Figure 2.4).

Ion lenses (lenses L0 and L1, Figure 2.3) were installed between each multiple ion guide. These lenses were only applied with DC potential, which focused ions into tighter packets before they entered the next multiple ion guide. A gate lens was placed in front of the Q1 octapole to control ion injection into the ion trap. When set at a high DC potential (shown in red in Figure 2.4), the gate lens prevented ions from entering the Q1 octapole which led into the ion trap. When set at a lower potential (shown in black in Figure 2.4), it facilitated ion movement into the Q1 octapole by creating a relatively large potential drop. The Q1 octapole then directly guided ions into the linear quadrupole ion trap.

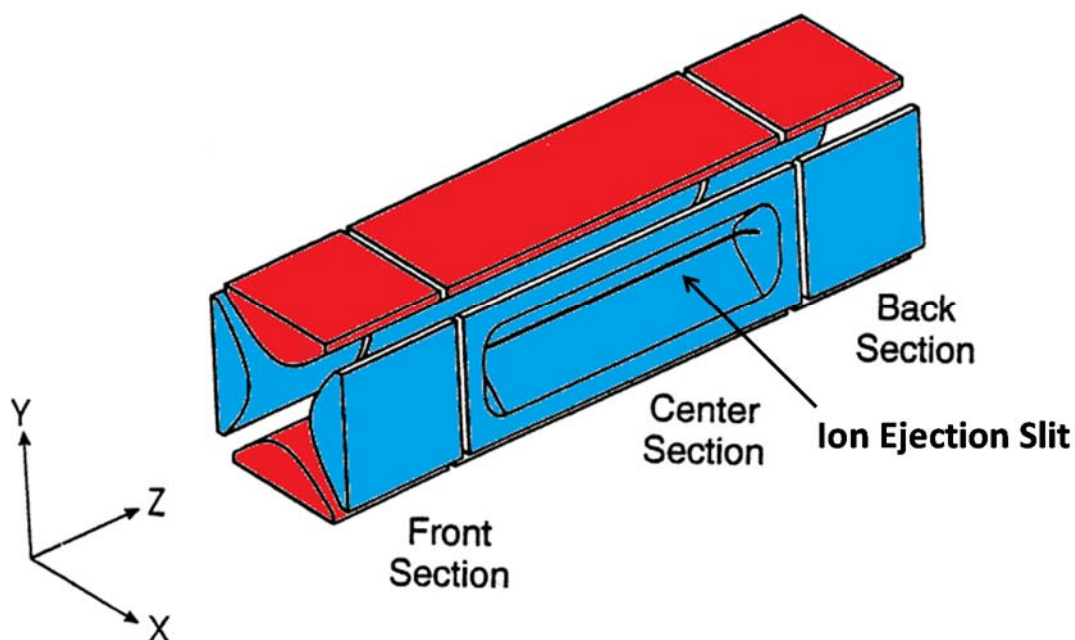


Figure 2.5 Schematic representation of the linear quadrupole ion trap used in Thermo scientific LTQ mass spectrometers.

The ion trap consisted of four hyperbolic rods that were cut into three sections: front section, center section, and back section (Figure 2.5). The four hyperbolic rods were divided into two sets of opposing rods (colored in red or blue in Figure 2.5). The two rods within each set were connected electrically and thus had the same RF potential applied to them. The voltages applied to the two rod sets were the same in amplitude but opposite in polarity. These RF voltages trapped ions in the x and y plane similarly as the multiple ion guides discussed above. Trapping of ions in the z direction was achieved by applying higher DC potential to the front and the back sections of the ion trap. The two rods in the center section in the x direction had a slit through which ions could be ejected into the detector. These two rods are referred to as the “x-rods”, or “exit rods”. Ion motion inside the ion trap will be further discussed below.

2.3.2 Ion Motion Inside Linear Quadrupole Ion-Trap

2.3.2.1 Ion Trapping in the X- and Y- Plane

The motion of the ions in a quadrupole field is mathematically described by the Mathieu equation^{24,25}:

$$\frac{d^2u}{d\xi^2} + (a_u + 2q_u \cos 2\xi)u = 0 \quad (1)$$

Here, u represents the x, y, and z coordinates, and a_u and q_u are the Mathieu stability parameters. The other parameter $\xi = \frac{\Omega t}{2}$, with Ω being the radio frequency of the potential applied to the quadrupole rods.

For the LQIT, the applied electric potential generated by the RF and DC voltages can be described using the equation below:

$$\phi_0 = U + V \cos \Omega t \quad (2)$$

where U is the applied DC potential, V is the amplitude of the applied RF potential, and Ω is the angular frequency of the RF potential. The quadrupole potential within the ion trap in the x and y plane can then be described as:

$$\phi_{x,y} = \phi_0 \frac{x^2 - y^2}{r_0^2} = \frac{(U + V \cos \Omega t)(x^2 - y^2)}{r_0^2} \quad (3)$$

According to Newton's Second Law of Motion, the force that an ion experiences in a certain direction is proportional to its acceleration in the same direction. Therefore, in the x and y plane, we have:

$$\begin{aligned} F_x &= ma = m \frac{d^2 x}{dt^2} = -ze \frac{\partial \phi_{x,y}}{\partial x} \\ F_y &= ma = m \frac{d^2 y}{dt^2} = -ze \frac{\partial \phi_{x,y}}{\partial y} \end{aligned} \quad (4)$$

where m is the mass of the ion, z is the number of charges of the ion, and e is the elementary charge. Combining equation 2 into equation 3 gives:

$$\begin{aligned} m \frac{d^2 x}{dt^2} &= -\frac{2ze}{r_0^2} (U + V \cos \Omega t)x \\ m \frac{d^2 y}{dt^2} &= \frac{2ze}{r_0^2} (U + V \cos \Omega t)y \end{aligned} \quad (5)$$

which can be further rearranged into:

$$\begin{aligned}\frac{d^2x}{dt^2} + \frac{2ze}{mr_0^2}(U + V \cos \Omega t)x &= 0 \\ \frac{d^2y}{dt^2} - \frac{2ze}{mr_0^2}(U + V \cos \Omega t)y &= 0\end{aligned}\tag{6}$$

Comparing equation 6 with equation 1, we can derive the following mathematic representation for the two Mathieu stability parameters, a and q:

$$\begin{aligned}a_u = a_x = -a_y &= \frac{8zeU}{mr_0^2\Omega^2} \\ q_u = q_x = -q_y &= -\frac{4zeV}{mr_0^2\Omega^2}\end{aligned}\tag{7}$$

For ions to maintain a stable trajectory in the x and y plane within the ion trap, the above two parameters must fall within a certain range, known as the stable region on the Mathieu stability diagram²⁵ (Figure 2.6). Ions with parameters outside of the stable region will be unstable in at least one direction and thus will be eliminated from the ion trap.

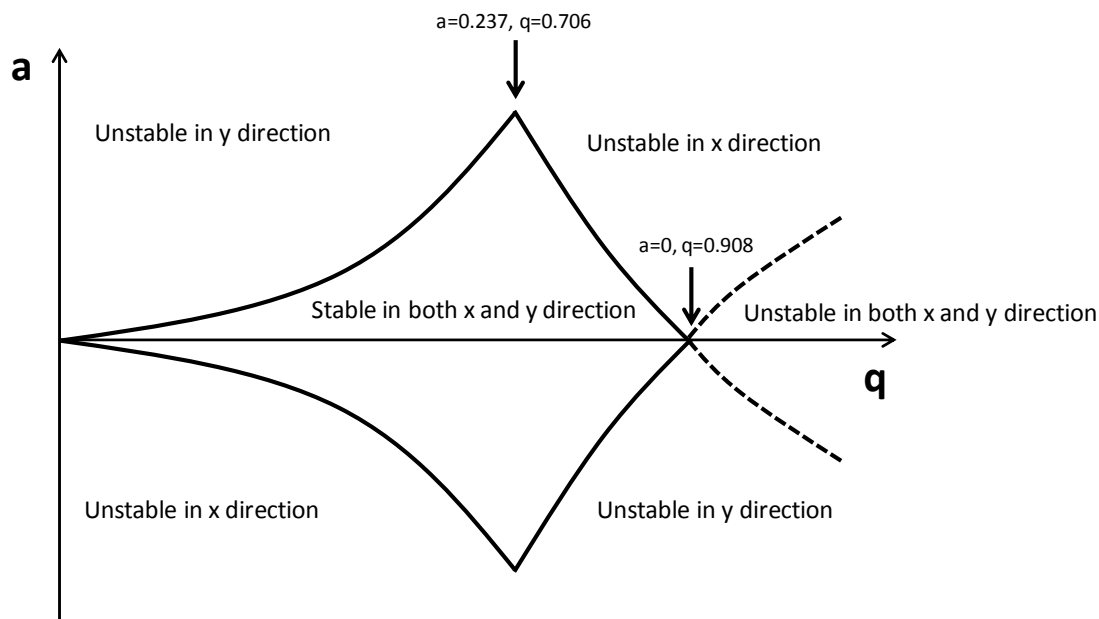


Figure 2.6 Illustration of the Mathieu stability diagram.

It is worth noting that smaller ions have larger a_u and q_u values. Therefore, in order to simultaneously trap ions with a broad range of m/z -values, the ion trap was typically operated at $a_u = 0$, which covers the widest range of q_u values. Under this setting, ions with q_u values ranging from 0 to 0.908 are stable inside the ion trap.

2.3.2.2 Ion Trapping in the Z Direction

Ion trapping in the z direction was achieved by applying different DC potentials to the three sections of the ion trap. Higher potentials were applied to the front and back sections, creating a DC potential well that confined ions into the center section. Different DC gradients were used during ion injection, ion trapping, and ion ejection (Figure 2.7).

Helium buffer gas filled the ion trap at a nominal pressure of ~ 3 mtorr as a supplementary method to confine ions into the center section of the ion trap.²⁶ Ions gained kinetic energy as they entered the ion trap following the DC potential gradient along the ion optics (discussed in 2.3.1). Upon entering the ion trap, ions' kinetic energy was reduced through multiple collisions with the helium buffer gas. Ions with lower kinetic energy are more efficiently trapped at the center of the ion trap, resulting in enhanced mass accuracy, resolution, and ion ejection efficiency.

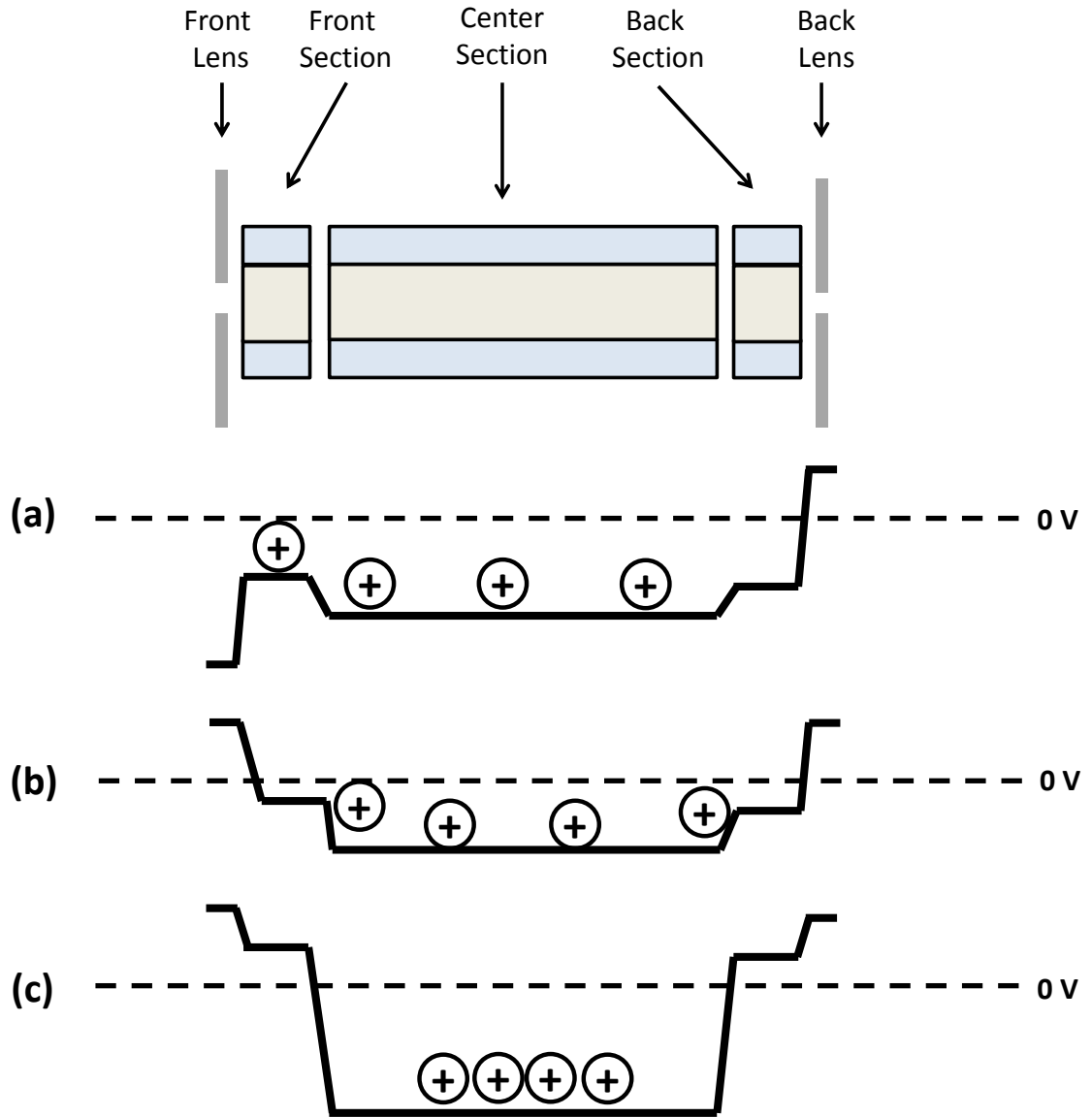


Figure 2.7 Representation of the DC potential well created during (a) ion injection, (b) ion trapping, and (c) ion ejection. Notice how the ions are focused into a much tighter packet during ion ejection by the sharper DC potential gradient.

2.3.3 Ion Ejection and Detection

As discussed in section 2.3.2.1, LQIT typically operates at a condition of $a = 0$. Under such conditions, ions line up on the x axis of the Mathieu stability diagram according to their m/z values, with bigger ions on the left side (Figure 2.8a). When the amplitude of the main RF voltage is ramped up, the q value of all ions increases, shifting them further right on the stability diagram. When the q value of a certain ion exceeds 0.908, it can no longer maintain a stable trajectory inside the ion trap and is ejected radially through the slits on the exit rods. This ejection method is referred to as the “mass selective instability scan” (Figure 2.8b).²⁷

In an attempt to enhance resolution, the contemporary Thermo Scientific LTQ mass spectrometers utilize an alternative ejection method known as “resonance ejection”.²⁸ During this ejection event, a supplementary ac voltage is applied to the exit rods. The frequency of this voltage is set to a value that is in resonance with the frequency of motion of ions at $q = 0.880$. As the amplitude of the main RF voltage is ramped up, ions with q value of 0.880 are brought into resonance with the frequency of the supplementary ac voltage, and start to oscillate at increasingly bigger amplitudes. When the oscillation amplitude is big enough, the ion is ejected from the trap (Figure 2.8c). Compared to the mass selective instability scan, resonance ejection allows ions to be ejected as a tighter packet, resulting in enhanced mass resolution.^{29,30}

Once ions are ejected, they are attracted to the conversion dynode³¹ by a strong electric field induced by a high voltage (+15 kV for negative ions, -15 kV for positive ions) applied to the conversion dynode. Ions hitting the conversion dynode generate secondary particles with opposite polarity (positive ions typically generate negative ions

or electrons, negative ions typically generate positive ions).²⁰ These secondary particles are then directed from the conversion dynode into the electron multiplier, where they are cascaded into a measurable current. The current produced is proportional to the number of ions originally ejected from the ion trap (Figure 2.9).

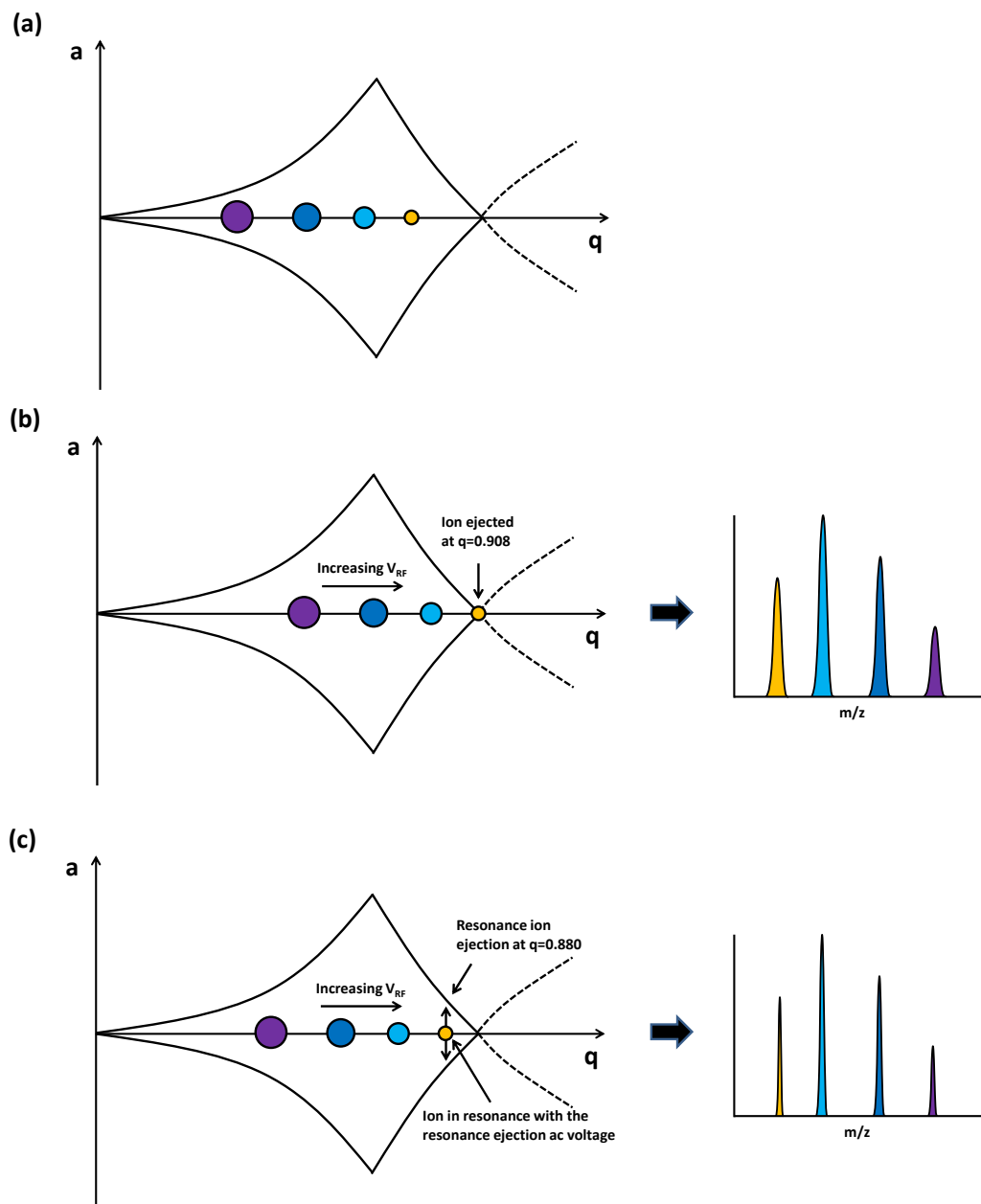


Figure 2.8 (a) Representation of ions trapped inside the ion trap in the Mathieu stability diagram. (b) Ion ejection by ramping the amplitude of the main RF voltage. (c) Resonance ion ejection using the supplementary resonance ejection ac voltage

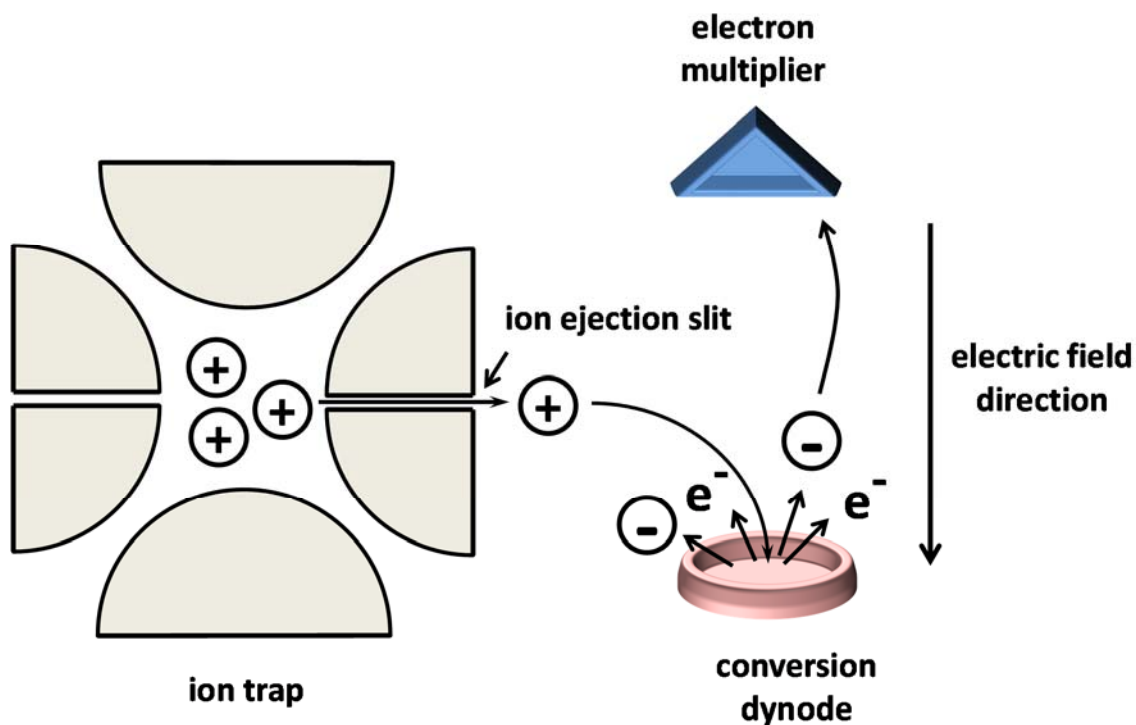


Figure 2.9 Schematic representation of the ion detection system. Ions were radially ejected through the exit rods and converted to secondary particles in the conversion dynode that were detected by the electron multiplier. Note that the electric field direction and the secondary particles generated correspond to positive ion detection.

2.4 Tandem Mass Spectrometry in LQIT

The ability to perform multiple tandem mass spectrometry experiments is a powerful feature of the linear quadrupole ion trap instruments.³² Generally, the ion of interest (parent ion) is isolated inside the ion trap by ejecting all other ions from the trap, and subjected to additional MS experiments, such as collision-activated dissociation³³ (CAD) or ion-molecule reactions.³⁴ These experiments produce fragment ions or product ions that are scanned out of the ion trap and detected. The LQIT is capable of doing multiple stages of tandem MS experiments (MS^n) by isolating an ion produced in the first MS experiment and subjecting it to further dissociation or bimolecular reaction. MS^n

capability is a feature unique to trapping instruments like LQIT and can be used to obtain in-depth structural information of the analyte ion.

2.4.1 Ion Isolation

Ion isolating is the first step involved in a tandem MS experiment. The main RF voltage was first ramped up to a value that set the ion of interest at a q value of 0.803. In this step, certain ions with lower m/z value than the ion of interest would be ejected from the trap. Then, a broad resonance excitation waveform was applied to the exit rods, which excited all ions inside the ion trap except for those with a q value of 0.803 (Figure 2.10). This can be accomplished because the excitation waveform covers a wide range of ion oscillation frequencies (5-500 kHz) but has a notch at the frequency corresponding to $q = 0.803$. The width of the notch is related to the isolation window, which can be defined by the software.

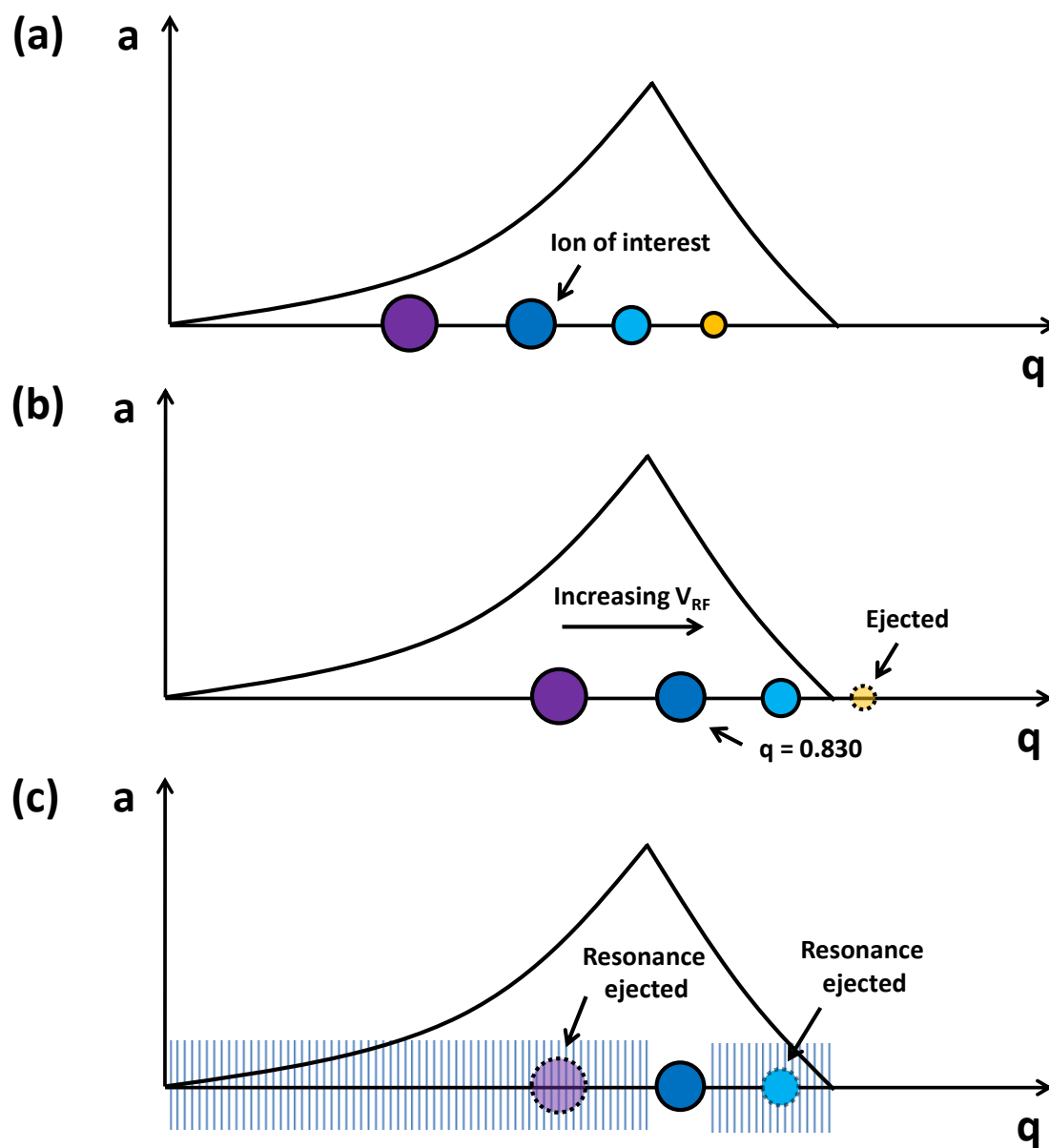


Figure 2.10 Position of the ions on the Mathieu stability diagram during (a) ion trapping, (b) RF ramp to increase the q value of ion of interest to 0.830, (c) application of resonance ejection waveform to remove all unwanted ions.

2.4.2 Collision-activated Dissociation

Collision-activated dissociation (CAD) is a common dissociation method aimed at fragmenting the isolated ion (Figure 2.11).³⁵ CAD process was started by lowering the amplitude of the main RF voltage so that the isolated ion had a lower q value (typically 0.25). Then, a supplementary ac voltage was applied to the x-rods of the quadrupole ion trap to bring the isolated ion into resonance. This supplementary voltage, known as the “tickle voltage”, had a lower amplitude compared with the resonance ejection voltage so that the ions were not excited too much that they leave the trap. The tickle voltage kinetically excited the ion of interest, which then underwent numerous collisions with the helium buffer gas present inside the ion trap. During these collision processes, kinetic energy of the ion was converted into internal energy. When the internal energy exceeded the barrier for unimolecular dissociation, the parent ion fragmented into smaller ions.

It should be noted here that the q value at which CAD occurs could influence the result of the experiment. In general, a lower q value was used in order to trap all fragment ions (which have lower m/z values and thus higher q values) inside the ion trap. However, at higher q values, parent ion could osculate at a higher frequency, allowing more kinetic energy to be deposited into the parent ion. In this way, the internal energy of the parent ion could be increased, making fragmentation pathways with higher barriers accessible.

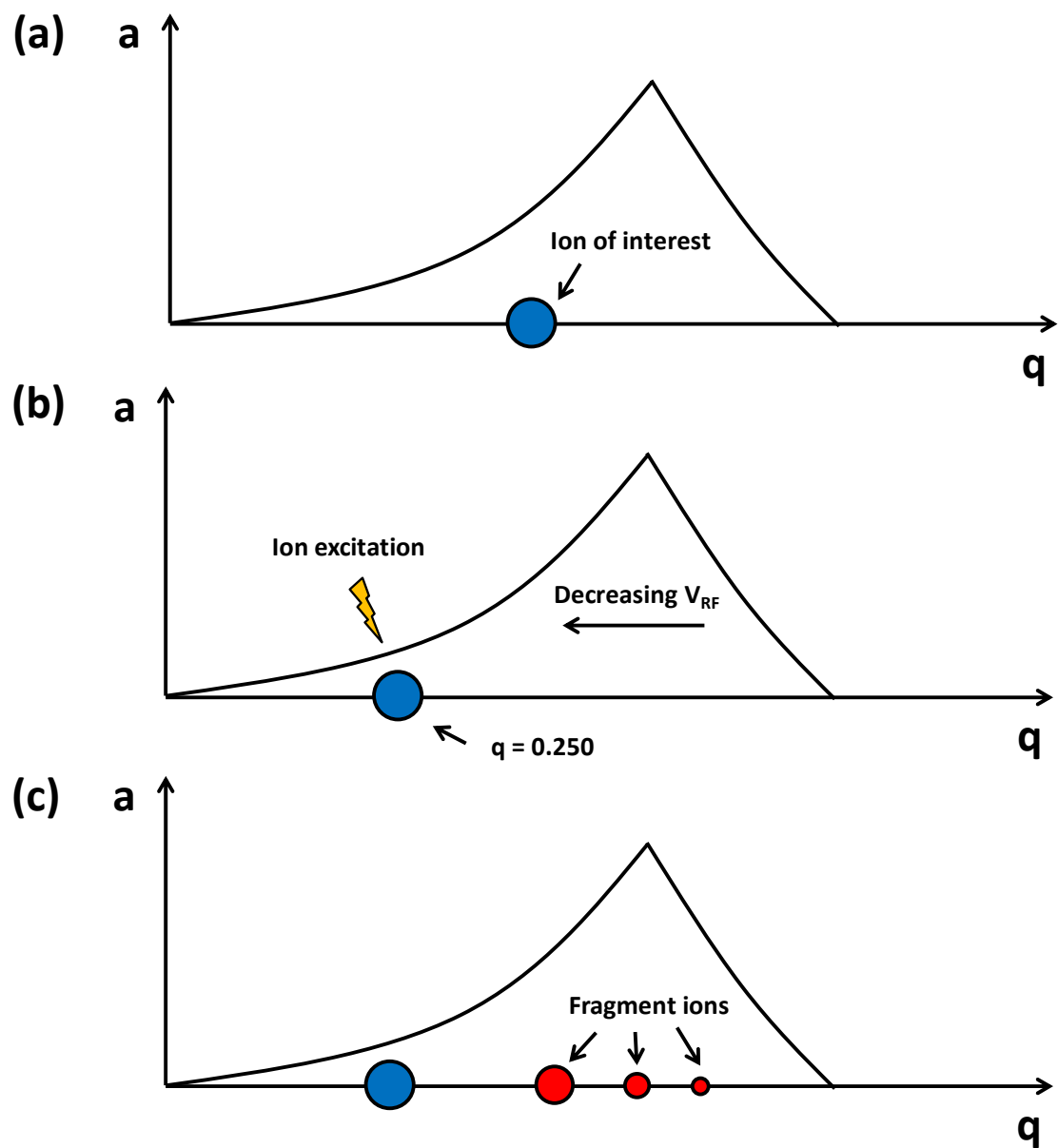


Figure 2.11 Position of the ions on the Mathieu stability diagram during (a) ion trapping, (b) ion excitation at q value of 0.250 (c) production of fragment ions.

2.4.3 Ion-molecule Reaction

Ion-molecule reaction is an alternative tandem MS technique to CAD.^{36,37} It can provide an extra dimension of structural information for the ionized analyte. As the name suggests, ion-molecule reaction occurs between the ionized analyte and a neutral reagent molecule. In general, neutral reagents were introduced into the ion trap via modification module installed on the mass spectrometer. Once inside the ion trap, they reacted with the isolated ion of interest, producing product ions that typically have larger m/z values (Figure 2.12).

Normal potential energy surface models do not apply to ion-molecule reaction which occurs in the gas-phase.³⁸ Instead, the Braumann double-well potential energy surface is used (Figure 2.13).³⁹ According to this model, the analyte ion and the neutral reagent first form a complex via ion-dipole interaction or ion-induced dipole interactions. Formation of the reactant complex lowers the overall energy through solvation. The solvation process gives the reactant complex enough energy to surpass the reaction barrier, forming a product complex which eventually dissociate into separated products. Because ion-molecule reactions occur in vacuum, total amount of energy in the reaction system is constant. Therefore, reactions with a barrier higher than the entrance energy level and reactions that are overall endothermic cannot occur.

In this dissertation, two methods are employed for the introduction of neutral reagents into the mass spectrometer (Figure 2.14). The first method is via an external reagent mixing manifold.^{3,40} This setup first mixed the neutral reagent into the helium buffer gas that entered the ion trap. A leak valve was used to regulate the amount of helium-reagent mixture into the ion trap. This method allowed the neutral reagent to be

continuously introduced and maintained at a constant concentration inside the trap. The second method is via a pulsed valve setup.⁴¹ Here, the neutral reagent was injected into a chamber that connects to the back of the ion trap via a pulsed valve. The pulsed valve opened for a short period of time upon triggering, allowing a packet of neutral reagent to enter the ion trap and react with the analyte ion.

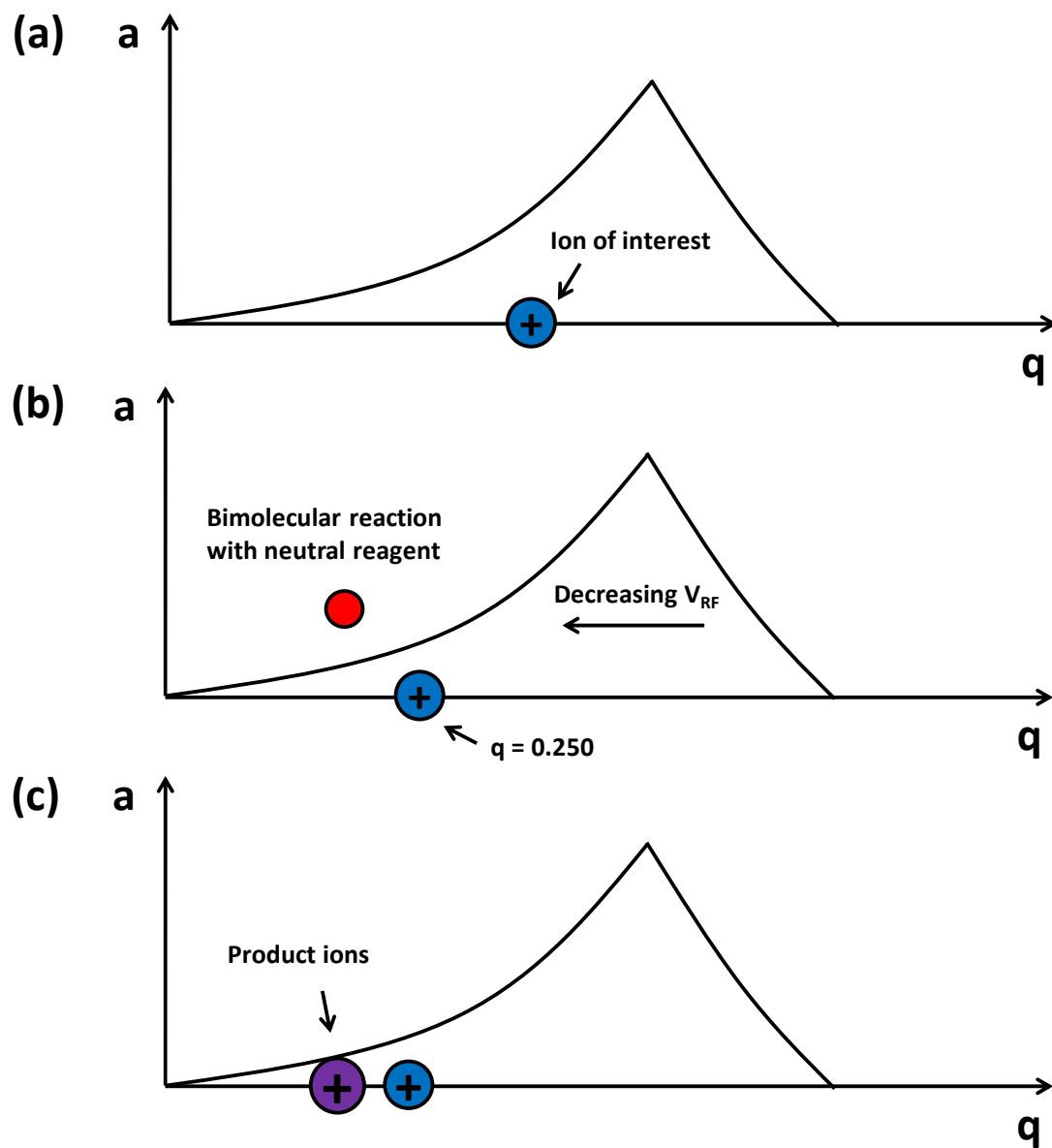


Figure 2.12 Position of the ions on the Mathieu stability diagram during (a) ion trapping, (b) RF ramp to increase the q value of ion of interest to 0.830, (c) application of resonance ejection waveform to remove all unwanted ions.

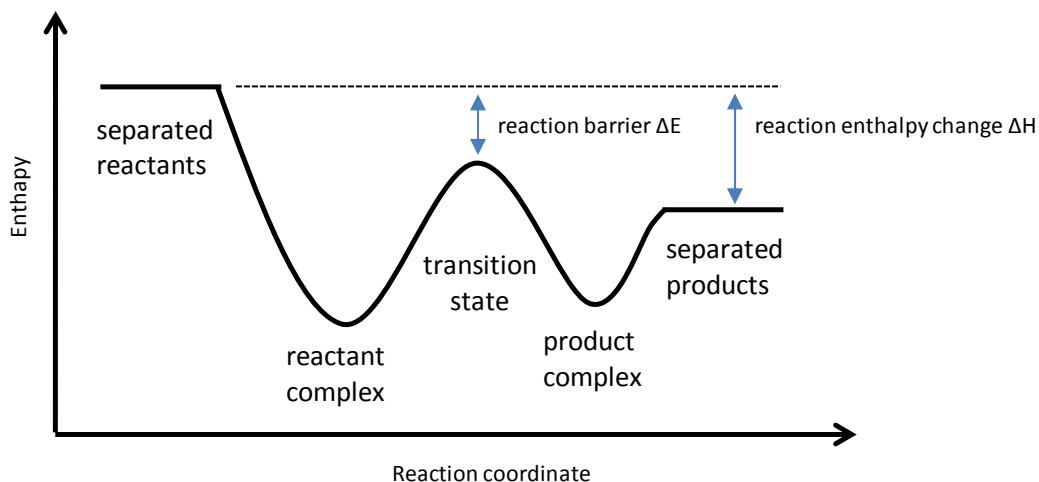


Figure 2.13 An example representation of the Braumann double well potential energy surface

2.5 Orbitrap Mass Spectrometer

The orbitrap has quickly become the most widely used high resolution mass analyzer since its introduction in 2005.⁴² Compared with other ion traps, the orbitrap only utilizes electrostatic field for ion trapping and mass analysis. Therefore, it is in general a simpler, more robust, and more compact ion trap mass analyzer. However, it should be noted that despite being an ion trap, the orbitrap on its own cannot perform tandem MS experiments. Therefore, hybrid instruments such as LQIT-Orbitrap are developed to perform tandem MS experiments with high mass resolution.⁴³

2.5.1 Instrument Setup

The Orbitrap mass spectrometer used in this dissertation is a Thermo Scientific LTQ Orbitrap XL mass spectrometer.^{43,44} It is a hybrid instrument made by coupling an orbitrap mass analyzer to the rear end of a linear quadrupole ion trap (Figure 2.14). Ions trapped inside the linear ion trap could be ejected axially into the C-trap by applying a DC potential gradient. The ejected ions then underwent collisions with the nitrogen gas to be focused into a thin packet along the curvature of the C-trap. The focused ions were then accelerated by a series of lenses before being pulsed into the orbitrap mass analyzer.

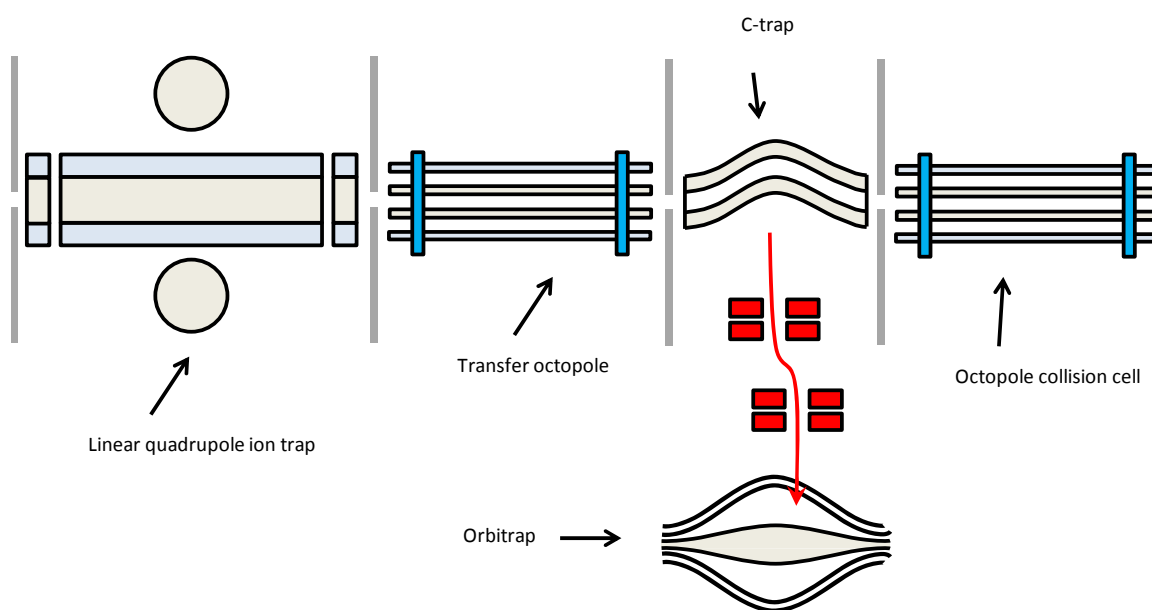


Figure 2.14 Schematic representation of the coupling between linear quadrupole ion trap and orbitrap in Thermo Scientific LTQ Orbitrap XL mass spectrometer. Parts in front of the linear quadrupole ion trap are identical with Thermo Scientific LTQ mass spectrometer (Fig 2.4). Ions are concentrated in the C-trap before being ejected off center into the orbitrap (red arrow).

2.5.2 Ion Motion Inside Orbitrap Mass Analyzer

Two ion motions are involved inside the orbitrap: 1) axial oscillation movement along the central electrode and 2) the rotational movement around the central electrode (Figure 2.15).⁴⁵ The axial movement can be described by the following equation:

$$z(t) = z_0 \cos(\omega t) + \left(\frac{2E_z}{k}\right)^{1/2} \sin(\omega t)$$

where z_0 is the initial axial coordinate, E_z is the initial ion kinetic energy along the axis, k is the axial restoring force parameter determined by the condition of the orbitrap, and ω is the frequency at which the ion oscillates. This oscillation movement induces an imaginary current that peaks whenever the ion moves across the center of the orbitrap. Therefore, oscillation frequency of the ions can be derived by performing Fourier transform on the imaginary current data. The frequency ω is further related to the m/z of the ion by the following equation:

$$\omega = \left(\frac{kq}{m}\right)^{1/2}$$

The rotational movement around the central electrode can be described as:

$$r = \frac{2qV}{qE}$$

where r is the radius at which the ion rotates, qV is the initial kinetic energy, and E is the electric field strength. Although the rotational movement is not used for mass analysis, it is still important as the ion's initial kinetic energy must be controlled in order to avoid collision with the outer electrode of the orbitrap.

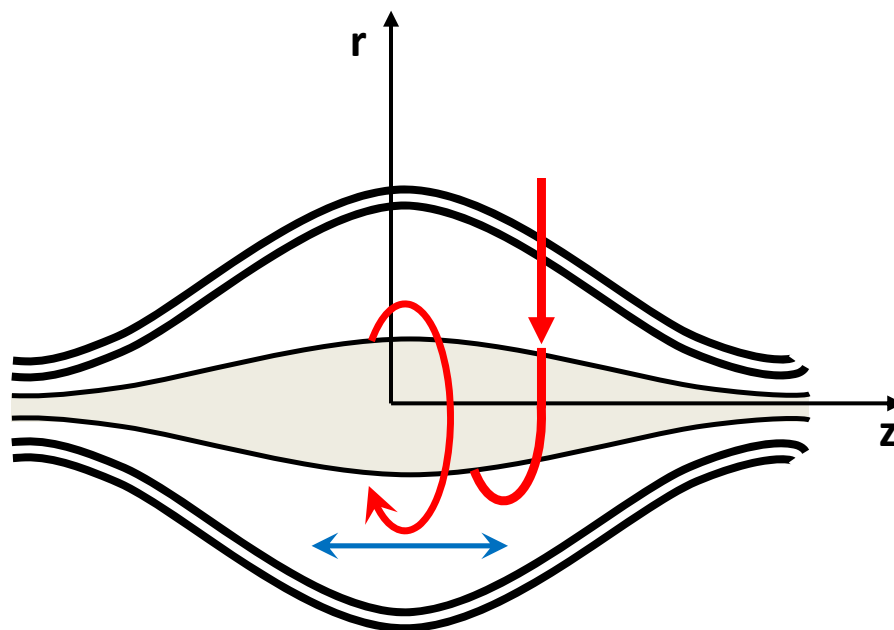


Figure 2.15 Schematic representation of an orbitrap mass analyzer. The ions are injected off center to induced a harmonic axial oscillation (blue arrows).

2.6 References

- (1) Cooks, R. G.; Busch, K. L.; Glish, G. L. *Science* **1983**, 222 (4621), 273–291.
- (2) McLafferty, F. W. *Int. J. Mass Spectrom.* **2001**, 212 (1–3), 81–87.
- (3) Gronert, S. *Mass Spectrom. Rev.* **2005**, 24 (1), 100–120.
- (4) Klein, G. C.; Angström, A.; Rodgers, R. P.; Marshall, A. G. *Energy Fuels* **2006**, 20 (2), 668–672.
- (5) Hernández, F.; Sancho, J. V.; Ibáñez, M.; Abad, E.; Portolés, T.; Mattioli, L. *Anal. Bioanal. Chem.* **2012**, 403 (5), 1251–1264.
- (6) Zhu, M.; Zhang, H.; Humphreys, W. G. *J. Biol. Chem.* **2011**, 286 (29), 25419–25425.
- (7) Dempster, A. J. *Phys. Rev.* **1918**, 11 (4), 316–325.
- (8) Munson, M. S. B.; Field, F. H. *J. Am. Chem. Soc.* **1966**, 88 (12), 2621–2630.
- (9) Tanaka, K.; Waki, H.; Ido, Y.; Akita, S.; Yoshida, Y.; Yoshida, T.; Matsuo, T. *Rapid Commun. Mass Spectrom.* **1988**, 2 (8), 151–153.
- (10) Fenn, J. B.; Mann, M.; Meng, C. K.; Wong, S. F.; Whitehouse, C. M. *Science* **1989**, 246 (4926), 64–71.
- (11) Carroll, D. I.; Dzidic, I.; Stillwell, R. N.; Horning, M. G.; Horning, E. C. *Anal. Chem.* **1974**, 46 (6), 706–710.
- (12) Robb, D. B.; Covey, T. R.; Bruins, A. P. *Anal. Chem.* **2000**, 72 (15), 3653–3659.
- (13) Takáts, Z.; Wiseman, J. M.; Gologan, B.; Cooks, R. G. *Science* **2004**, 306 (5695), 471–473.
- (14) Konermann, L.; Ahadi, E.; Rodriguez, A. D.; Vahidi, S. *Anal. Chem.* **2013**, 85 (1), 2–9.
- (15) Wilm, M. S.; Mann, M. *Int. J. Mass Spectrom. Ion Process.* **1994**, 136 (2), 167–180.
- (16) Taflin, D. C.; Ward, T. L.; Davis, E. J. *Langmuir* **1989**, 5 (2), 376–384.
- (17) Duft, D.; Achtzehn, T.; Müller, R.; Huber, B. A.; Leisner, T. *Nature* **2003**, 421 (6919), 128–128.
- (18) Iribarne, J. V.; Thomson, B. A. *J. Chem. Phys.* **1976**, 64 (6), 2287–2294.

- (19) Iavarone, A. T.; Williams, E. R. *J. Am. Chem. Soc.* **2003**, *125* (8), 2319–2327.
- (20) Schwartz, J. C.; Senko, M. W.; Syka, J. E. P. *J. Am. Soc. Mass Spectrom.* **2002**, *13* (6), 659–669.
- (21) Hager, J. W. *Rapid Commun. Mass Spectrom.* **2002**, *16* (6), 512–526.
- (22) Douglas, D. J.; Frank, A. J.; Mao, D. *Mass Spectrom. Rev.* **2005**, *24* (1), 1–29.
- (23) Bier, M. E.; Syka, J. E. P. Ion trap mass spectrometer system and method. US5420425 A, May 30, 1995.
- (24) March, R. E. *Int. J. Mass Spectrom. Ion Process.* **1992**, *118*, 71–135.
- (25) Johnson, J. V.; Peddeer, R. E.; Yost, R. A.; March, R. E. *Rapid Commun. Mass Spectrom.* **1992**, *6* (12), 760–764.
- (26) Stafford, G. C.; Kelley, P. E.; Syka, J. E. P.; Reynolds, W. E.; Todd, J. F. *J. Int. J. Mass Spectrom. Ion Process.* **1984**, *60* (1), 85–98.
- (27) Franzen, J. *Int. J. Mass Spectrom. Ion Process.* **1993**, *125* (2), 165–170.
- (28) Kaiser, R. E.; Graham Cooks, R.; Stafford, G. C.; Syka, J. E. P.; Hemberger, P. H. *Int. J. Mass Spectrom. Ion Process.* **1991**, *106*, 79–115.
- (29) Williams, J. D.; Cox, K. A.; Cooks, R. G.; McLuckey, S. A.; Hart, K. J.; Goeringer, D. E. *Anal. Chem.* **1994**, *66* (5), 725–729.
- (30) Schwartz, J. C.; Syka, J. E. P.; Jardine, I. *J. Am. Soc. Mass Spectrom.* **1991**, *2* (3), 198–204.
- (31) A, D. L. Electron multiplier-ion detector system. US3898456 A, August 5, 1975.
- (32) Louris, J. N.; Cooks, R. G.; Syka, J. E. P.; Kelley, P. E.; Stafford, G. C.; Todd, J. F. *J. Anal. Chem.* **1987**, *59* (13), 1677–1685.
- (33) McLuckey, S. A. *J. Am. Soc. Mass Spectrom.* **1992**, *3* (6), 599–614.
- (34) Gronert, S. *Chem. Rev.* **2001**, *101* (2), 329–360.
- (35) Cooks, R. G. *J. Mass Spectrom.* **1995**, *30* (9), 1215–1221.
- (36) Brodbelt, J. S. *Mass Spectrom. Rev.* **1997**, *16* (2), 91–110.
- (37) Campbell, K. M.; Watkins, M. A.; Li, S.; Fiddler, M. N.; Winger, B.; Kenttämaa, H. I. *J. Org. Chem.* **2007**, *72* (9), 3159–3165.
- (38) Brauman, J. I. *J. Mass Spectrom.* **1995**, *30* (12), 1649–1651.

- (39) Olmstead, W. N.; Brauman, J. I. *J. Am. Chem. Soc.* **1977**, *99* (13), 4219–4228.
- (40) Gronert, S. *J. Am. Soc. Mass Spectrom.* **1998**, *9* (8), 845–848.
- (41) Jarrell, T.; Riedeman, J.; Carlsen, M.; Replogle, R.; Selby, T.; Kenttämää, H. *Anal. Chem.* **2014**, *86* (13), 6533–6539.
- (42) Hu, Q.; Noll, R. J.; Li, H.; Makarov, A.; Hardman, M.; Graham Cooks, R. *J. Mass Spectrom.* **2005**, *40* (4), 430–443.
- (43) Makarov, A.; Denisov, E.; Kholomeev, A.; Balschun, W.; Lange, O.; Strupat, K.; Horning, S. *Anal. Chem.* **2006**, *78* (7), 2113–2120.
- (44) Hardman, M.; Makarov, A. A. *Anal. Chem.* **2003**, *75* (7), 1699–1705.
- (45) Perry, R. H.; Cooks, R. G.; Noll, R. J. *Mass Spectrom. Rev.* **2008**, *27* (6), 661–699.

CHAPTER 3. FUNCTIONAL GROUP IDENTIFICATION IN DEPROTONATED ANALYTES VIA ION-MOLECULE REACTIONS WITH DEMB AND WATER

3.1 Introduction

Mass spectrometry (MS) is a powerful analytical technique for the identification of unknown compounds within complex mixtures.¹⁻⁴ By accurately measuring the m/z value of the ionized analyte, molecular weight and elemental compositions of the unknown molecules can be obtained.⁵ In order to further elucidate the structure of the unknown molecules, tandem mass spectrometry (MS^n) experiments that involve multiple stages of ion isolation and dissociation experiments can be performed.³ During these experiments, the ion of interest (parent ion) is fragmented into smaller fragmentation ions. Analyte ions with certain functional groups often produce characteristic fragmentation ions.⁶ In this way, the functional groups present in the unknown molecule can be identified. The most commonly used method to fragment ions is via collision activated dissociation (CAD).⁷ However, for compounds with multiple functional groups, MS^n based on CAD does not always provide adequate structural information for the identification of all functional groups present.⁸ Therefore, additional structural elucidation methods need to be developed.

Past studies have shown that tandem mass spectrometry based on ion-molecule reactions can be a powerful tool for structural elucidation of ionized analytes.⁹ Functional

groups can be identified by using neutral reagents that only exhibit reactivity towards ions with these functional groups.¹⁰⁻¹³ However, most of the ion-molecule reactions developed require the target analyte to be protonated as proton transfer from the protonated analyte to the neutral reagent is a key step in the reaction mechanism.¹² Therefore, these methods are suboptimal for acidic analytes that are easier to ionize under negative ion mode. One example of such analytes is lignin related compounds that generally contain the phenol functional groups.¹⁴ The best ionization method for these compounds was shown to be negative ion mode electrospray ionization (ESI) with sodium hydroxide dopant, which exclusively forms deprotonated molecules with no fragmentation for lignin model compounds.¹⁵ Other ionization methods, such as positive ion mode ESI or atmospheric pressure chemical ionization (APCI), either cause extensive fragmentation or form multiple ion types for each compound. Another example is drug metabolites that contain phosphate, sulfate, or glucuronide functional group. Negative ion mode ESI were shown to provide a lower detection limit compared with positive ion mode ESI, which is desirable for the trace analysis of these compounds in complex biologic matrixes.¹⁶ For those acidic compounds, functional group selective ion-molecule reactions for deprotonated analytes need to be developed.

Boron reagents were shown to be reactive towards deprotonated analytes.¹⁷⁻¹⁹ Trimethyl borate (TMB) were shown to react with phosphate containing species by forming an adduct that losses one or more methanol molecules.¹⁸ Diethylmethoxyborane (DEMB) was able to differentiate phosphorus- and sulfocarbohydrates as it only reacted with phosphorus carbohydrates.²⁰ However, the reactivity of boron reagents towards

deprotonated analytes containing other functional groups, such as carboxylate or phenoxide, was not yet studied.

In the work presented in this chapter, two ion-molecule reaction systems were developed for the functional group identification in deprotonated analytes. In the first part, DEMB is explored as a reagent for the identification of the phenol functionality which is commonly observed in lignin-related analytes. DEMB was introduced into the mass spectrometer via a reagent mixing manifold. In the second part, a novel ion-molecule reaction setup was developed that allowed separate introduction of two neutral reagents, DEMB and H₂O, into the ion trap. Using this setup, a new reagent, diethylhydroxylborane (DEHB) was produced inside the ion trap. Its reactivity with deprotonated analyte containing phenoxides, carboxylates, phosphates, and sulfates functional group was studied. This reaction system was later implemented to the analysis of an artificial drug metabolite mixture.

3.2 Experimental

3.2.1 Chemicals

Diethylmethoxyborane (97%), phenol (99%), 2-ethoxyphenol (98%), 3-methoxyphenol (96%), 4-ethoxyphenol (99%), 2-methoxy-4-propylphenol (99%), isoeugenol (98%), methyl ferulate (99%), catechol (99%), resorcinol (99%), hydroquinone (99%), 2-hydroxybenzyl alcohol (99%), 3-hydroxybenzyl alcohol (99%), benzoic acid (99.5%), 3,5-dimethoxybenzoic acid (97%), 3,4,5-trimethoxybenzoic acid (99%), phenylacetic acid (99%), *trans*-cinnamic acid (99%), octanoic acid (98%),

heptanoic acid (97%), levulinic acid (98%), D-serine (98%), phthalic acid (99.5%), isophthalic acid (99%), terephthalic acid (98%), 3-nitrophenol (99%), 4-nitrophenol (99%), 2-hydroxybenzaldehyde (98%), 3-hydroxybenzaldehyde (99%), 4-hydroxybenzaldehyde (98%), methyl 2-hydroxybenzoate (99%), methyl 3-hydroxybenzoate (99%), methyl 4-hydroxybenzoate (99%), 2-hydroxybenzoic acid (99%), 3-hydroxybenzoic acid (99%), 4-hydroxybenzoic acid (99%), 2-hydroxycinnamic acid (99%), 3-hydroxycinnamic acid (98%), 4-hydroxycinnamic acid (97%), 2-hydroxyphenacetic acid (97%), 3-hydroxyphenacetic acid (99%), 4-hydroxyphenacetic acid (98%), vanillic acid (97%), syringic acid (95%), sinapic acid (98%), 4-methoxybenzoic acid (99%), 4-methylumbelliferyl β -D-glucuronide hydrate (98%), phenylphosphonic acid (98%), 2-aminoethylphosphonic acid (99%), 4-methylumbelliferyl phosphate, 4-methylumbelliferyl sulfate potassium salt, *p*-toluenesulfonic acid monohydrate (98.5%), benzenesulfonic acid (98%), morphine-6- β -D-glucuronide solution (1.0 mg/mL in methanol: water (2:8)), *p*-acetamidophenyl β -D-glucuronide sodium salt, 4-nitrophenyl β -D-glucuronide (98%), phenolphthalein β -D-glucuronide, Water- ^{18}O (97 atom % ^{18}O) and 4-hydroxy-3-methylbenzoic acid (97%) were purchased from Sigma Aldrich and used as received. Vanillin (99%) was purchased from Fisher Scientific and used as received. Guaiacylglycerol guaiacyl ether (97%) was purchased from TCI America and used as received. Water (LC/MS grade) was purchased from ProteoChem (Hurricane, UT) and used as received. Deuterium oxide (99.5%) was purchased from Cambridge Isotope Laboratories (Tewksbury, MA) and used as received. Lignin β -5 dimer was synthesized via a previously reported method.²¹ Converted *Miscanthus* biomass was obtained via a previously published procedure.²² For the

Hymecromone metabolite mixture, 4-methylumbelliferone (Hymecromone), 4-methylumbelliferyl sulfate potassium salt, 4-methylumbelliferyl phosphate, and 4-methylumbelliferyl β -D-glucuronide hydrate were dissolved in 50/50 v/v methanol/water to achieve a final concentration of 0.1 mM for each compound.

3.2.2 Mass Spectrometry

All experiments were performed on a Thermo Scientific linear quadrupole ion trap (LQIT) mass spectrometer equipped with an electrospray ionization (ESI) source operated in the negative ion mode. Sample solutions were prepared at a concentration of 1 mmol in 50/50 water/methanol (v/v) solution. 10 μ L of 1 mM NaOH water solution were added into 5 mL of sample solution to facilitate the formation of deprotonated analyte molecules. The NaOH doped sample solutions were injected into the ion source at a flow rate of 10 μ L/min. The injected solutions were mixed via a T-connector with 50/50 water/methanol (v/v) at a flow rate of 100 μ L/min to maintain stable spray current. Typical ESI conditions were: 3.5 kV spray voltage, 20 (arbitrary unit) sheath gas (N_2) flow, 10 (arbitrary unit) auxiliary gas (N_2) flow, and 2 (arbitrary unit) sweep gas (N_2) flow.

3.2.3 Ion-molecule Reactions

Ion-molecule reactions were studied using a combination of a custom build external reagent mixing manifold and a custom build pulsed valve interface.^{23,24} DEMB was injected into the external reagent mixing manifold via a syringe drive at a flow rate of 3 $\mu\text{L}/\text{min}$ and diluted with helium at a flow rate of 250 mL/min . The manifold was heated to 70 $^{\circ}\text{C}$ for efficient evaporation of DEMB into helium. The DEMB-helium mixture then entered a variable leak valve that allowed part of the mixture gas to enter the ion trap while the excess was directed into waste. The variable leak valve was set to maintain the pressure (measured via an ion gauge) within the trap region of the instrument at 0.5×10^{-5} Torr. Analyte ions were isolated and allowed to react with the neutral reagents for 200 ms before being ejected for detection.

H_2O was introduced into the trap region of the mass spectrometer via a custom build pulsed valve system. 5 μL of H_2O was injected into a stainless steel channel through a rubber septum via a syringe. The stainless steel channel was heated to 90 $^{\circ}\text{C}$ for promote water evaporation. A pulsed valve connected to the stainless steel channel were triggered manually via a waveform generator to open for 500 μS to allow H_2O to enter the linear quadrupole trap region. Analyte ions were isolated and allowed to react with the neutral reagents for 200 ms before being ejected for detection.

3.2.4 High-performance Liquid Chromatography

HPLC experiments were performed on a Surveyor Plus HPLC system consisting of a quaternary pump, an autosampler, and a Zorbax SB-C18 column. For the separation of drug metabolite mixtures, a non-linear gradient of water with 5 mMol ammonium

acetate (A) and methanol with 5 mMol ammonium acetate (B) was used: 0.00 min, 100% A; 10.00 min, 70% A and 30% B; 20.00 min, 60% A and 40% B; 25.00 min, 30% A and 70 % B; 30.00min, 30% A and 70% B; 31.00 min, 100% A; 40.00 min, 100% A. For all other separations, non-linear gradient of water (A) and acetonitrile (B) was used as follows: 0.00 min, 95% A and 5% B; 10.00 min, 95% A and 5% B; 30.00 min, 40% A and 60% B; 35.00 min, 5% A and 95 %; 38.00min, 5% A and 95% B; 38.50 min, 95% A and 5% B; 45.00 min, 95% A and 5% B. The flow rate of the mobile phase was kept at 500 $\mu\text{L}/\text{min}$ for both gradient methods. PDA detector was set at the wavelength of 254 nm.

HPLC eluents were ionized via an ESI source operating under negative ion mode with the following conditions: 3.25 kV spray voltage; 50 (arbitrary unit) sheath gas (N_2) flow and 20 (arbitrary unit) auxillary gas (N_2) flow. For phenolic compounds, HPLC eluents were mixed via a T-connector with 1% sodium hydroxide solution at a flow rate of 0.1 $\mu\text{L}/\text{min}$ before entering the ESI source.

3.2.5 Computational Details

All density functional theory (DFT) calculations were performed using the Gaussian 09 software package. Geometry optimizations were performed using the hybrid functional M06-2X with the 6-31+G(d,p) basis set. Vibrational frequencies calculations for the optimized geometries were performed at the same level of theory to obtain enthalpy values as well as to confirm that all minima had no negative frequencies and all transition states had one negative frequency. Intrinsic reaction coordinate (IRC) analyses were performed for all transition states to confirm that they connect to the correct reactant

and product. Natural Bond Orbital (NBO) analyses were performed at the M06-2X/6-311++G(2d,p) level of theory.

3.3 Results and Discussions

The first part of chapter 3.3 discusses the reactions between DEMB and deprotonated analytes containing phenoxide, phosphate, sulfate, or carboxylate functionality. The deprotonated analytes were generated via negative ion mode ESI with NaOH as dopant, isolated inside the ion trap, and subjected to reaction with DEMB. Results suggested that DEMB is a useful reagent for the identification of the phenol functionality in deprotonated analytes. DEMB was then used to identify phenols in a catalytically converted biomass sample containing multiple phenolic compounds.

The second part of chapter 3.3 discusses the reactions between DEHB/H₂O and deprotonated analytes containing phenoxide, phosphate, sulfate, or carboxylate functionality. This reaction system was found to be able to identify ions containing phenoxide, phosphate, or carboxylate functionality. Ion-molecule reactions with DEHB/H₂O were then applied to the analysis of a drug metabolite artificial mixture.

3.3.1 Ion-molecule Reactions with DEMB and H₂O

DEMB and H₂O, the two neutral reagents used in this study, were introduced into the mass spectrometer separately. DEMB was introduced continuously via a reagent mixing manifold and was maintained at a constant concentration inside the ion trap. H₂O was introduced into the mass spectrometer via a pulsed valve system. Upon triggering the

pulsed valve, H₂O molecules entered the ion trap and reacted with the isolated analytes ions.

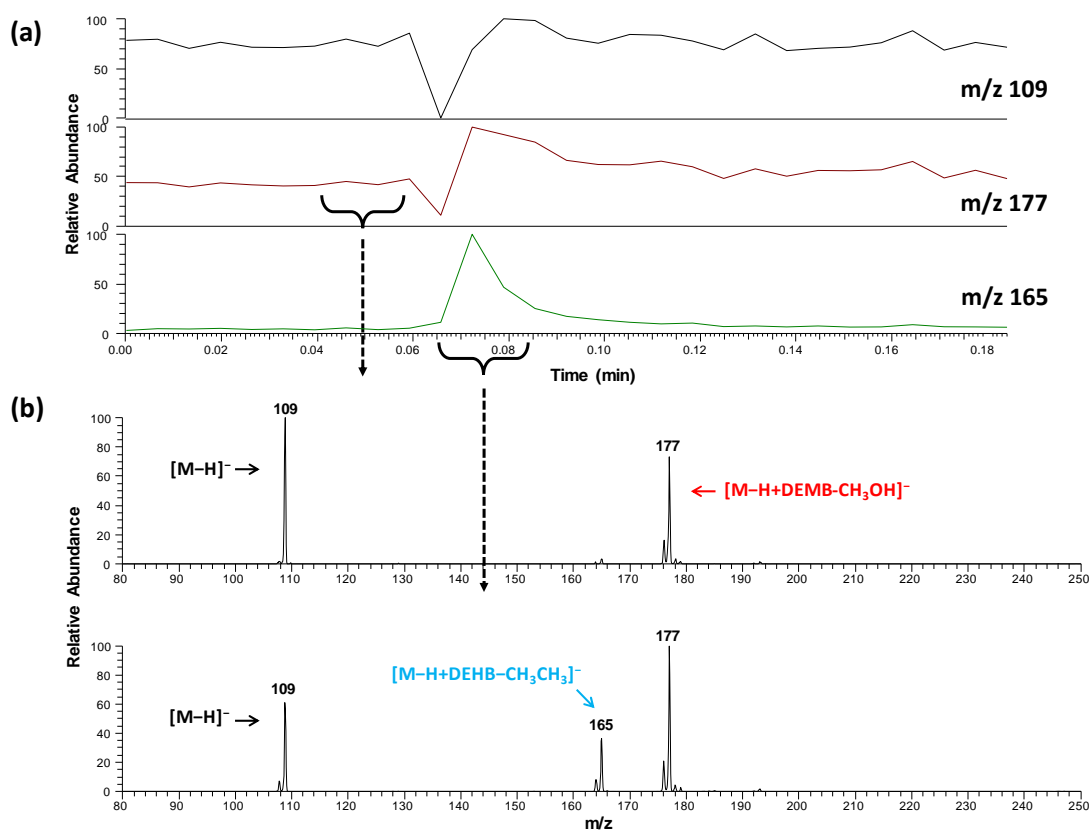


Figure 3.1 Reactions of deprotonated catechol (m/z 109) with DEMB and DEHB/H₂O. (a) Extracted ion current of the reactant ion (m/z 109), DEMB product ion (m/z 177), and DEHB/H₂O product ion (m/z 165) over time. (b) Averaged mass spectra measured (top) before and (bottom) after one pulsed introduction of H₂O

Figure 3.1 shows the mass spectra collected during the ion-molecule reaction involving deprotonated catechol, DEMB, and H₂O. Before H₂O introduction, DEMB was the only neutral reagent present inside the ion trap. Deprotonated catechol (m/z 109) reacted with DEMB, forming a DEMB adduct-CH₃OH product ion (m/z 177).

Abundance of the DEMB adduct-CH₃OH product ion (*m/z* 177) did not change over time because DEMB concentration was held constant. Upon H₂O introduction via the pulsed valve, DEMB hydrolyzed into DEHB and proceeded to react with the analyte ion. As a result, the abundance of a new product ion (*m/z* 165) increased. A corresponding decrease in the abundance of the reactant ion (deprotonated catechol of *m/z* 109) and the DEMB adduct-CH₃OH product ion (*m/z* 177) was also observed. The ion of *m/z* 165 was later identified to be DEHB adduct-CH₃CH₃. Therefore, this reaction setup can be used to study the reactivity of both DEMB and DEHB/H₂O towards deprotonated analytes.

3.3.2 Reactions Between DEMB and Deprotonated Analytes

3.3.2.1 Reactions Between DEMB and Phenoxide Containing Ions

Upon reactions with DEMB, most phenoxide containing analyte ions formed a DEMB adduct ion ($[M-H+DEMB]^-$) that has 100 units greater *m/z*-value than the analyte ion (Tables 3.1). Larger analytes such as two lignin dimers with β-O-4 and β-5 linkages also exclusively produced DEMB adducts (Table 3.1). However, there are three types of exceptions where the DEMB adduct was not observed for phenoxide containing analyte ions.

Table 3.1 Ionic products formed upon reactions of deprotonated model compounds with diethylmethoxyborane (DEMB) for 200 ms.

Analyte ion (m/z of [M-H] ⁻)	Ion structure	Products formed upon reactions with DEMB ^a (m/z)
phenol (91)		91+DEMB (191)
2-ethoxyphenol (137)		137+DEMB (237)
3-methoxyphenol (137)		123+DEMB (223)
4-ethoxyphenol (123)		137+DEMB (237)
2-methoxy-4-propylphenol (165)		165+DEMB (265)
isoeugenol (163)		163+DEMB (263)
methyl ferulate (207)		207+DEMB (307)
catechol (109)		109+DEMB-CH ₃ OH (177)
resorcinol (109)		109+DEMB (209)
hydroquinone (109)		109+DEMB (209)
2-hydroxybenzyl alcohol (123)		123+DEMB-CH ₃ OH (191)
3-hydroxybenzyl alcohol (123)		123+DEMB (223)
guaiacylglycerol guaiacyl ether (319)		319+DEMB (419)
lignin β-5 dimer (325)		325+DEMB (425)

^aOnly products with 5% or greater relative abundance reported. DEMB adduct colored in red, DEMB adduct-MeOH colored in blue.

The first exception was deprotonated phenols with an adjacent hydroxyl group such as catechol and 2-hydroxybenzyl alcohol. These analyte ions produced DEMB adduct-CH₃OH instead of DEMB adduct upon reaction with DEMB. Formation of this type of a product ion was not observed for the resorcinol, hydroquinone, or 3-hydroxybenzyl alcohol whose hydroxyl and phenol groups are further away from each other (Table 3.1). These observations suggest that the additional phenol or hydroxyl functionality close to the deprotonation site are likely involved in the formation of DEMB adduct-CH₃OH. The potential energy surface for the proposed mechanism, calculated via density functional theory, is shown in Figure 3.2.

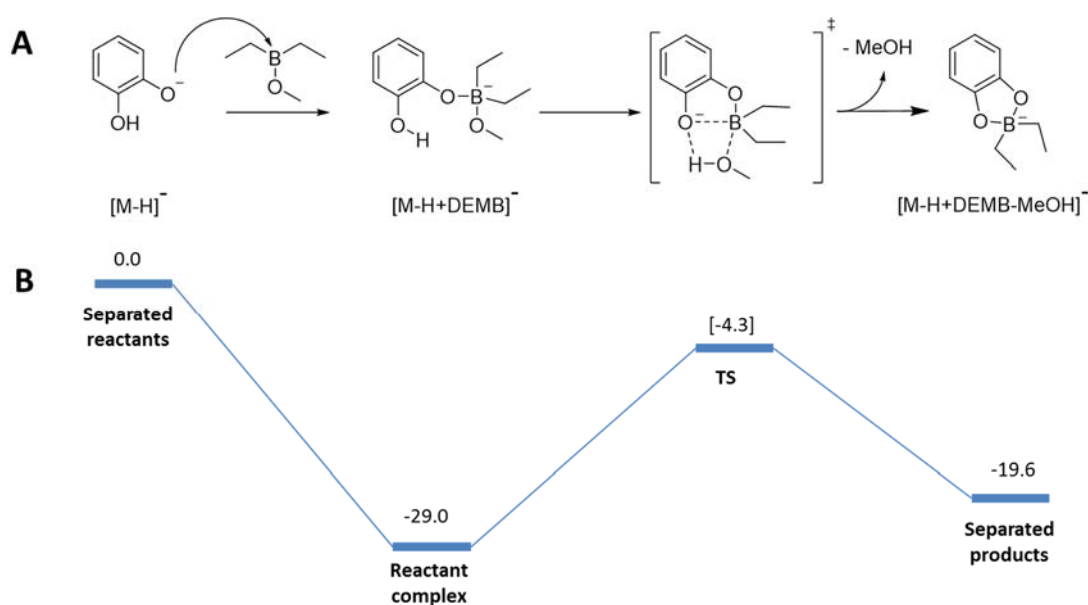
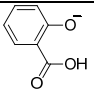
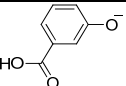
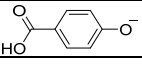
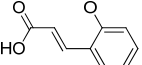
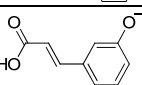
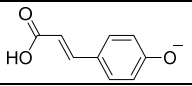
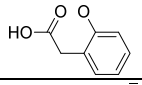
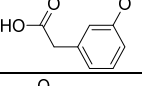
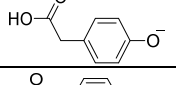
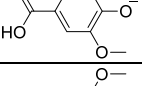
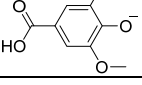
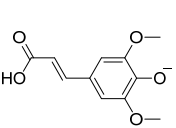


Figure 3.2 (A) Proposed mechanism and (B) calculated potential energy surface (enthalpy in kcal/mol) for the formation of a DEMB adduct that has lost methanol upon reactions between deprotonated catechol and DEMB (M06-2X/6-31+G(d,p) level of theory).

The second exception was phenols with a conjugated carboxylic acid. Multiple compounds with both phenol and carboxylic acid functional group were deprotonated and reacted with DEMB (Table 3.2). DEMB adduct-CH₃OH was observed for 4-hydroxybenzoic acid, 2-hydroxycinnamic acid and 4-hydroxycinnamic acid, whose phenol and carboxylic acid functionalities are conjugated. The above proposed mechanism in Figure 3.2 cannot explain the formation of DEMB adduct-CH₃OH for 4-hydroxybenzoic acid since the distance between the carboxylic acid and phenol functionalities is too great. Therefore, a different mechanism must be involved. One issue that must be considered here is that 4-hydroxybenzoic acid has two possible deprotonation sites. Hence it is important to figure out which deprotonation form is involved in the formation of DEMB adduct-CH₃OH.

Past studies have shown that ESI solvent conditions can influence the site of deprotonation of 4-hydroxybenzoic acid.^{25,26} In general, aprotic solvents favor the formation of the phenoxide while protic solvent favor the formation of carboxylate. The above conclusion was verified via CAD experiments performed on deprotonated 4-hydroxybenzoic acid generated under different solvent conditions (Figure 3.3). Regardless of the CAD energy used, deprotonated 4-hydroxybenzoic acid generated with acetonitrile showed more CO₂ loss than the deprotonated 4-hydroxybenzoic acid generated with H₂O and NaOH.

Table 3.2 Ionic products formed upon reactions of deprotonated model compounds containing a phenol and a carboxylic acid functional group with DEMB for 200 ms

Analyte ion (m/z of [M-H] ⁻)	Structure	Products formed upon reactions with DEMB ^a (m/z)
2-hydroxybenzoic acid (137)		none
3-hydroxybenzoic acid (137)		137+DEMB (251)
4-hydroxybenzoic acid (137)		137+DEMB-CH ₃ OH (177)
2-hydroxycinnamic acid (137)		137+DEMB-CH ₃ OH (177)
3-hydroxycinnamic acid (137)		137+DEMB (251)
4-hydroxycinnamic acid (137)		137+DEMB-CH ₃ OH (177)
2-hydroxyphenacetic acid (151)		none
3-hydroxyphenacetic acid (151)		151+DEMB (251)
4-hydroxyphenacetic acid (151)		151+DEMB (251)
vanillic acid (167)		167+DEMB-CH ₃ OH (235)
syringic acid (197)		197+DEMB-CH ₃ OH (265)
sinapic acid (223)		223+DEMB-CH ₃ OH (291)

^aOnly products with 5% or greater relative abundance reported.

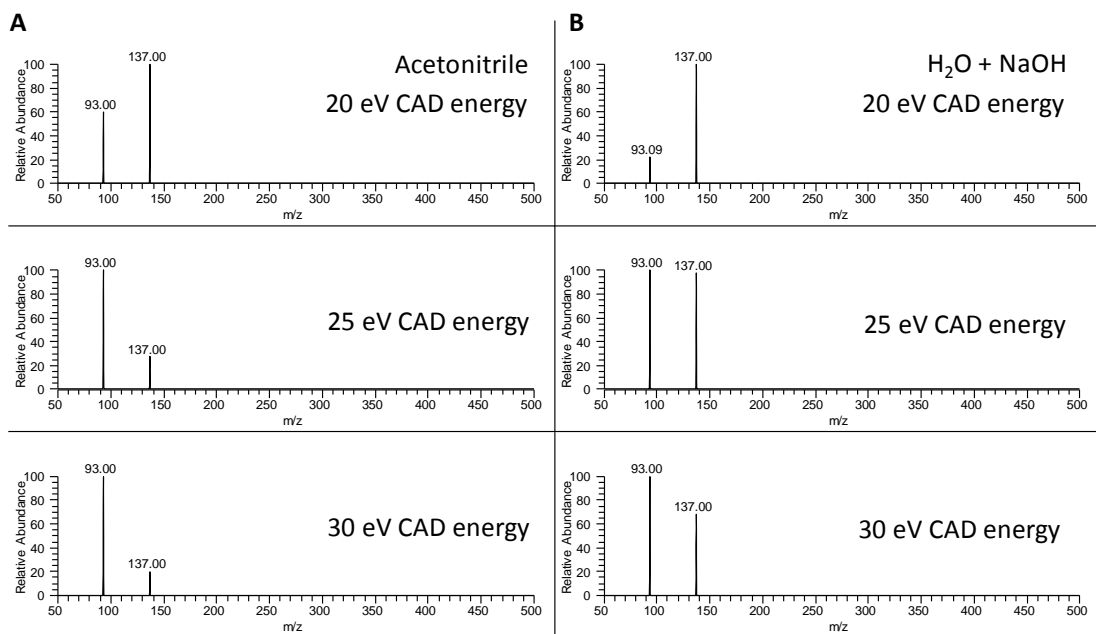


Figure 3.3 MS² CAD spectra measured for deprotonated 4-hydroxybenzoic acid (m/z 137) generated using ESI with (A) acetonitrile solution and (B) NaOH doped water solution.

CO₂ loss for phenoxide and carboxylate form of 4-hydroxybenzoic acid happen via different mechanisms and have different barriers. The calculated CO₂ loss barrier for phenoxide is lower than that for carboxylate (Figure 3.4). This suggests that CO₂ loss is easier for phenoxide upon CAD. The above two pieces of information proves that the deprotonated 4-hydroxybenzoic acid generated with acetonitrile contains a larger percentage of the phenoxide tautomer.

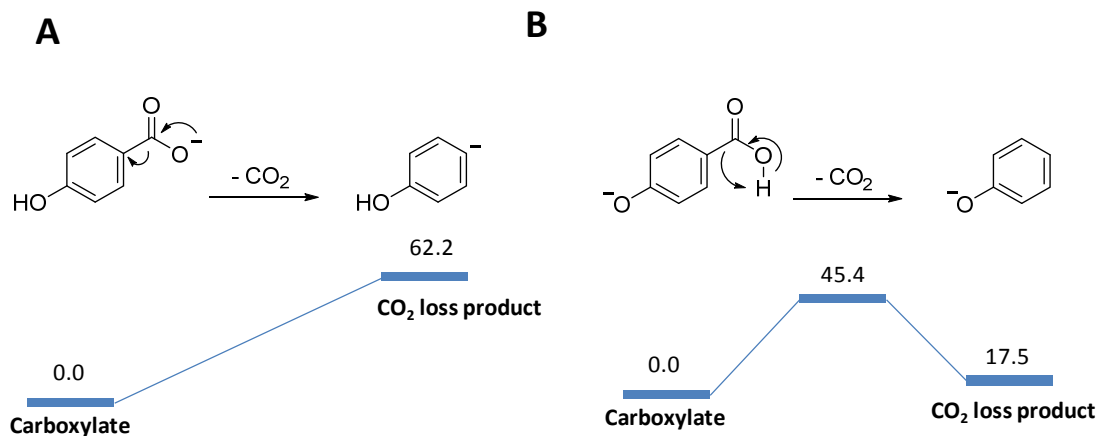


Figure 3.4 Calculated potential energy surface for the loss of CO₂ upon CAD of deprotonated 4-hydroxybenzoic acid carboxylate form (A) and phenoxide form (B) (M06-2X/6-31+G(d,p) level of theory).

Afterwards, the abundances of 4-hydroxybenzoic acid deprotonated using acetonitrile and water with 0.1% NaOH and its DEMB adduct-CH₃OH product were measured as a function of reaction time. Ion-molecule reactions studied under the conditions utilized here follow pseudo-first order kinetics. Hence, a plot of the logarithm of the reactant ion's relative abundance versus reaction time is a straight line with a negative slope equal to the rate constant multiplied by DEMB concentration. With the concentration of DEMB staying constant under the conditions employed here (the concentration of reactant ions is substantially smaller than the concentration of the reagent molecules), the rate constant is proportional to the value of the negative slope, which is larger (0.007 vs 0.005) when the reactant ions were generated using acetonitrile (Figure 3.5A). As discussed above, deprotonated 4-hydroxybenzoic acid generated with acetonitrile contains a larger percentage of the phenoxide tautomer, therefore, it is

reasonable to conclude that the formation of DEMB adduct-MeOH involves the phenoxide form of deprotonated 4-hydroxybenzoic acid.

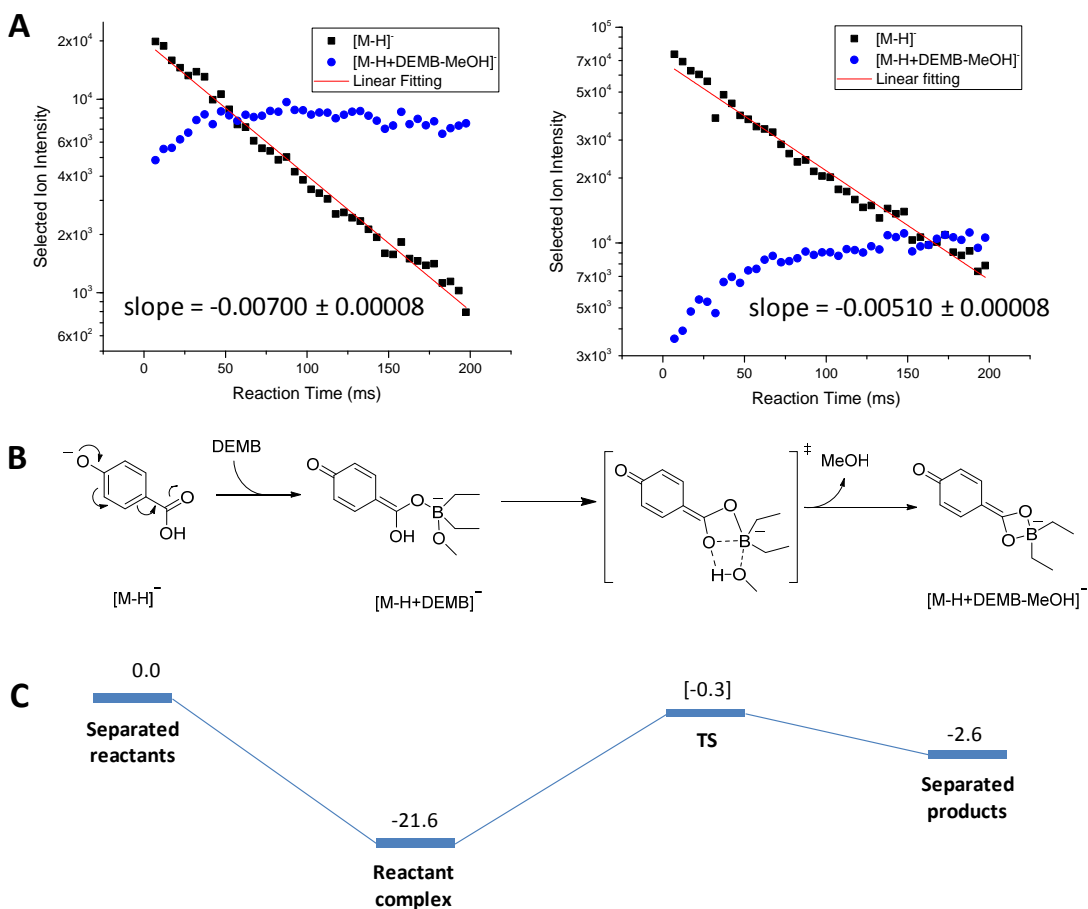


Figure 3.5 (A) Logarithm of the abundances of deprotonated 4-hydroxybenzoic acid (black symbols) and DEMB adduct- CH_3OH product ion (blue symbols) plotted as a function of reaction time for the reaction between DEMB and deprotonated 4-hydroxybenzoic acid generated using NaOH doped water solution (left) and acetonitrile solution (right). (B) Mechanism proposed for the formation of DEMB adduct that has lost methanol. (C) Calculated potential energy surface (enthalpies in kcal/mol) for the formation of DEMB adduct- CH_3OH (M06-2X/6-31+G(d,p) level of theory).

Based on above findings, a new mechanism is proposed for the formation of DEMB adduct- CH_3OH (Figure 3.5B) for deprotonated 4-hydroxybenzoic acid. The charge on the deprotonated phenol moiety can resonate onto the carboxylic acid oxygen,

which enables nucleophilic attack by the carboxylic acid moiety at the boron atom in DEMB. After addition, the carboxylic acid moiety can donate a proton to a methoxy group to eliminate methanol. Potential energy surface calculated for the proposed mechanism shows a low barrier of -0.3 kcal/mol for DEMB adduct-CH₃OH formation for the reaction between deprotonated 4-hydroxybenzoic acid and DEMB (Figure 3.5C).

The third exception was phenols with an electron-withdrawing functional group (aldehyde, nitro, and carboxylic acid ester) in the *ortho*- or *para*-position (Table 3.3). Deprotonated phenols with an electron-withdrawing substituent at the *ortho*- or *para*-position were found to exhibit no reactivity towards DEMB while the *meta*-substituted isomers formed the DEMB adduct ion. An explanation for this behavior was sought by quantum chemical calculations.

Table 3.3 Ionic products formed upon reactions of deprotonated phenol and its derivatives containing electron-withdrawing substituents with DEMB for 200 ms, calculated NBO charges of the deprotonated phenols, and calculated energy differences between the reactants and their products

Analyte ion (m/z of [M-H] ⁻)	Ion structure	Products formed upon reactions with DEMB ^a (m/z)	Calculated NBO charge ^b	Energy difference (kcal/mol) ^d
phenol (91)		91+DEMB (191)	-0.808 ^c	-34.2
vanillin (151)		No products observed	-0.721 ^c	-25.1
3-nitrophenol (138)		138+DEMB (238)	-0.782 ^c	-28.8
4-nitrophenol (138)		No products observed	-0.726 ^c	-23.4
2-hydroxybenzaldehyde (121)		121+DEMB (221) minor	-0.766 ^c	-27.3
3-hydroxybenzaldehyde (121)		121+DEMB (221)	-0.793 ^c	-31.0
4-hydroxybenzaldehyde (121)		No products observed	-0.743 ^c	-26.4
methyl 2-hydroxybenzoate (151)		151+DEMB (251) minor	-0.724 ^c	-27.6
methyl 3-hydroxybenzoate (151)		151+DEMB (251)	-0.798 ^c	-31.9
methyl 4-hydroxybenzoate (151)		151+DEMB (251) minor	-0.752 ^c	-27.2

^aProducts with 5% or greater relative abundance colored in red. Products with relative abundance between 0.1% and 5% considered as minor.

^bNBO = natural bond orbital. Calculated at M06-2X/6-311G++(2d,p)

^cCharge on the phenoxide oxygen atom

^dRelative energy difference in enthalpy between product ion and separated reactants. Calculated at M06-2X/6-311G++(2d,p) level of theory

Calculations based on density functional theory showed that the electron density on the phenoxide oxygen atom in deprotonated phenols is reduced in the presence of an *ortho*- or *para*-positioned electron-withdrawing substituent when compared to *meta*-substituted phenols (Table 3.3). The reduced electron density makes them weaker nucleophiles that are less likely to attack the electron-deficient boron atom in DEMB. At the same time, DEMB adduct formation is also less exothermic for phenols an *ortho*- or *para*-positioned electron-withdrawing substituent, producing adduct with higher energies. In the gas phase, adducts are generally not stable unless stabilized by emission of IR light or by collisions with the helium buffer gas. The lower the energy of the adduct, the longer its lifetime, and the more likely it is that it gets stabilized via one of these processes. The above two reasons likely explains the selectivity for stable DEMB adduct formation for different deprotonated phenols.

3.3.2.2 Reactions Between Carboxylate, Sulfonate or Phosphate Containing Ions and DEMB

The reactions between phosphate, carboxylate, or sulfonate containing analyte ions and DEMB were also studied (Table 3.4). Most phosphate containing analyte ions formed DEMB adduct-CH₃OH product ions upon reaction with DEMB, which is consistent with past literature findings.¹⁷ Most carboxylate and sulfonate containing analyte ions were unreactive towards DEMB. The only exceptions were glucuronides which formed DEMB adduct-CH₃OH. Given the fact that there are multiple hydroxyl groups close to the charge site in glucuronides, a mechanism similar to the one in Figure 3.2 was proposed (Figure 3.6).

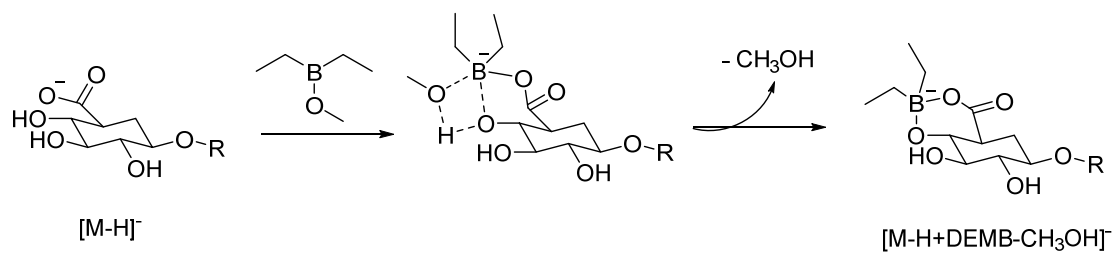


Figure 3.6 Proposed mechanism for the formation of DEMB adduct- CH_3OH product ion upon reactions between deprotonated glucuronides and DEMB

Table 3.4 Ionic products formed upon reactions of deprotonated model compounds with diethylmethoxyborane (DEMB) for 200 ms.

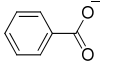
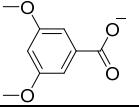
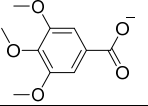
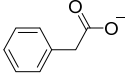
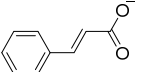
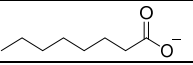
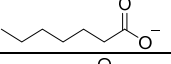
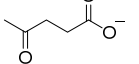
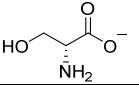
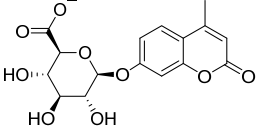
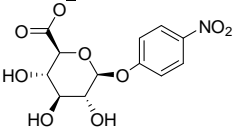
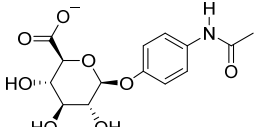
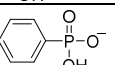
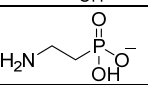
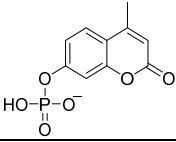
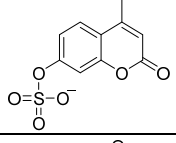
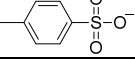
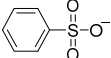
Analyte ion (m/z of [M-H] ⁻)	Ion structure	Products formed upon reactions with DEMB (m/z)
benzoic acid (121)		none
3,5-dimethoxybenzoic acid (181)		none
3,4,5-trimethoxybenzoic acid (211)		none
phenylacetic acid (135)		none
cinnamic acid (147)		none
octanoic acid (143)		none
heptanoic acid (129)		none
levulinic acid (115)		none
D-serine (104)		none
4-methylumbelliferyl β-D-glucuronide (351)		351+DEMB-CH ₃ OH (419)
4-nitrophenyl β-D-glucuronide (314)		314+DEMB-CH ₃ OH (382)
<i>p</i> -acetamidophenyl β-D-glucuronide (326)		326+DEMB-CH ₃ OH (392)
phenylphosphonic acid (157)		157+DEMB-CH ₃ OH (225)
2-aminoethylphosphonic acid (124)		124+DEMB-CH ₃ OH (192)

Table 3.4, continued

Analyte ion (m/z of [M-H] ⁻)	Ion structure	Products formed upon reactions with DEMB (m/z)
4-methylumbelliferyl phosphate (255)		255+DEMB-CH ₃ OH (323)
4-methylumbelliferyl sulfate (255)		none
p-toluenesulfonic acid (171)		none
benzenesulfonic acid (157)		none

3.3.2.3 DEMB Ion-molecule Reactions Coupled with HPLC

From the above two sections, it can be concluded that DEMB adduct formation is characteristic for most phenols. Therefore, this method can be used to identify phenol containing compounds in complex mixtures. Here, DEMB ion molecule reaction was coupled to HPLC for the rapid identification of phenolic compounds in a product mixture obtained by catalytic conversion of *miscanthus* biomass (Figure 3.7). The mixture was separated via a water/acetonitrile gradient. HPLC elutes were ionized by negative ion mode ESI and the most abundant ion formed for each elute was isolated and allowed to react with DEMB for 200 ms. Although the total ion current is highly complex, by monitoring ions that produce an ion with 100 units greater m/z value, an extracted ion chromatogram can be obtained that represents compounds with the phenol functionality (Figure 3.7A). For the product mixture studied, four major phenols were identified. Their

structures were elucidated via CAD of their deprotonated forms and comparison to CAD of model compounds (Figure 3.8B).²²

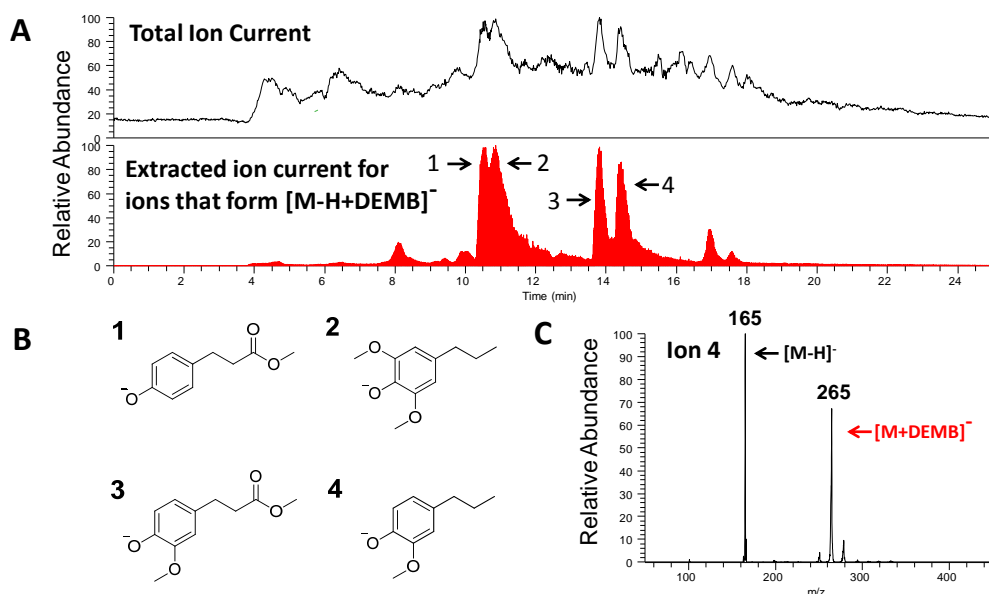


Figure 3.7 (A) (top) Total ion current HPLC chromatogram for a mixture obtained via catalytic conversion of *miscanthus* biomass. (bottom) Selected ion HPLC chromatogram for all ions that form a DEMB adduct. (B) Structures of the four major phenols that were identified in the mixture. (C) MS^2 spectrum measured after isolation of ion 4 (m/z 165) and reaction with DEMB for 200 ms.

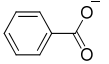
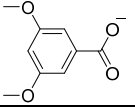
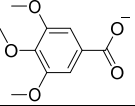
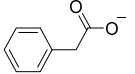
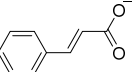
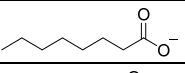
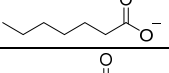
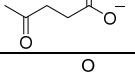
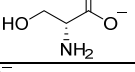
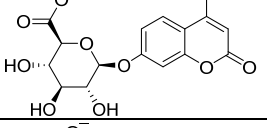
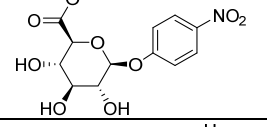
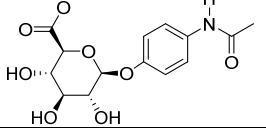
3.3.3 Reactions Between Deprotonated Analytes and DEHB/H₂O

Although DEMB proved to be a useful reagent in the identification of phenol functional group, it does not provide adequate information to differentiate carboxylates and sulfonates, which all remained unreactive towards DEMB. In the work presented discussed in this section, the DEHB/H₂O ion-molecule reaction system was explored in attempt to obtain additional information for the functional group identification in deprotonated analytes.

3.3.3.1 Reactions Between Carboxylate Containing Analyte Ions and DEHB/H₂O

Upon reaction with DEHB/H₂O, most analyte ions containing the carboxylate functionality formed a DEHB adduct followed by the addition of a water molecule and the elimination of an ethane molecule ($[M-H+DEHB+H_2O-CH_3CH_3]^-$) as the major product. The product ion has 74 units greater m/z -value than the analyte ion. The formation of the product ion was observed for both aromatic and aliphatic carboxylates, as well as more complex compounds such as deprotonated amino acids and glucuronides (Table 3.5). A minor DEHB adduct product ($[M-H+DEHB]^-$) was observed as well.

Table 3.5. Product ions observed upon reactions between diethylhydroxylborane (DEHB) and water (H₂O) with analyte ions containing carboxylate functionality for 200 ms.

Analyte ion (m/z of [M-H] ⁻)	Ion structure	Products formed upon reactions with DEHB/H ₂ O ^a (m/z)
benzoic acid (121)		121+DEHB (207) 121+DEHB+H ₂ O-CH ₃ CH ₃ (195)
3,5-dimethoxybenzoic acid (181)		181+DEHB (267) 181+DEHB+H ₂ O-CH ₃ CH ₃ (255)
3,4,5-trimethoxybenzoic acid (211)		211+DEHB (297) 211+DEHB+H ₂ O-CH ₃ CH ₃ (285)
phenylacetic acid (135)		135+DEHB (221) 135+DEHB+H ₂ O-CH ₃ CH ₃ (209)
cinnamic acid (147)		147+DEHB (233) 147+DEHB+H ₂ O-CH ₃ CH ₃ (221)
octanoic acid (143)		143+DEHB (229) 143+DEHB+H ₂ O-CH ₃ CH ₃ (217)
heptanoic acid (129)		129+DEHB (215) 129+DEHB+H ₂ O-CH ₃ CH ₃ (203)
levulinic acid (115)		115+DEHB (201) 115+DEHB+H ₂ O-CH ₃ CH ₃ (189)
D-serine (104)		104+DEHB (190) 104+DEHB+H ₂ O-CH ₃ CH ₃ (178)
4-methylumbelliferyl β-D-glucuronide (351)		351+DEHB (437) 351+DEHB+H ₂ O-CH ₃ CH ₃ (425)
4-nitrophenyl β-D-glucuronide (314)		314+DEHB (400) 314+DEHB+H ₂ O-CH ₃ CH ₃ (388)
<i>p</i> -acetamidophenyl β-D-glucuronide (326)		326+DEHB (412) 326+DEHB+H ₂ O-CH ₃ CH ₃ (400)

^a Major products colored in red

In order to elucidate the structures of the product ions and gain a better understanding on their formation mechanisms, deprotonated benzoic acid (m/z 121) was allowed to react with DEHB/ H_2O , DEHB/ D_2O , and DEHB/ $H_2^{18}O$ (Figure 3.8a). For unlabeled H_2O , product ions of m/z 195 and 207 (with a mass difference of 10 units) were observed, while product ions of m/z 197 and 208 (with a mass difference of 11 units) were observed for D_2O , and ions of m/z 199 and 209 (with a mass difference of 10 units) were observed for $H_2^{18}O$. These results suggest that the larger product ions (m/z 207, 208 and 209) contain one hydrogen atom and an oxygen atom that originate from water and hence that one hydrogen atom that originates from water has been eliminated. These findings are in agreement with reaction of DEMB with water to form diethylhydroxyborane (DEHB) via elimination of CH_3OH (containing one H atom originating from water) that then forms a stable adduct with the benzoate ion analyte, or reaction of the benzoate ion with DEMB to form a stable adduct that then reacts with water to eliminate a methanol molecule (containing one hydrogen atom originating from water). As benzoic acid is unreactive toward DEMB, the former possibility appears more likely.

In light of above findings, a pathway involving two water molecules is proposed to explain the formation of the two product ions for carboxylates (Figure 3.8b). Based on this pathway, the reaction is initiated by the hydrolysis of DEMB into DEHB. This is followed by addition of DEHB to the analyte ion to generate a DEHB adduct ion (a stable adduct was observed for all carboxylates; Table 3.5), the larger of the two observed product ions. Reaction of this adduct ion ($[M - H + DEHB]^-$) with H_2O leads to the elimination of an ethane molecule, yielding the smaller product ion, DEHB adduct + H_2O

– CH_3CH_3 . DFT calculations were carried out to evaluate the proposed mechanism (Figure 3.8c). The highest barrier found for the formation of DEHB adduct + H_2O – CH_3CH_3 for benzoate ion was – 0.3 kcal/mol, suggesting that the above mechanism is energetically feasible.

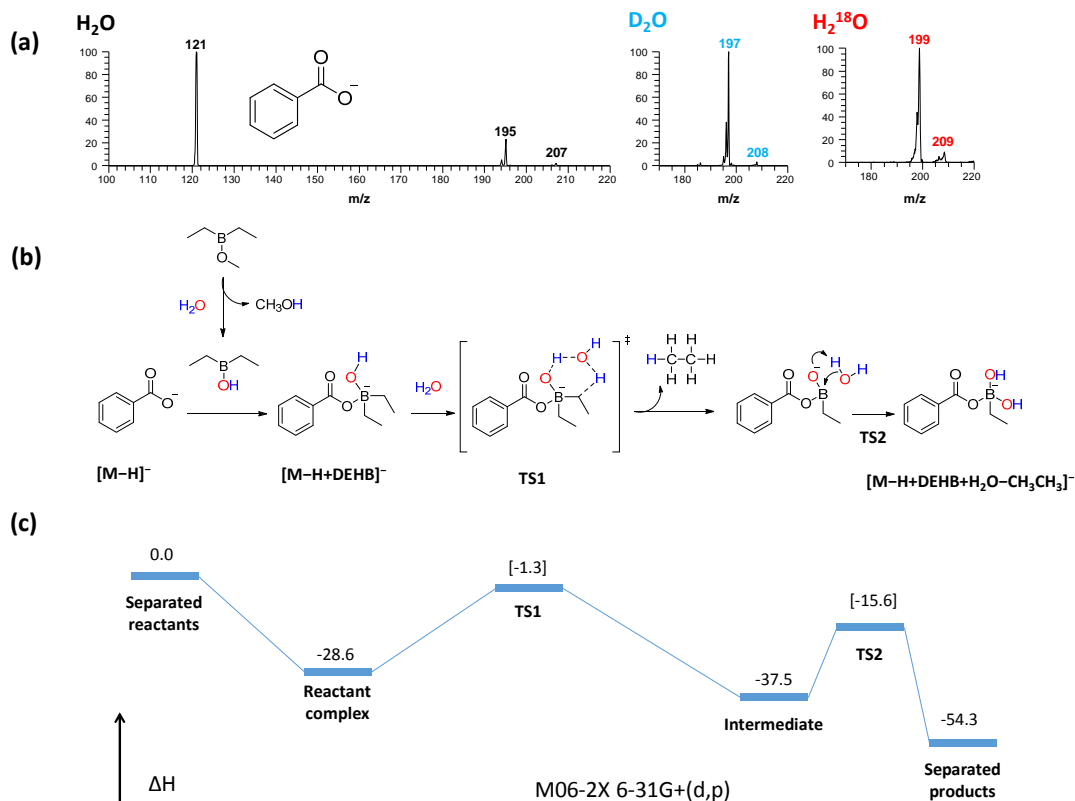


Figure 3.8 (a) Mass spectrum measured after 200 ms reaction of deprotonated benzoic acid (m/z 121) with (left) $\text{H}_2\text{O}/\text{DEHB}$, (middle) $\text{D}_2\text{O}/\text{DEHB}$, and (right) $\text{H}_2^{18}\text{O}/\text{DEHB}$. (b) Proposed mechanism for the formation of DEHB adduct + H_2O – CH_3CH_3 product ion (m/z 195) upon reaction of deprotonated benzoic acid with DEHB/ H_2O . Hydrogen and oxygen atoms that originate from the H_2O reagent are colored in blue and red, respectively. (c) Calculated potential energy surface (enthalpy in kcal/mol) for the mechanism shown in (b) (M06-2X/6-31G+(d,p) level of theory).

3.3.3.2 Reactions Between Phenoxide Containing Analyte Ions and DEHB/H₂O

Most analyte ions containing the phenoxide functionality also formed a stable DEHB adduct and a DEHB adduct + H₂O – CH₃CH₃ product ion upon reaction with DEHB/H₂O (Table 3.6). The results obtained using isotopically labeled water (D₂O and H₂¹⁸O) were analogous to those reported above for carboxylates (Figure 3.9). Therefore, phenoxides and carboxylates are assumed to form the DEHB adduct and DEHB adduct + H₂O – CH₃CH₃ product ions via a similar mechanism (Figure 3.9). It is worth mentioning that the DEHB/H₂O reagent system can still be used to differentiate phenoxides and carboxylates as only phenoxides form the characteristic DEMB adduct prior to H₂O introduction as the result of reaction with DEMB

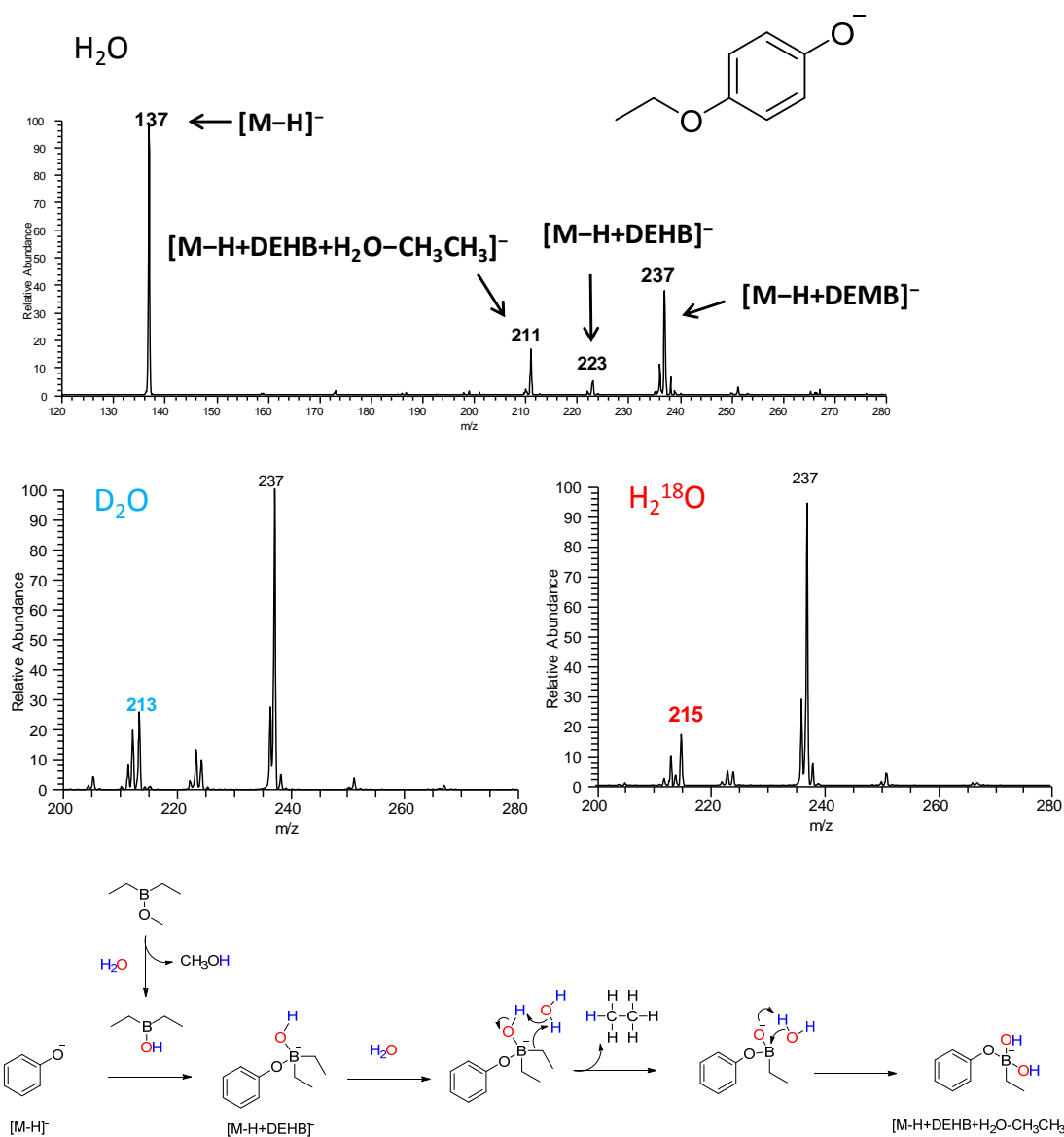


Figure 3.9 (Top) Mass spectrum measured after the reaction between deprotonated 4-ethoxyphenol (m/z 137) with $\text{H}_2\text{O}/\text{DEHB}$, $\text{D}_2\text{O}/\text{DEHB}$, and $\text{H}_2^{18}\text{O}/\text{DEHB}$ for 200 ms. (bottom) Proposed mechanism for the formation of $\text{DEHB}+\text{H}_2\text{O}-\text{CH}_3\text{CH}_3$ product ion upon reaction between deprotonated phenol and $\text{DEHB}/\text{H}_2\text{O}$.

Table 3.6 Product ions observed after 200 ms reactions of analyte ions containing a phenoxide, phosphate, or sulfate functionality with diethylhydroxyborane (DEHB) and water.

Analyte ion (m/z of [M-H] ⁻)	Ion structure	Products formed upon reactions with DEHB/H ₂ O ^a (m/z)
phenol (91)		91+DEHB (177) 91+DEHB+H ₂ O-CH ₃ CH ₃ (165)
4-ethoxyphenol (137)		137+DEHB (223) 137+DEHB+H ₂ O-CH ₃ CH ₃ (211)
catechol (109)		109+DEHB-CH ₃ CH ₃ (165)
resorcinol (109)		109+DEHB (195) 109+DEHB+H ₂ O-CH ₃ CH ₃ (183)
hydroquinone (109)		109+DEHB (195) 109+DEHB+H ₂ O-CH ₃ CH ₃ (183)
2-hydroxybenzyl alcohol (123)		123+DEHB-CH ₃ CH ₃ (179)
3-hydroxybenzyl alcohol (123)		123+DEHB (209) 123+DEHB+H ₂ O-CH ₃ CH ₃ (197)
phenylphosphonic acid (157)		157+DEHB-CH ₃ CH ₃ (213)
2-aminoethylphosphonic acid (124)		124+DEHB-CH ₃ CH ₃ (180)
4-methylumbelliferyl phosphate (255)		255+DEHB-CH ₃ CH ₃ (311)
4-methylumbelliferyl sulfate (255)		none
p-toluenesulfonic acid (171)		none
benzenesulfonic acid (157)		none

However, a new product ion, DEHB adduct-CH₃CH₃, was observed for deprotonated catechol and deprotonated 2-hydroxybenzylalcohol upon their reaction with DEHB/H₂O (Table 3.6). This product was not observed for resorcinol,

hydroquinone, and 3-hydroxybenzylalcohol, which all have its hydroxyl group further away from the deprotonation site. Therefore, it was proposed that a hydroxyl group adjacent to the deprotonation site participated in the formation of this new product ion.

Labeling experiments with D_2O and $H_2^{18}O$ revealed that the DEHB adduct- CH_3CH_3 product ion contains one hydrogen atom and one oxygen atom from the H_2O reactant (Figure 3.11). In addition, the product ion dissociates back to the analyte ion upon CAD (likely via loss of $O=B-CH_2CH_3$), suggesting that the linkage formed between the neutral reagent and the analyte ion is relatively weak (Figure 3.10). A mechanism consistent with the above observations was proposed and evaluated via DFT calculation (Figure 3.11).

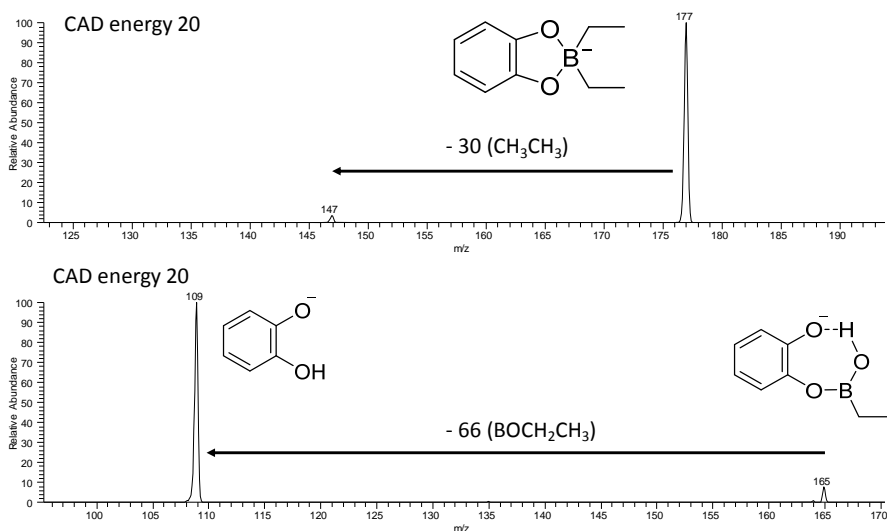


Figure 3.10 CAD mass spectrum obtained at 20 (arbitrary units) collision energy for product ion of (top) reaction between deprotonated catechol with DEMB and (bottom) reaction between deprotonated catechol with DEHB/ H_2O

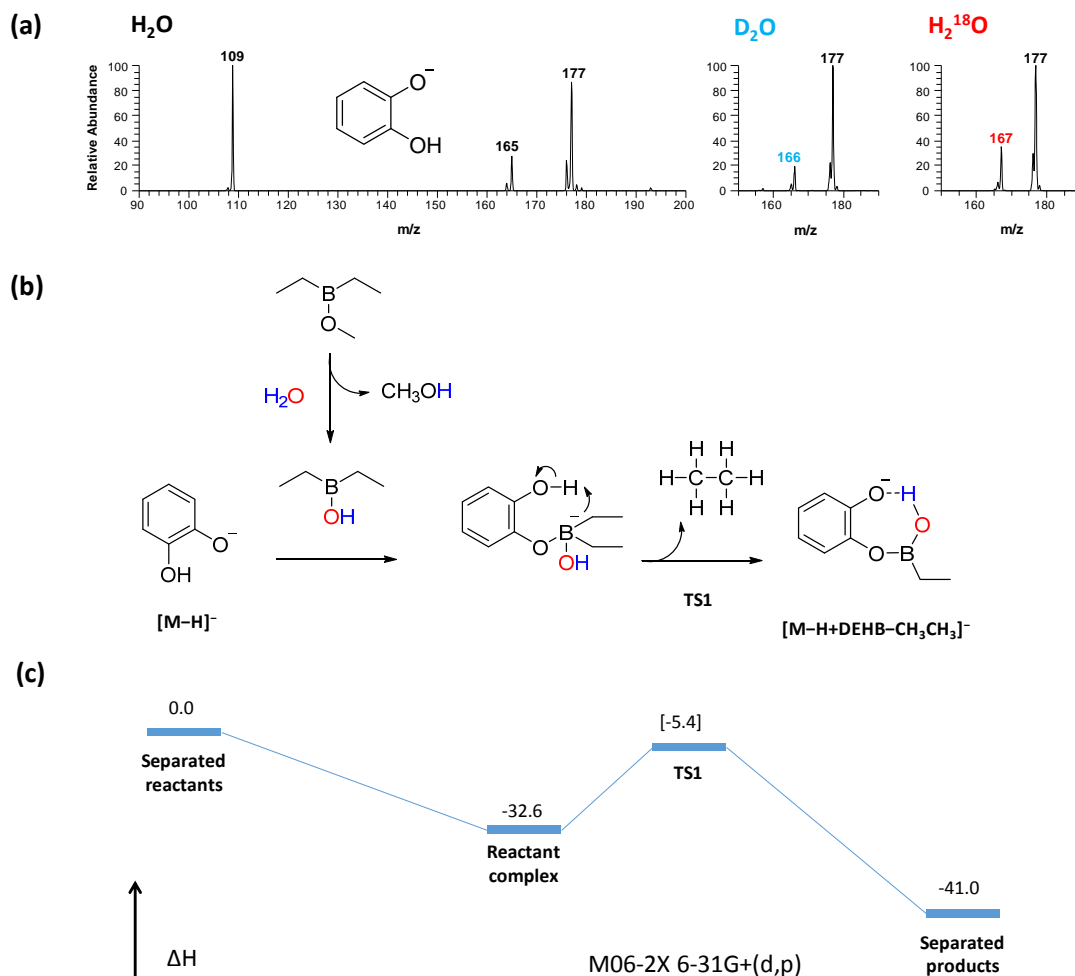


Figure 3.11 (a) Mass spectrum measured after 200 ms reactions of deprotonated catechol (m/z 109) with (left) $\text{H}_2\text{O}/\text{DEHB}$, (middle) $\text{D}_2\text{O}/\text{DEHB}$, and (right) $\text{H}_2^{18}\text{O}/\text{DEHB}$. (b) Proposed mechanism for the formation of DEHB adduct- CH_3CH_3 product ion upon reactions between deprotonated catechol and DEHB/ H_2O . Hydrogen and oxygen atoms that originate from the H_2O reactant are colored in blue and red, respectively. (c) Calculated potential energy surface (enthalpy in kcal/mol) for the mechanism shown in (b) (M06-2X/6-31G+(d,p) level of theory).

3.3.3.3 Reactions Between Phosphate Containing Analyte Ions and DEHB/H₂O

Phosphates containing analyte ions also have a hydroxyl groups close to the deprotonation site, similar to catechol. Therefore, it was not surprising that they also formed DEHB adduct-CH₃CH₃ upon reactions with DEHB/H₂O (Table 3.6). Reaction mechanism was proposed based on isotope labeling experiments that confirmed that the DEHB adduct-CH₃CH₃ product observed for deprotonated phenylphosphonic acid also contains one hydrogen atom and oxygen atom from the H₂O reactant (Figure 3.12).

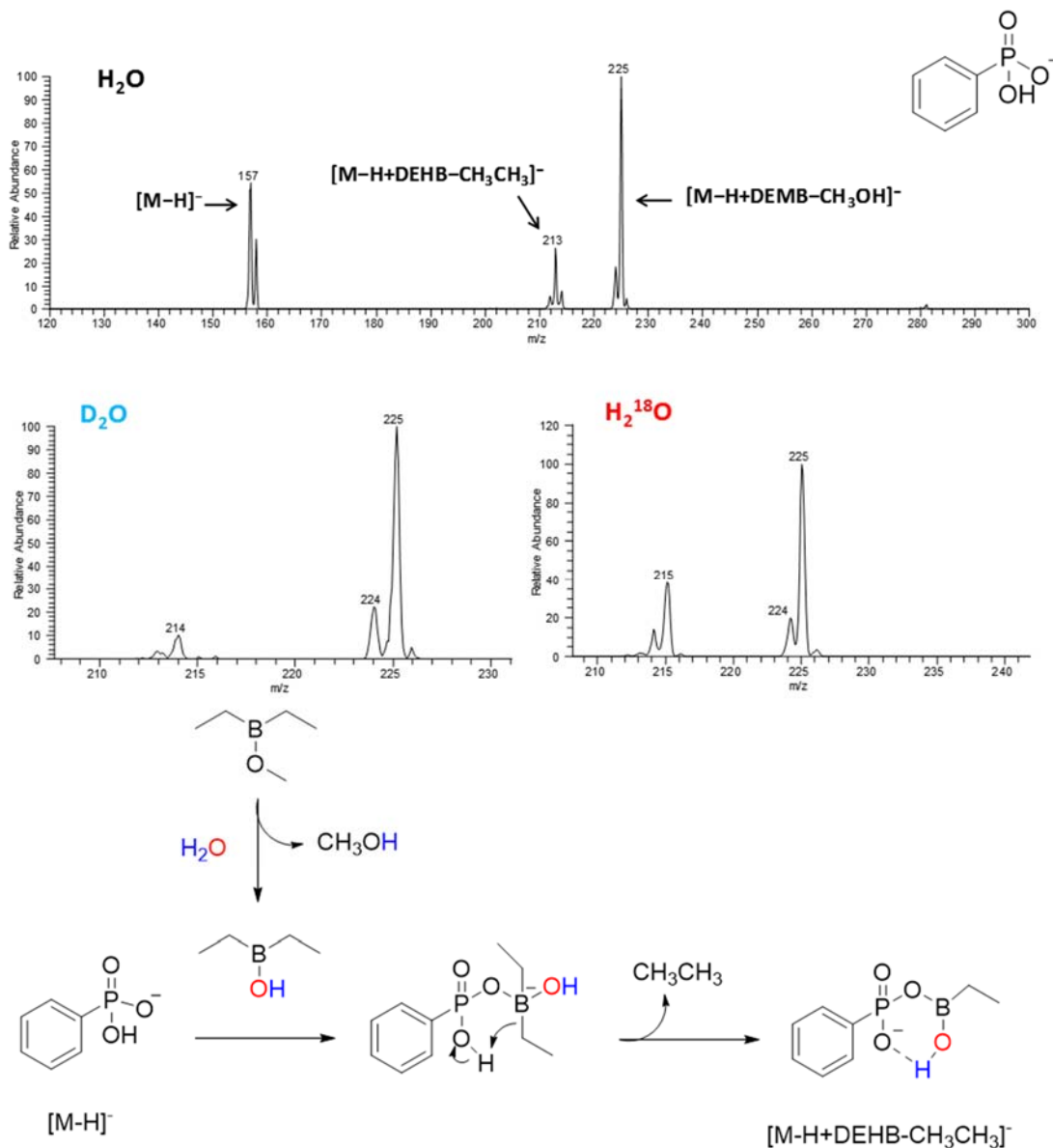


Figure 3.12 (top) Mass spectra measured after 200 ms reactions of deprotonated phenylphosphonic acid (m/z 157) with H₂O/DEHB, D₂O/DEHB, and H₂¹⁸O/DEHB. (Bottom) Proposed mechanism for the formation of DEHB-CH₃CH₃ product ion upon reaction between deprotonated phenylphosphonic acid and DEHB/H₂O.

3.3.3.4 DEHB/H₂O Ion-molecule Reactions Coupled with HPLC

HPLC separation prior to MS experiments is necessary for the analysis of mixture containing isobaric or isomeric analytes. The feasibility of coupling ion-molecule reaction experiments with DEHB/H₂O to HPLC was tested using an artificial mixture containing Hymecromone (4-methylumbelliferone), a choleric and antispasmodic drug, and its three metabolites: 4-methylumbelliferyl phosphate, 4-methylumbelliferyl sulfate, and 4-methylumbelliferyl- β -D-glucuronide (Figure 3.13). The mixture was separated via reverse phase HPLC, ionized under ESI negative ion mode, and subjected to ion-molecule reaction with DEHB/H₂O for 200 ms. Upon elution of the analyte, H₂O was pulsed into the ion trap every 6 seconds for the duration of the HPLC peak. A typical HPLC peak 15-30 seconds wide could allow for 2-5 H₂O pulses with 5-10 individual ion-molecule reaction experiments performed within each pulse. Deprotonated 4-methylumbelliferyl phosphate formed the characteristic DEHB adduct-CH₃CH product ion while its isobar, 4-methylumbelliferyl sulfate, showed no reactivity (Figure 3.13). Both deprotonated 4-methylumbelliferone (contains phenoxide functionality) and 4-methylumbelliferyl- β -D-glucuronide (contains carboxylate functionality) formed DEMB adduct+H₂O-CH₃CH product ion. However, they are still differentiated as the phenoxide containing deprotonated 4-methylumbelliferone formed the characteristic DEMB adduct upon reaction with DEMB (Figure 3.13).

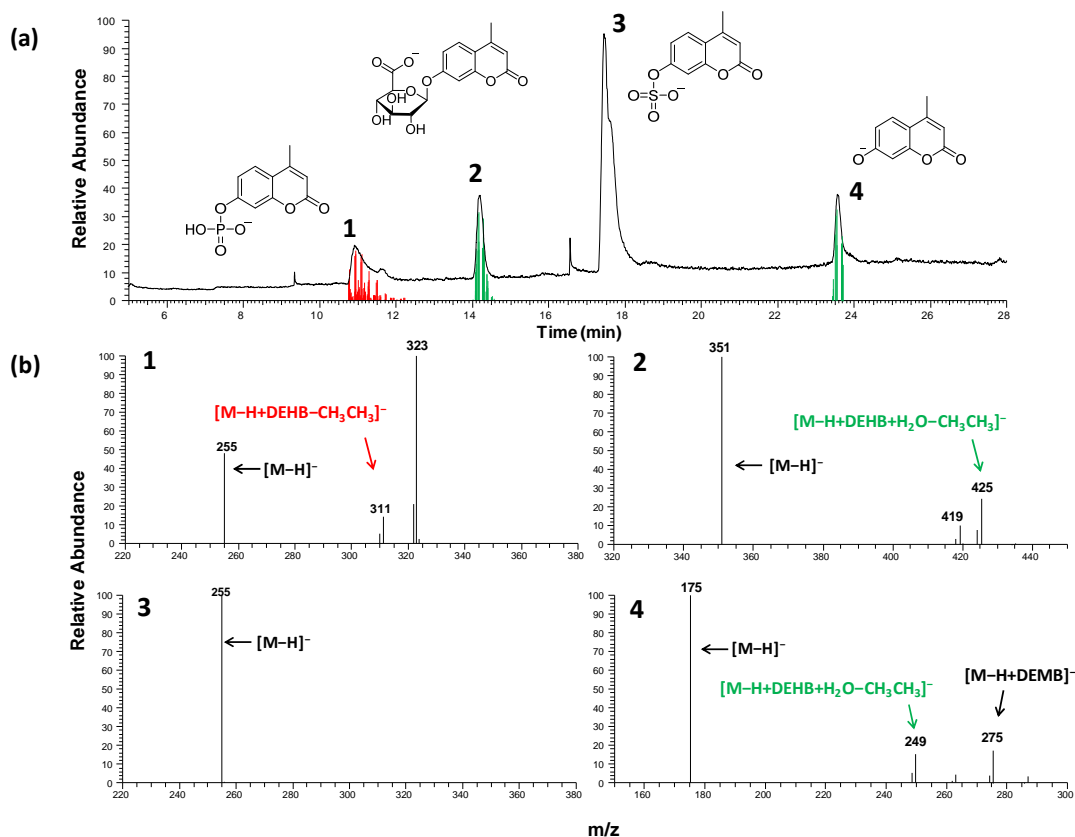


Figure 3.13 (a) HPLC chromatogram measured for an artificial mixture of 4-methylumbelliferyl phosphate (1), 4-methylumbelliferyl β-D-glucuronide (2), 4-methylumbelliferyl sulfate (3), and 4-methylumbelliferone (4). The total ion current is plotted in black. Selected ion current for ion-molecule reaction product ions with DEHB/H₂O are plotted in red (DEHB adduct-CH₃CH₃) and green (DEHB adduct+H₂O-CH₃CH₃). (b) Mass spectra measured after reactions between the deprotonated HPLC eluents (4-methylumbelliferyl phosphate (1), 4-methylumbelliferyl β-D-glucuronide (2), 4-methylumbelliferyl sulfate (3), and 4-methylumbelliferone) with DEHB/H₂O for 200ms

3.4 Conclusions

Two ion-molecule reaction systems were explored for the functional group identification in deprotonated analytes. The first ion-molecule reaction system used DEMB as the neutral reagent. Aside from three types of exceptions, most phenoxide containing deprotonated analytes formed exclusively DEMB adducts upon reactions with DEMB. Deprotonated phenols with an adjacent hydroxyl group or a conjugated carboxylic acid functional group formed DEMB adduct-CH₃CH₃ product ions instead. Deprotonated phenols with an electron-withdrawing substituent in the *ortho*- or *para*-position were unreactive toward DEMB. By coupling above technique with HPLC, a catalytically converted *miscanthus* biomass sample was analyzed, demonstrating the potential of tandem mass spectrometry based on ion-molecule reactions as a high-throughput screening tool.

The second reaction system introduced both DEMB and H₂O to generated a new reagent, DEHB, inside the ion trap. Deprotonated analytes containing the carboxylate functionality or the phenoxide functionality reacted with DEHB/H₂O via the formation of DEHB adduct+H₂O-CH₃CH₃ product ions. Phosphates and phenoxides with an adjacent hydroxyls formed DEHB adduct-CH₃CH₃. Sulfates were still unreactive in this reaction system. Coupling the above technique with HPLC allowed the identification of the functional groups in multiple metabolites of a drug molecule, demonstrating the potential of tandem mass spectrometry based on ion-molecule reactions as a powerful analytical tool for drug metabolite identification in mixtures.

3.5 References

- (1) Dettmer, K.; Aronov, P. A.; Hammock, B. D. *Mass Spectrom. Rev.* **2007**, *26* (1), 51–78.
- (2) Chen, C.; Gonzalez, F. J.; Idle, J. R. *Drug Metab. Rev.* **2007**, *39* (2-3), 581–597.
- (3) McLafferty, F. W. *Int. J. Mass Spectrom.* **2001**, *212* (1–3), 81–87.
- (4) Cooks, R. G.; Jarmusch, A. K.; Wleklinski, M. *Int. J. Mass Spectrom.* **2015**, *377*, 709–718.
- (5) Hernández, F.; Sancho, J. V.; Ibáñez, M.; Abad, E.; Portolés, T.; Mattioli, L. *Anal. Bioanal. Chem.* **2012**, *403* (5), 1251–1264.
- (6) Mitchell Wells, J.; McLuckey, S. A. Enzymology, B.-M. in, Ed.; Biological Mass Spectrometry; Academic Press, 2005; Vol. 402, pp 148–185.
- (7) Cooks, R. G. *J. Mass Spectrom.* **1995**, *30* (9), 1215–1221.
- (8) Amundson, L. M.; Owen, B. C.; Gallardo, V. A.; Habicht, S. C.; Fu, M.; Shea, R. C.; Mossman, A. B.; Kenttämää, H. I. *J. Am. Soc. Mass Spectrom.* **2011**, *22* (4), 670–682.
- (9) Campbell, K. M.; Watkins, M. A.; Li, S.; Fiddler, M. N.; Winger, B.; Kenttämää, H. I. *J. Org. Chem.* **2007**, *72* (9), 3159–3165.
- (10) Eismin, R. J.; Fu, M.; Yem, S.; Widjaja, F.; Kenttämää, H. I. *J. Am. Soc. Mass Spectrom.* **2011**, *23* (1), 12–22.
- (11) Sheng, H.; Tang, W.; Yerabolu, R.; Kong, J. Y.; Williams, P. E.; Zhang, M.; Kenttämää, H. I. *Rapid Commun. Mass Spectrom.* **2015**, *29* (8), 730–734.
- (12) Sheng, H.; Tang, W.; Yerabolu, R.; Max, J.; Kotha, R. R.; Riedeman, J. S.; Nash, J. J.; Zhang, M.; Kenttämää, H. I. *J. Org. Chem.* **2016**, *81* (2), 575–586.
- (13) Sheng, H.; Williams, P. E.; Tang, W.; Zhang, M.; Kenttämää, H. I. *Analyst* **2014**, *139* (17), 4296–4302.
- (14) Zakzeski, J.; Bruijninx, P. C. A.; Jongerius, A. L.; Weckhuysen, B. M. *Chem. Rev.* **2010**, *110* (6), 3552–3599.
- (15) Hauptert, L. J.; Owen, B. C.; Marcum, C. L.; Jarrell, T. M.; Pulliam, C. J.; Amundson, L. M.; Narra, P.; Aqueel, M. S.; Parsell, T. H.; Abu-Omar, M. M.; Kenttämää, H. I. *Fuel* **2012**, *95*, 634–641.

- (16) Quéméner, B.; Vigouroux, J.; Rathahao, E.; Tabet, J. C.; Dimitrijevic, A.; Lahaye, M. *J. Mass Spectrom.* **2015**, *50* (1), 247–264.
- (17) Piatkivskiy, A.; Pyatkivskyy, Y.; Ryzhov, V. *Eur. J. Mass Spectrom. Chichester Engl.* **2014**, *20* (4), 337–344.
- (18) Gronert, S.; O’Hair, R. A. J. *J. Am. Soc. Mass Spectrom.* **2002**, *13* (9), 1088–1098.
- (19) Gao, H.; Petzold, C. J.; Leavell, M. D.; Leary, J. A. *J. Am. Soc. Mass Spectrom.* **2003**, *14* (8), 916–924.
- (20) Piatkivskiy, A.; Pyatkivskyy, Y.; Hurt, M.; Ryzhov, V. *Eur. J. Mass Spectrom.* **2014**, *20* (2), 177.
- (21) Forsythe, W. G.; Garrett, M. D.; Hardacre, C.; Nieuwenhuyzen, M.; Sheldrake, G. N. *Green Chem.* **2013**, *15* (11), 3031–3038.
- (22) Luo, H.; Klein, I. M.; Jiang, Y.; Zhu, H.; Liu, B.; Kenttämä, H. I.; Abu-Omar, M. M. *ACS Sustain. Chem. Eng.* **2016**, *4* (4), 2316–2322.
- (23) Gronert, S. *Chem. Rev.* **2001**, *101* (2), 329–360.
- (24) Jarrell, T.; Riedeman, J.; Carlsen, M.; Replogle, R.; Selby, T.; Kenttämä, H. *Anal. Chem.* **2014**, *86* (13), 6533–6539.
- (25) Schröder, D.; Buděšínský, M.; Roithová, J. *J. Am. Chem. Soc.* **2012**, *134* (38), 15897–15905.
- (26) Steill, J. D.; Oomens, J. *J. Am. Chem. Soc.* **2009**, *131* (38), 13570–13571.

CHAPTER 4. DIFFERENTIATION OF REGIOISOMERIC BENZENEDIOLS VIA ION-MOLECULE REACTIONS WITH THIONYL CHLORIDE

4.1 Introduction

Due to its high aromatic content, lignin is viewed as a promising feedstock for converting biomass into valuable aromatic chemicals.¹⁻³ Chemical characterization of the aromatic product mixtures is necessary for obtaining mass balance data that are used to evaluate the conversion processes.⁴ Mass spectrometry is a powerful analytical technique suitable for complex mixture analysis, providing valuable information such as molecular weight and elemental compositions.⁵ For isomeric and isobaric compounds, tandem mass spectrometry based on CAD can provide insight into their structure.⁶ However, the differentiation of aromatic regioisomers is still challenging and often require time-consuming derivatization processes because they often exhibit similar CAD fragmentation pattern.⁷ Therefore, additional analytical methods for analyzing mixtures with high aromatic content such as converted lignin are still desired.

Ion-molecule reactions have proven to be a powerful method for functional group identification in ionized analytes and hence isomer differentiation. Functional groups that can be identified via this method include hydroxyl,⁸ epoxide,⁹ amido,¹⁰ hydroxylamino,¹¹ N-oxide,¹² sulfoxide,¹³ and sulfone.^{14,15} The differentiation of isomeric ions that are not discernable via CAD experiments has been achieved.^{16,17} However, most of the aforementioned ion-molecule reactions require the target analyte to be protonated as the

reactions are initiated via proton transfer from the protonated analyte to the reagent.¹²

Hence, these methods are not suitable for lignin mixture analysis as lignin is shown to be better ionized under negative ion mode.¹⁸

In this chapter, thionyl chloride is explored as a neutral reagent for the differentiation of regioisomeric deprotonated lignin model compounds. The neutral reagent was introduced into the mass spectrometer via a novel pulsed valve setup. Reactions between thionyl chloride and deprotonated catechols, resorcinols, and hydroquinones, the isomeric dihydroxybenzenes, are discussed. This is the first report of using thionyl chloride as a neutral reagent for ion-molecule reactions.

4.2 Experimental

4.2.1 Chemicals

Thionyl chloride (99%), catechol (99%), resorcinol (99%), hydroquinone (99%), 2-nitroresorcinol (98%), 2-aminoresorcinol (99%), 3,4,5-trimethylhydroquinone (99%) were purchased from Sigma Aldrich (Saint Louis, MO) and used as received.

4.2.2 Mass Spectrometry

All experiments were performed on a Thermo Scientific linear quadrupole ion trap (LQIT) mass spectrometer equipped with an electrospray ionization (ESI) source operated under negative ion mode. Sample solutions were prepared at a concentration of 1 mmol in 50/50 water/methanol (v/v) solution. 10 μ L of 1mM NaOH water solution were added into 5 mL of sample solution to facilitate the formation of deprotonated

analyte molecules. The NaOH doped sample solutions were injected into the T-connector via a syringe driver at a flow rate of 10 $\mu\text{L}/\text{min}$, before being mixed with 50/50 water/methanol (v/v) at a flow rate of 100 $\mu\text{L}/\text{min}$. Typical ESI conditions used were: 3.5 kV spray voltage, 20 (arbitrary unit) sheath gas (N_2) flow, 10 (arbitrary unit) auxiliary gas (N_2) flow, and 2 (arbitrary unit) sweep gas (N_2) flow.

4.2.3 Ion-molecule Reactions

Ion-molecule reactions between deprotonated analytes and SOCl_2 were performed using a Thermo Scientific linear quadrupole ion trap (LQIT) mass spectrometer with a custom build multiported pulsed valve interface system.¹⁹ 5 μL of SOCl_2 were introduced via a syringe into a stainless steel channel through a rubber septum. The stainless steel channel was heated to 70 $^\circ\text{C}$ for efficient evaporation of the neutral reagent. The pulsed valve connected to the stainless steel channel was triggered manually via a waveform generator to open for 500 μs to allow SOCl_2 to enter the linear quadrupole ion trap region of the mass spectrometer. Analyte ions isolated inside the ion trap were allowed to react with SOCl_2 for 30 ms before all ions were ejected for detection.

4.2.4 Density Functional Theory Calculations

All Density Functional Theory (DFT) calculations were performed using the Gaussian 09 software package. Geometry optimizations were performed using hybrid functional M06-2X with 6-31+G(d,p) basis set. Vibrational frequencies were calculated for the optimized structures at the same level of theory to confirm the absence of imaginary frequency and to obtain thermal corrected enthalpy.

4.3 Results and Discussions

4.3.1 Ion-molecule reactions

Neutral introduction during ion-molecule reactions between SOCl_2 and analyte ions was achieved via a pulsed valve setup connected to the back of the ion trap. A valve that can be electronically triggered open separated SOCl_2 from the ion trap region. Upon triggering the pulsed valve, SOCl_2 entered the ion trap and reacted with the isolated analytes ions.

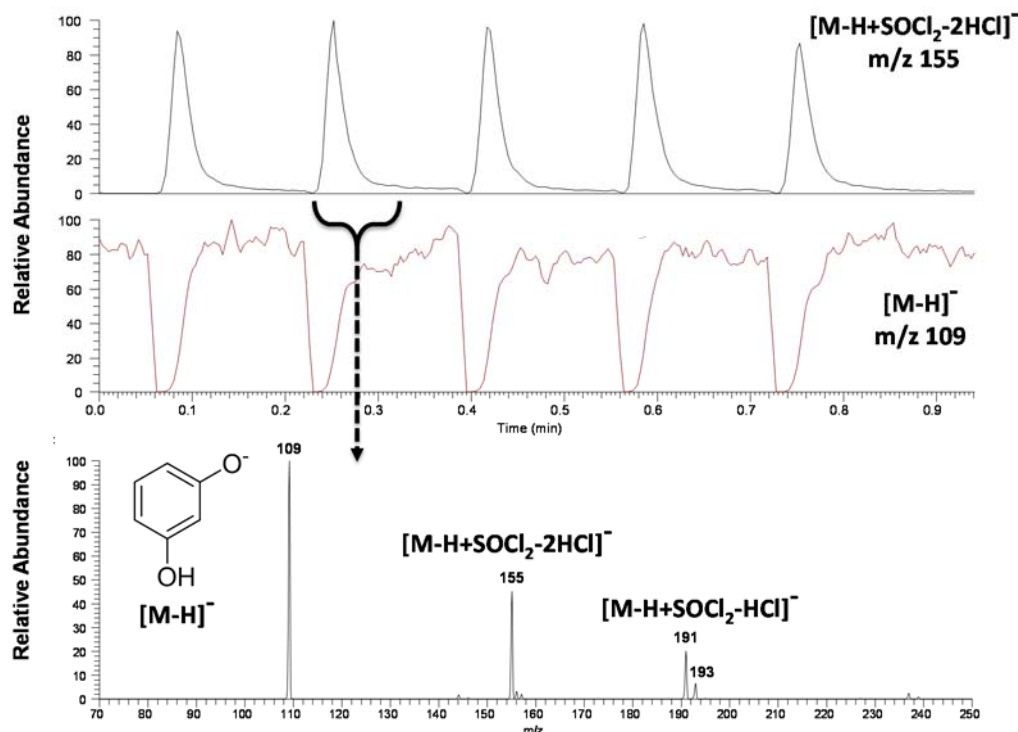


Figure 4.1 Reaction between deprotonated resorcinol (m/z 109) and SOCl_2 introduced via the pulsed valve system. (Top) Extracted ion current of the reactant ion (m/z 109) and product ion (m/z 155) over time. (Bottom) Averaged mass spectra measured during one pulsed introduction of SOCl_2 .

As shown in Figure 4.1, after triggering of the pulsed valve, the abundance of the reactant ion (m/z 109) sharply decreased followed by a corresponding increase in the abundance of the product ion (m/z 155). This observation showed that SOCl_2 reacted with the analyte ion. SOCl_2 was introduced 5 times within 1 min by repeatedly opening the pulsed valve. The residence time of SOCl_2 was estimated to be roughly 5 seconds. The MS spectra obtained were averaged spectra across one pulsed event.

Deprotonated catechol, resorcinol, and hydroquinone were subjected to reaction with SOCl_2 . Different product ions were observed for each one of the three regioisomers (Figure 4.2).

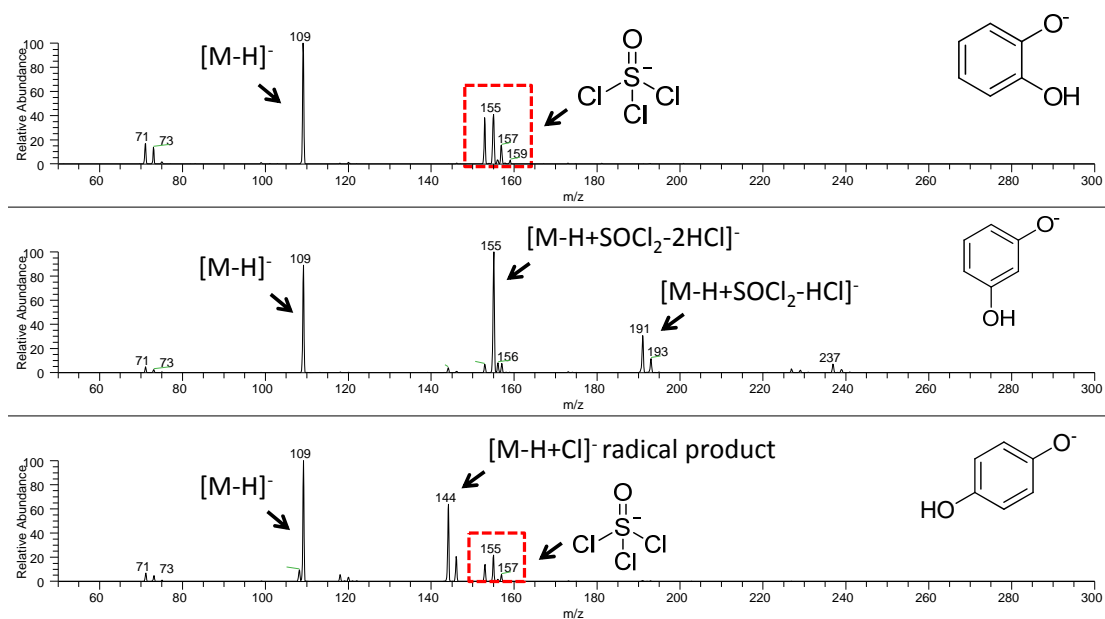


Figure 4.2 Mass spectrum measured for (top) deprotonated resorcinol, (middle) deprotonated resorcinol, and (bottom) deprotonated hydroquinone after reaction with $SOCl_2$ for 30 ms.

4.3.2 Reactions between deprotonated catechol and $SOCl_2$

The major product ion observed for reactions between deprotonated catechol and $SOCl_2$ is a series of ions (m/z 153, m/z 157, and m/z 159) which were later identified as the sulfur trichloride monoxide anion ($SOCl_3^-$). The monoisotopic mass of this product is 153. Ions of m/z 157 and m/z 159 contained one and two ^{37}Cl atoms, respectively. Minor HCl_2^- ions (m/z 71) were also observed aside from the major product ion.

As the major observed product ion ($SOCl_3^-$) does not contain any part of the reactant ion (deprotonated catechol), a negative charge must have been eliminated from the reactant complex during the reaction. Also, both product ions ($SOCl_3^-$ and HCl_2^-) can be seen as a chloride adduct ion of $SOCl_2$ or HCl . Therefore, it was likely that an adduct

was formed between deprotonated catechol and SOCl_2 followed by the elimination of a Cl^- .

A mechanism was proposed based on the above discussions (Figure 4.3). According to the proposed mechanism, adducts were formed between deprotonated catechol and SOCl_2 via the nucleophilic attack from the charge oxygen atom onto the sulfur atom in SOCl_2 . An HCl molecule and a Cl^- were then eliminated from the adduct via the assistance of the neighboring hydroxyl group. The eliminated Cl^- further reacted with another SOCl_2 molecule to form the SOCl_3^- product ion, or with another HCl molecule to form the HCl_2^- product ion.

As Cl^- elimination requires the presence of a neighboring hydroxyl group, it was only possible for a molecule that has two neighboring hydroxyl groups such as catechol. This likely explains why SOCl_3^- and HCl_2^- were not the major product ions in reactions between SOCl_2 and resorcinol or hydroquinone.

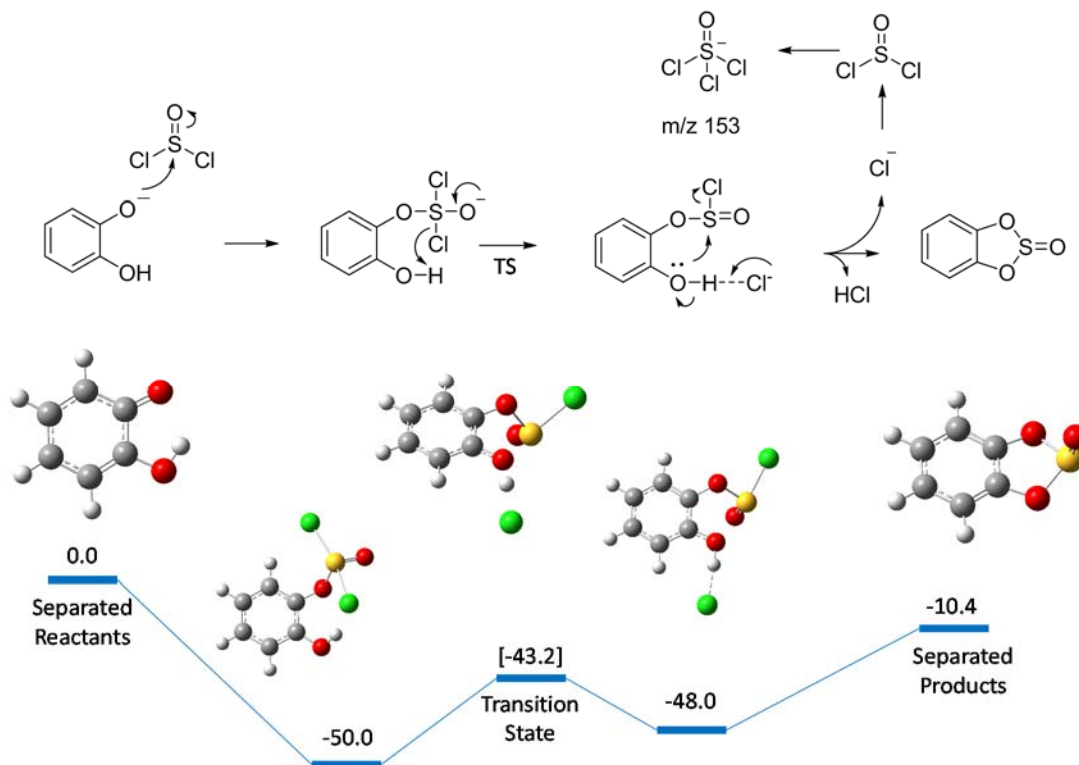


Figure 4.3 (Top) proposed mechanism and (bottom) calculated potential energy surface (enthalpy in kcal/mol) for the formation of SOCl_3^- product ion upon reaction between deprotonated catechol and SOCl_2 (M06-2X/6-31+G(d,p) level of theory).

The proposed reaction mechanism was evaluated via DFT calculations (Figure 4.3, bottom). All reaction barriers were found to lie below the entrance energy level and the overall reaction is exothermic by 10.4 kcal/mol. These results suggest that the proposed mechanism is energetically feasible.

4.3.3 Reactions between deprotonated resorcinol and SOCl_2

Deprotonated resorcinol formed two major product ions upon reaction with SOCl_2 : SOCl_2 adduct ion that had lost one HCl molecule ($[\text{M}-\text{H}+\text{SOCl}_2-\text{HCl}]^-$ of m/z 191) and SOCl_2 adduct ion that had lost two HCl molecules ($[\text{M}-\text{H}+\text{SOCl}_2-2\text{HCl}]^-$, m/z

155). These two product ions can be identified via the isotopic distribution of sulfur (4% ^{34}S to 100% ^{32}S) and chlorine (33% ^{37}Cl to 100% ^{35}Cl).

The structure of the SOCl_2 adduct-2HCl was of particular interest because upon its formation, two HCl molecules were eliminated but deprotonated resorcinol only contains one active hydrogen atom. Therefore, one aromatic hydrogen must also be involved in the reaction. Also, the aromatic hydrogen involved cannot be too far away from the hydroxyl group on carbon 3 because both hydrogens need to be close to the chloride atoms in order to form the HCl molecules. Thus, the above reaction most likely involves the aromatic hydrogen on carbon 2 or carbon 4.

In order to determine which aromatic hydrogen is involved, reaction between SOCl_2 and deprotonated 2-methylresorcinol, whose hydrogen on carbon 2 was replaced with a methyl group, was studied (Figure 4.3). Deprotonated 2-methylresorcinol also formed the SOCl_2 adduct-2HCl product ion upon reaction with SOCl_2 . The above result suggested that for resorcinol, the aromatic hydrogen on carbon 2 was not necessarily involved in the formation of SOCl_2 adduct-2HCl product ion.

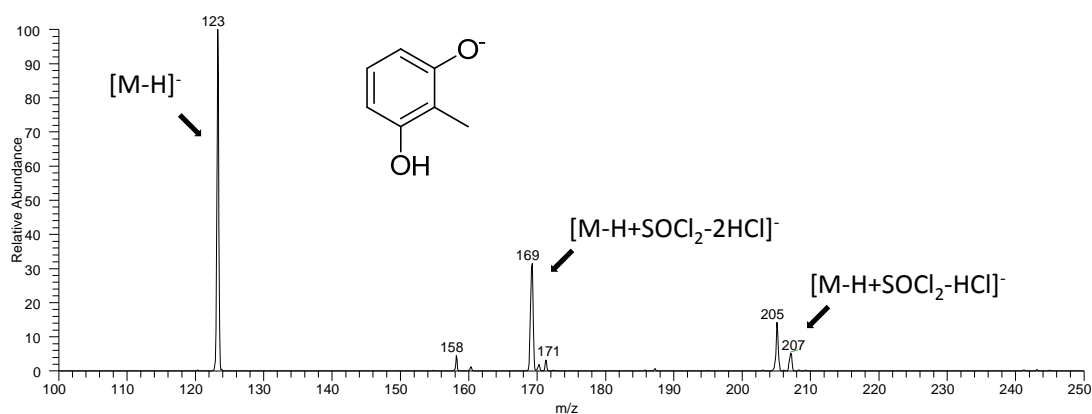


Figure 4.4 Mass spectrum measured for the reaction between deprotonated 2-methylresorcinol and SOCl₂.

In light of above results, a mechanism involving the aromatic hydrogen on carbon 4 was proposed (Figure 4.5). This mechanism is initiated by forming adduct between deprotonated resorcinol and SOCl₂ via a nucleophilic attack from carbon 4 on deprotonated resorcinol onto the sulfur atom in SOCl₂. For deprotonated resorcinol, the electron density on its 4 position carbon is increased by its 1 position phenoxide group and 3 position phenol group, which are both *ortho/para* directing groups. The increased electron density makes the nucleophilic attack more likely to occur. After adduct formation, the hydroxyl hydrogen and the aromatic hydrogen at carbon 4 were lost in the form of a HCl molecule. The barriers for the proposed mechanism were calculated via DFT. The highest barrier was only -40.9 kcal/mol and the overall reaction was exothermic by 16.2 kcal/mol (Figure 4.5).

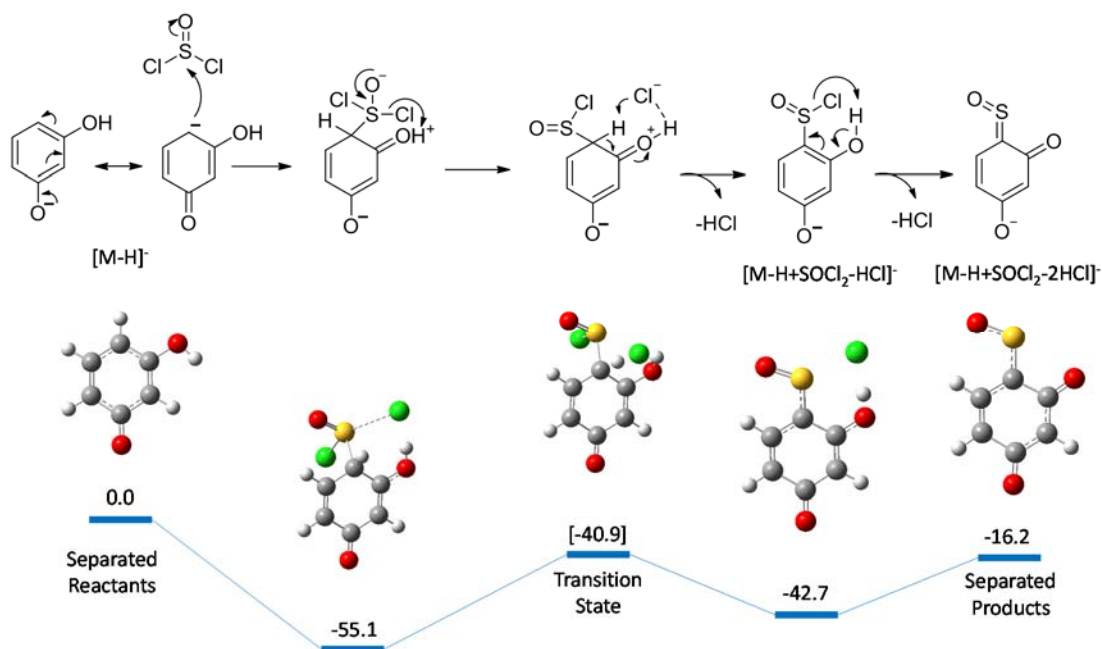


Figure 4.5 (Top) Proposed mechanism and (bottom) calculated potential energy surface (enthalpy in kcal/mol) for the formation of SOCl_2 adduct-2HCl product ion upon reaction between deprotonated resorcinol and SOCl_2 (M06-2X/6-31+G(d,p) level of theory).

4.3.4 Reactions between deprotonated hydroquinone and SOCl_2

Deprotonated hydroquinone formed a chlorine atom adduct anion ($[\text{M}-\text{H}+\text{Cl}]^-$ of m/z 144) upon reactions with SOCl_2 . The product ion was identified as a radical species because it had an even mass but contained no nitrogen atoms. The formation of this product ion was observed for a highly substituted hydroquinone as well (Figure 4.7). Upon CAD, the product ion dissociated into a *p*-benzoquinone radical anion (m/z 108) by losing a HCl molecule, suggesting that the chlorine atom was bound to the hydroxyl group.

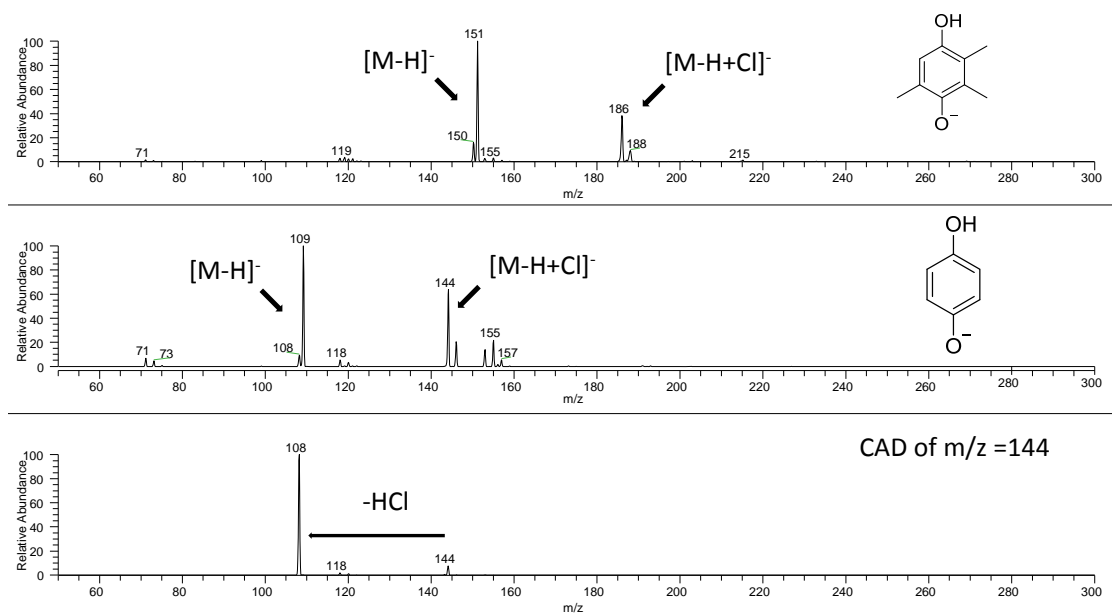


Figure 4.6 Mass spectrum measured for the reaction between SOCl_2 and (top) deprotonated 3,4,5-trimethylhydroquinone and (middle) deprotonated hydroquinone. (Bottom) CAD mass spectrum measured for the $[M-H+Cl]^-$ product ion at 20 (arbitrary unit) collision energy.

A mechanism for the formation of above product ion was proposed and evaluated via DFT calculations. This mechanism involves nucleophilic addition of carbon 4 of the deprotonated hydroquinone to the sulfur atom followed by elimination of HCl and a SOCl radical.

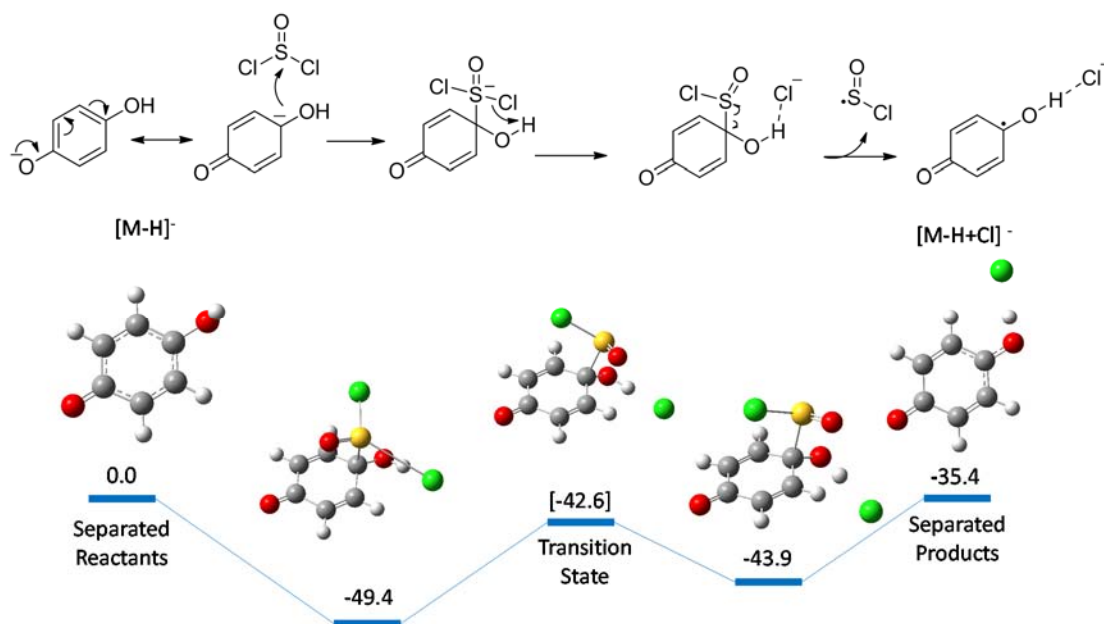


Figure 4.7 (Top) proposed mechanism and (bottom) calculated potential energy surface (enthalpy in kcal/mol) for the formation of Cl adduct ion upon reaction between deprotonated hydroquinone and SOCl_2 (M06-2X/6-31+G(d,p) level of theory).

4.4 Conclusions

Catechol, resorcinol, and hydroquinone were successfully differentiated via ion-molecule reactions between the deprotonated analytes and SOCl_2 . Deprotonated catechol formed SOCl_3^- product ion. Deprotonated resorcinol formed SOCl_2 adduct-2HCl product ion. Deprotonated hydroquinone formed Cl anion adduct ion. The formation of these distinct product ions was related to the structural characteristic of each regioisomer. DFT calculations performed on the proposed mechanisms found them to be energetically feasible.

4.5 References

- (1) Azadi, P.; Inderwildi, O. R.; Farnood, R.; King, D. A. *Renew. Sustain. Energy Rev.* **2013**, *21*, 506–523.
- (2) Calvo-Flores, F. G.; Dobado, J. A. *ChemSusChem* **2010**, *3* (11), 1227–1235.
- (3) Weng, J.-K.; Li, X.; Bonawitz, N. D.; Chapple, C. *Curr. Opin. Biotechnol.* **2008**, *19* (2), 166–172.
- (4) Hatzis, C.; Riley, C.; Philippidis, G. P. *Appl. Biochem. Biotechnol.* *57-58* (1), 443.
- (5) Cooks, R. G.; Jarmusch, A. K.; Wleklinski, M. *Int. J. Mass Spectrom.* **2015**, *377*, 709–718.
- (6) McLafferty, F. W. *Int. J. Mass Spectrom.* **2001**, *212* (1–3), 81–87.
- (7) Nakazono, Y.; Tsujikawa, K.; Kuwayama, K.; Kanamori, T.; Iwata, Y. T.; Miyamoto, K.; Kasuya, F.; Inoue, H. *Forensic Toxicol.* **2013**, *31* (2), 241–250.
- (8) Fu, M.; Duan, P.; Gao, J.; Kenttämää, H. I. *The Analyst* **2012**, *137* (24), 5720.
- (9) Eismin, R. J.; Fu, M.; Yem, S.; Widjaja, F.; Kenttämää, H. I. *J. Am. Soc. Mass Spectrom.* **2011**, *23* (1), 12–22.
- (10) Campbell, K. M.; Watkins, M. A.; Li, S.; Fiddler, M. N.; Winger, B.; Kenttämää, H. I. *J. Org. Chem.* **2007**, *72* (9), 3159–3165.
- (11) Sheng, H.; Tang, W.; Yerabolu, R.; Kong, J. Y.; Williams, P. E.; Zhang, M.; Kenttämää, H. I. *Rapid Commun. Mass Spectrom.* **2015**, *29* (8), 730–734.
- (12) Sheng, H.; Tang, W.; Yerabolu, R.; Max, J.; Kotha, R. R.; Riedeman, J. S.; Nash, J. J.; Zhang, M.; Kenttämää, H. I. *J. Org. Chem.* **2016**, *81* (2), 575–586.
- (13) Sheng, H.; Williams, P. E.; Tang, W.; Zhang, M.; Kenttämää, H. I. *Analyst* **2014**, *139* (17), 4296–4302.
- (14) Sheng, H.; Williams, P. E.; Tang, W.; Riedeman, J. S.; Zhang, M.; Kenttämää, H. I. *J. Org. Chem.* **2014**, *79* (7), 2883–2889.
- (15) Tang, W.; Sheng, H.; Kong, J. Y.; Yerabolu, R.; Zhu, H.; Max, J.; Zhang, M.; Kenttämää, H. I. *Rapid Commun. Mass Spectrom.* **2016**, *30* (12), 1435–1441.
- (16) Fu, M.; Duan, P.; Li, S.; Habicht, S. C.; Pinkston, D. S.; Vinueza, N. R.; Kenttämää, H. I. *The Analyst* **2008**, *133* (4), 452.

- (17) Gao, H.; Petzold, C. J.; Leavell, M. D.; Leary, J. A. *J. Am. Soc. Mass Spectrom.* **2003**, *14* (8), 916–924.
- (18) Hauptert, L. J.; Owen, B. C.; Marcum, C. L.; Jarrell, T. M.; Pulliam, C. J.; Amundson, L. M.; Narra, P.; Aqueel, M. S.; Parsell, T. H.; Abu-Omar, M. M.; Kenttämäa, H. I. *Fuel* **2012**, *95*, 634–641.
- (19) Jarrell, T.; Riedeman, J.; Carlsen, M.; Replogle, R.; Selby, T.; Kenttämäa, H. *Anal. Chem.* **2014**, *86* (13), 6533–6539.
- (20) Bachrach, S. M.; Hayes, J. M.; Check, C. E.; Sunderlin, L. S. *J. Phys. Chem. A* **2001**, *105* (41), 9595–9597.

CHAPTER 5. IDENTIFICATION OF MICROBIAL LIGNIN DEGRADATION PRODUCTS VIA HIGH PERFORMANCE LIQUID CHROMATOGRAPHY COUPLED WITH TANDEM MASS SPECTROMETRY

5.1 Introduction

Conversion of biomass into smaller compounds is a promising alternative route of obtaining the valuable chemicals mainly derived from crude oil.¹⁻⁴ The degradation of lignin, one of the primary biomass components, is of particular interest.⁵⁻⁷ Lignin is the second most abundant natural occurring polymer and can constitute up to 35% of the total biomass.⁸ While the exact chemical structure of lignin is hitherto unknown, the current consensus is that it is a biopolymer consisting of phenolic monomers linked together via a variety of linkages.⁸ Due to its high aromatic carbon content, lignin is viewed as a promising feedstock for biomass conversion processes that produce valuable aromatic compounds.⁹

The primary obstacle of utilizing lignin lies in its complexity. Due to the diverse types of phenolic monomers and linkages in lignin, most conversion processes degrade lignin into complex mixtures of aromatic compounds that are difficult to analyze. Yet, chemical characterization of these product mixtures is essential for the optimization of the conversion processes. Past research has shown that ESI in negative ion mode with NaOH as dopant is an effective ionization method for the phenolic compounds commonly observed in lignin degradation products.¹⁰ Its main advantage is that it yields one ion type

(deprotonated molecule) per analyte without fragmentation or aggregation. This ionization method can be further coupled with HPLC for the analysis of complex lignin degradation mixtures such as organosolv lignin.^{11,12}

Microbial degradation of lignin is an alternative approach aimed at producing relatively simple degradation product mixtures.^{13,14} This is generally achieved by using lignolytic microbes that produce enzymes targeting specific linkages within lignin, breaking it into smaller fragments.¹⁵ In this chapter, the analyses of two different microbial lignin degradation products are discussed. The first sample was a cordgrass sample degraded by *Phaeosphaeria spartinicola* (a type of salt marsh fungi) prepared by our collaborator, Dr. Alice Buchan at the University of Tennessee. Gene expressions during cordgrass degradation had already been measured via RNAseq experiments. Chemical characterization of the degradation product mixture was needed to correlate gene expression with lignin degradation pathways. The second sample was a lignin β -O-4 dimer incubated with mimivirus enzyme R135, which has a similar structure as an aryl-oxidase that participates in lignin biodegradation in plant cell walls.¹⁶ Chemical characterization of the incubation solution was required to determine whether mimivirus enzyme R135 can degrade lignin.

Both samples had a high salt concentration needed to maintain proper microbe functions. HPLC-MS analysis with NaOH dopant could not be directly applied to these mixtures because the high salt content would interfere with the ESI ionization process.¹⁷ Thus, certain sample preparation was necessary. Preparative HPLC was used to desalt the cordgrass degradation sample and solid phase extraction (SPE) were used to desalt lignin

dimer mimivirus degradation sample. The desalted samples were subsequently subjected to HPLC-MS analysis.

5.2 Experimental

5.2.1 Chemicals

4-Ethoxyphenol (99%) and vanillin (98%) was obtained from Sigma-Aldrich (St. Louis, Mo, USA). 4-Hydroxybenzoic acid (99%) and 4-hydroxy-3-methoxybenzoic acid (99%) were purchased from Alfa Aesar (Ward Hill, MA, USA). Guaiacyl glycerol- β -guaiacyl ether (99%) was purchased from TCI America (Portland, OR, USA). HPLC grade water and HPLC acetonitrile were purchased from Fisher Scientific (Pittsburgh, PA, USA). All chemicals were used without further purification.

All following cordgrass degradation samples were prepared by Dr. Alison Buchan at the University of Tennessee. These samples include: incubation mixtures of lignolic fungus and cordgrass (three replicas, CGSS-RepA, CGSS-RepB, and CGSS-RepC); an incubation mixture of lignolic fungus without cordgrass (two replicas, GSS-RepA, and GSS-RepB); and an incubation mixture of cordgrass without lignolic fungus (fungal-free). The incubation medium used were: 2% (w/v) sea salt (Sigma), 23.5 mM NaNO₃, 10.3 mM KH₂PO₄, and 17.2 mM K₂HPO₄. The CGSS sample replicas were further diluted 10 times and incubated with salt water lignolic bacteria for different periods of time (T₀-T₆ samples, T₀ incubated for 0 hr, T₆ incubated for 24 hr).

The lignin dimer mimivirus degradation samples were obtained from Dr. Michael Rossmann at Purdue University. Mimivirus R135 and its wildtype were incubated with 1

mM guaiacylglycerol- β -guaiacyl ether in PBS at 37°C for 48 hr. 1 mM guaiacylglycerol- β -guaiacyl ether in PBS incubated at 37°C for 48 hr without any mimivirus was used as a negative control.

5.2.2 Sample Preparation

Preparative HPLC separation was carried out to desalt the *Phaeosphaeria spartinicola* degraded cordgrass sample by using a modified Spectrasystem P4000 (Thermo Scientific) HPLC with a SN4000 PDA detector (Thermo Scientific) and a Synergi Polar-RP column (5 μ m particle size, 250 mm \times 21.2 mm). An injection volume of 2 mL was used for all degradation samples. A gradient composed of water (A) and acetonitrile (B) was used as follows: 0.00 min, 95% A and 5% B; 10.00 min, 95% A and 5% B; 35.00 min, 100% B; 40.00 min, 100 % B; 41.00min, 95% A and 5% B; and 50.00 min, 95% A and 5% B. Mobile phase flow rate was kept at 12 mL/min. HPLC elutes that exhibit UV absorbance at 254 nm were collected for further analysis.

The lignin dimer mimivirus degradation samples were desalted via solid phase extraction experiments using Waters Oasis HLB 3 cc Vac Cartridges. The cartridges were equilibrated with 10 mL of methanol followed by 10 mL of water. 2 mL of sample solutions were loaded and washed with 10 mL of water before eluted with 2 mL of methanol. 25 μ L eluents were injected for HPLC-MS analysis.

5.2.3 High-Performance Liquid Chromatography

All desalted samples were separated via HPLC with a Surveyor Plus HPLC system consisting of a quaternary pump, an autosampler, and a Zorbax SB-C18 column or SB-phenyl column. For separations using the SB-C18 column, a non-linear gradient of water (A) and acetonitrile (B) was used: 0.00 min, 100% A; 15.00 min, 100% A; 25.00 min, 100% B; 26.00 min, 100% A; and 35.00min, 100% A. For separations using the SB-phenyl column, a different gradient of water (A) and acetonitrile (B) was used: 0.00 min, 80% A and 20% B; 23.00 min, 25% A and 75%B; 25.00 min, 100% B; 26.00 min, 80% A and 20% B; and 35.00min, 80% A and 20% B. The flow rate of the mobile phase was kept at 500 $\mu\text{L}/\text{min}$ for both gradients.

4.2.3 Mass Spectrometry

All mass spectrometry experiments were carried out on a Thermo Scientific linear quadrupole ion trap mass spectrometer (LQIT) equipped with an electrospray ionization source (ESI). The mass spectrometer was coupled to a Surveyor Plus HPLC with a quaternary pump, auto sampler, and photodiode array (PDA) detector. During HPLC-MS analysis, HPLC eluents were mixed with 1% NaOH solution introduced at a flow rate of 0.1 $\mu\text{L}/\text{min}$ via a tee connector before introduced into the ESI source. ESI conditions were set as follows: 3.5 kV spray voltage, N_2 sheath gas at flow of 20 (arbitrary units), N_2 auxiliary gas at flow of 10 (arbitrary units), and a 275 $^\circ\text{C}$ transfer capillary temperature. Detection was done under negative ion mode. The most abundant ion measured within a scan were isolated with an an isolation width of 2 m/z units and subjected to collision-

activated dissociation (CAD) experiments. All CAD experiments were performed with at a q value of 0.25, collision energy of 30 (arbitrary units), and collision time of 30 ms.

5.3 Results and Discussion

5.3.1 Preparative HPLC Separation of Cordgrass Samples

The cordgrass samples were desalted using preparative HPLC experiments with a reversed phase column. This was done for two reasons: 1) the salt content would not retain in the reversed phase column and therefore would elute out first; 2) the degradation mixture might be complex, so this step would act as the first dimension of separation. A UV detector was used as all lignin degradation products are aromatic.

A cordgrass sample (CGSS) and two control samples (GSS and Fungal-free) were respectively subjected to prep-HPLC (Figure 5.1). The cordgrass sample (CGSS) contained both cordgrass and fungus, while the control samples either only contain cordgrass (Fungal-free) or only contain the fungus (GSS). For the CGSS sample, eluates eluting between 4-10 min (shown in red in figure 5.1) and 22-24 min (shown in blue in figure 5.1) showed the strongest UV absorbance. For the control samples, only elutes between 4-10 min showed strong UV absorbance (Figure 5.1). All three samples contained a compound eluting at 25 min (shown in green in figure 5.1). However, this compound was later identified as stripped column packing material as it was also observed in blank runs.

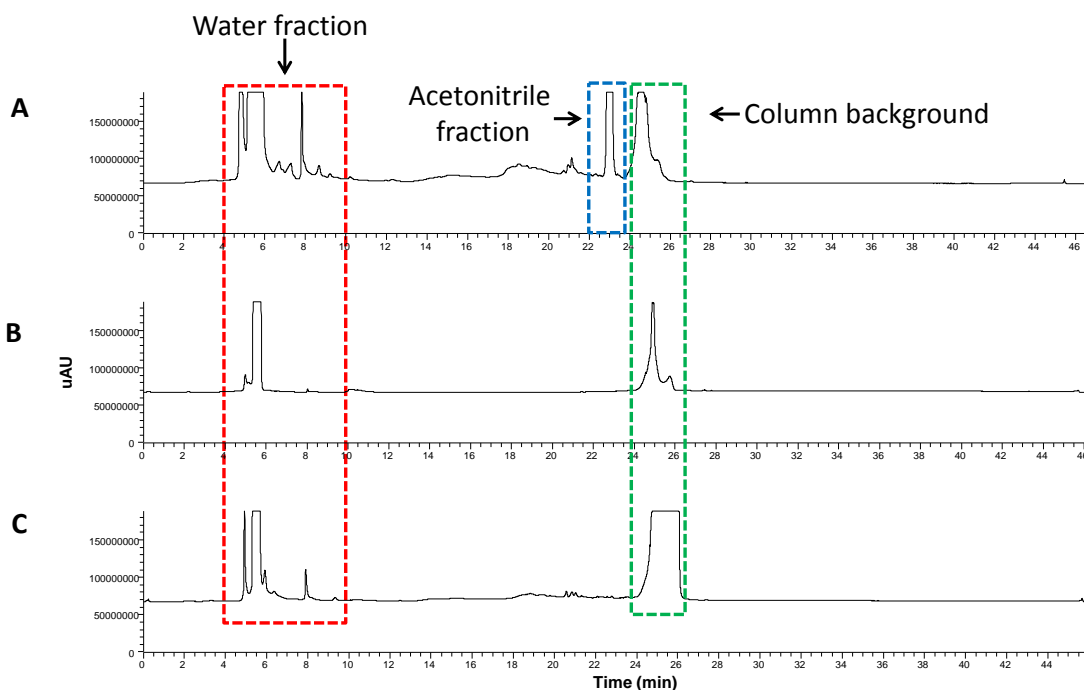


Figure 5.1 Preparative HPLC separations of the cordgrass samples. (A) Culture medium that contains both cordgrass and fungus (CGSS samples). (B) Culture medium that only contains fungus GSS. (C) Culture medium that only contains cordgrass (Fungal-free). UV signals were detected at 254 nm.

The fractions eluting between 4-10 min and between 22-24 min were collected for CGSS samples. Based on the mobile phase composition when they eluted, they are referred to as the “water fraction” and the “acetonitrile fraction”, respectively. For the control samples, only the water fractions were collected. These fractions were subjected to HPLC-MS analysis.

5.3.2 HPLC-MS Analysis of Cordgrass Samples

A C-18 column was used for the water fractions and a phenyl column was used for the acetonitrile fractions. HPLC eluates were analyzed by both UV detection and tandem mass spectrometry.

The HPLC chromatogram for the CGSS sample water fraction exhibited two peaks eluting at around 20.7 min and 20.9 min that had both strong ion current signal and UV absorbance signal (Figure 5.2). The mass spectra measured for the compounds eluted in these two peaks showed that their deprotonated forms had a m/z value of 137 and 167. The other large peaks eluting at around 5 min did not show strong UV signal, therefore most likely not correspond with aromatic compounds. The structures of the ions of m/z 137 and 167 were probed via CAD experiments (Table 5.1). Their structures were proposed via comparison with a literature database.¹⁸ The peaks eluting at 20.70 min and 20.94 min were not observed for the water fractions of the two control samples (GSS and the fungal free), suggesting that the above two identified compounds are likely the product of cordgrass fungal degradation (Figure 5.3).

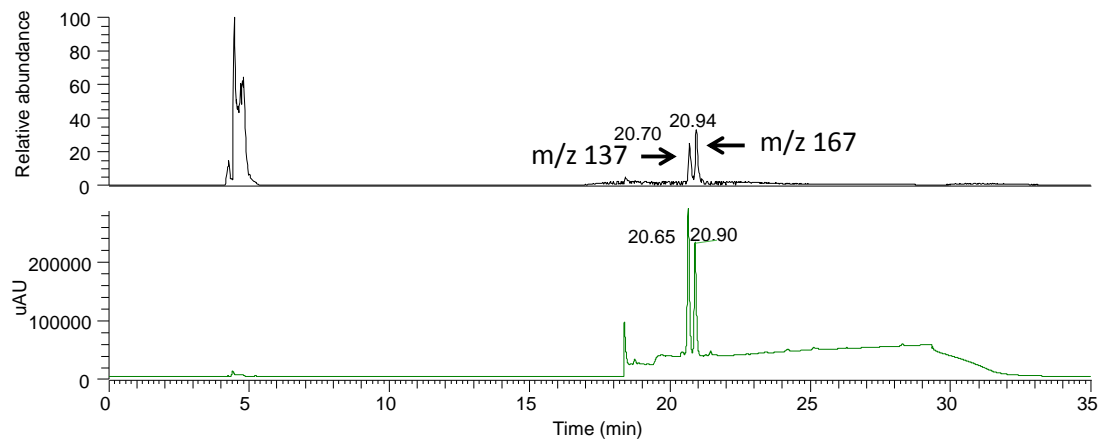


Figure 5.2 (Top) Total ion current chromatogram and (bottom) UV absorbance chromatogram at 254 nm for CGSS water fraction.

In the chromatography of the CGSS acetonitrile fraction, only one peak eluting at 13.60 min was observed (Figure 5.4). The compound in the peak had a m/z value of 151 when analyzed via mass spectrometer. Its structure was proposed by comparing its CAD pattern with a literature database (Table 5.1).¹⁸

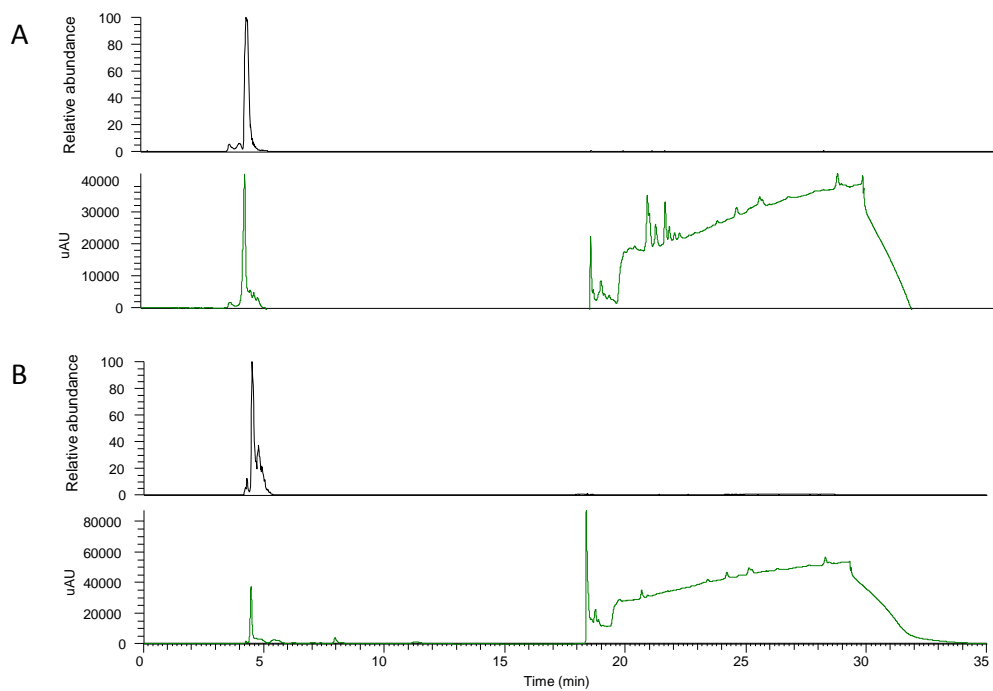
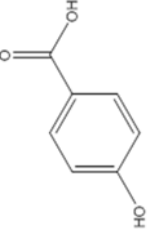
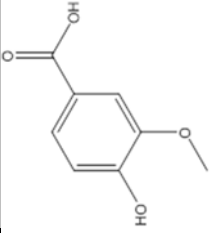
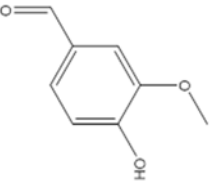


Figure 5.3 Total ion current chromatogram (top) and UV absorbance chromatogram (bottom) at 254 nm for (A) GSS water fraction and (B) fungal free water fraction.

Table 5.1 m/z value of the deprotonated major components in CGSS sample, their MS² and MS³ fragmentation ions and proposed structures

Fraction	Deprotonated analyte m/z	MS ² product ions (m/z) and their relative abundances	MS ³ product ions (m/z) and their relative abundances	Proposed structure
	137	137-CO ₂ (93, 100%)	No further fragmentation observed	
water	167	167-CH ₃ (152, 70%) 167-CO ₂ (123, 100%) 167-CO ₂ -CH ₃ (108, 10%)	123-CH ₃ (108, 100%)	
acetonitrile	151	151-CH ₃ (136, 100%)	136-CO (108, 40%) 136-CO ₂ (92, 100%)	

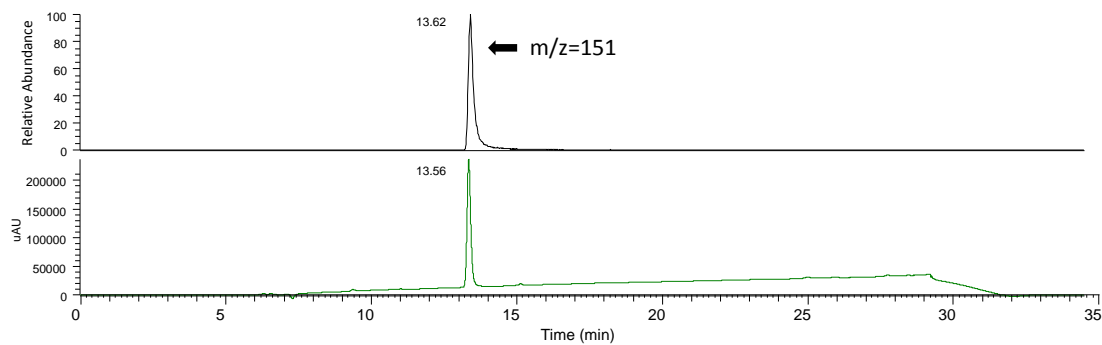


Figure 5.4 (Top) Total ion current chromatogram and (bottom) UV absorbance chromatogram at 254 nm for CGSS acetonitrile fraction.

To test the structural assignments, an artificial mixture of the three identified compounds was prepared and analyzed via preparative HPLC separation and subsequent HPLC-MS analysis (Figure 4.5). The retention times and the CAD spectra of the compounds in the artificial mixture were similar to the compounds detected in the degradation sample, suggesting that the structural assignment was correct.

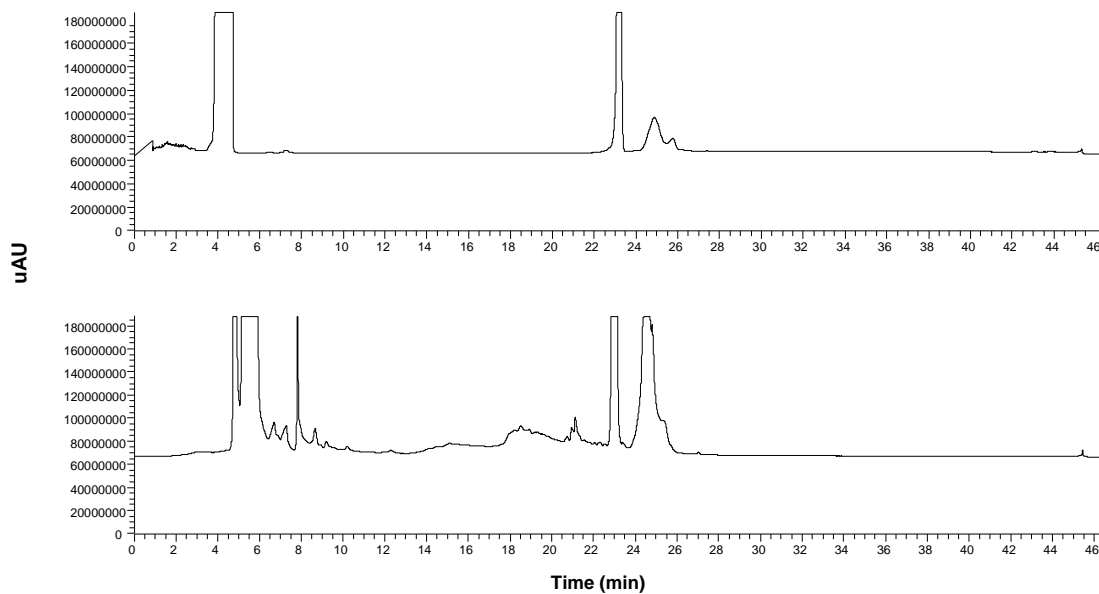


Figure 5.5 Preparative HPLC separations of the (top) artificial mixture and (bottom) CGSS sample. UV signal was detected at 254 nm.

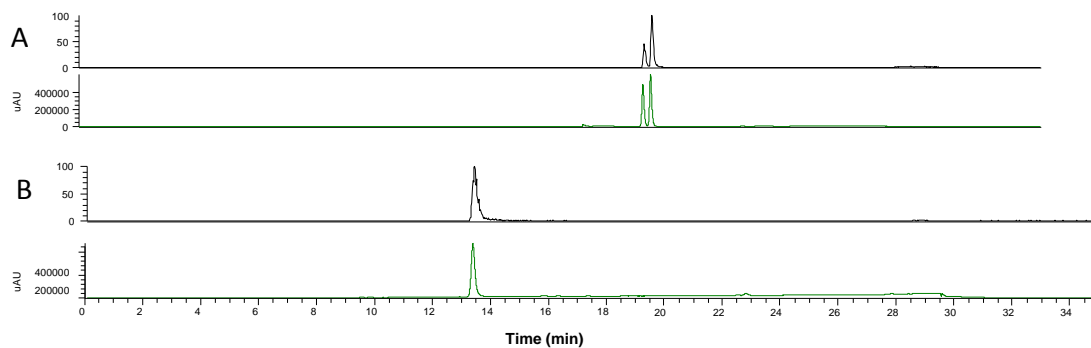


Figure 5.6 Total ion current chromatogram and UV absorbance chromatogram at 254 nm for (A) water fraction of the artificial mixture and (B) acetonitrile fraction of the artificial mixture.

5.3.3 Vanillin Quantification in Cordgrass Time Series Samples

Samples T₀ through T₆ were diluted CGSS samples incubated with another type of salt water bacteria for different time length. T₀ sample had the shortest incubation time while T₆ sample had the longest incubation time. In theory, the aromatic compounds in the CGSS samples will be consumed by the salt water bacteria. Concentration of vanillin, the major component identified in the CGSS sample, was determined in samples T₀-T₆ by using 4-ethoxyphenol as the internal standard. HPLC-MS analysis of these samples showed that vanillin concentration was too low to be effectively quantified via UV detection (Figure 5.7). The low concentration is likely due to that samples T₀-T₆ were diluted 10 times and further subjected to bacteria consumption. To solve this issue, mass spectrometry was explored as an alternative detection method for quantification of vanillin in lignin degradation samples. A comparison between UV detection and mass spectrometric detection (Figure 5.7) for vanillin showed that mass spectrometry has a much higher signal to noise ratio. The low limit of detection using mass spectrometry was determined to be 25 nM for a S/N of 3 (Figure 5.8).

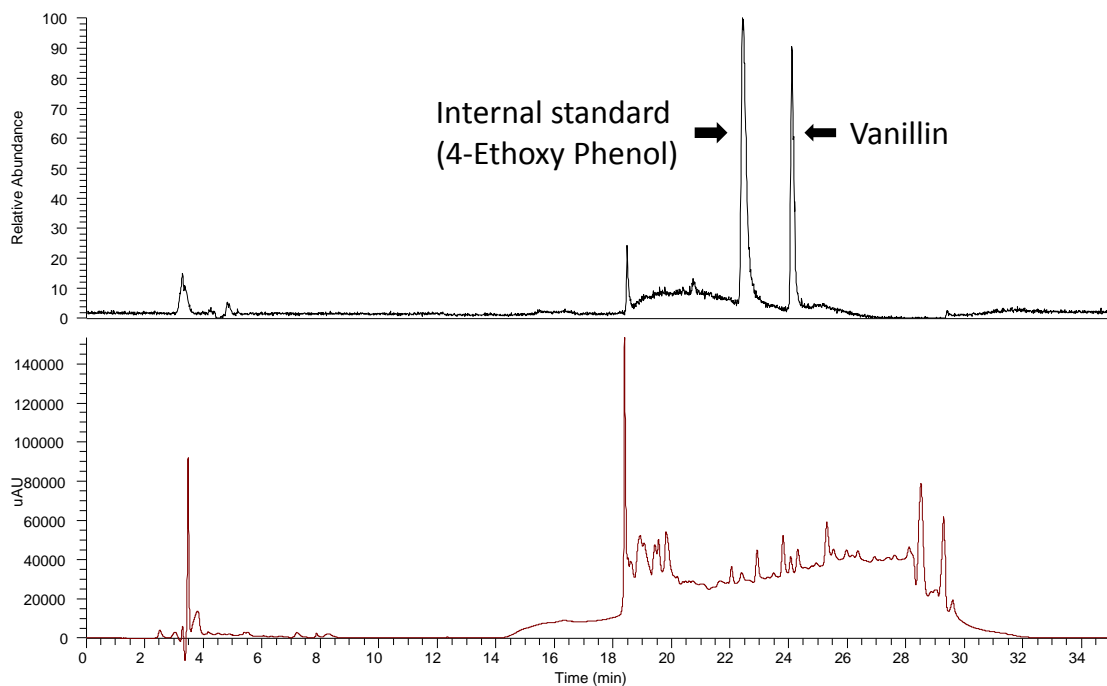


Figure 5.7 Analysis of the T_0 time series sample using (top) mass spectrometry detection by monitoring extracted ion current and (bottom) UV detection at 254 nm.

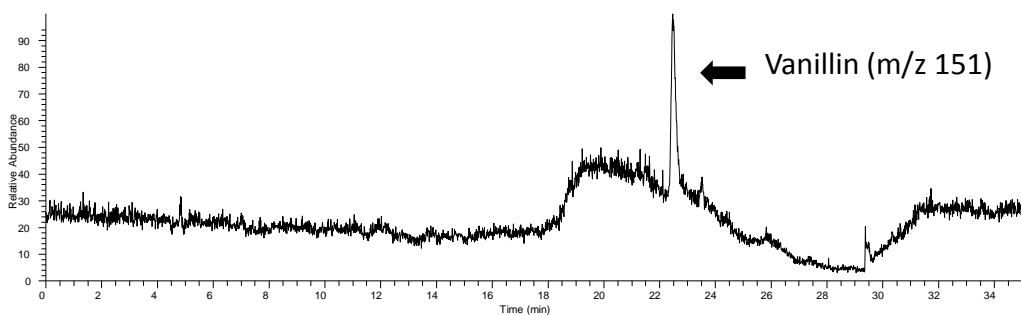


Figure 5.8 Selected ion current chromatogram of deprotonated vanillin (m/z 151) measured for a vanillin sample with a concentration of 25 nmol

A calibration curve for vanillin concentration and peak area ratio of vanillin over the internal standard was generated (Figure 5.9). A good linear correlation ($R^2 = 0.994$) between the peak area ratio and vanillin concentration was achieved. Quantification results of the time series samples are summarized in Figure 5.10.

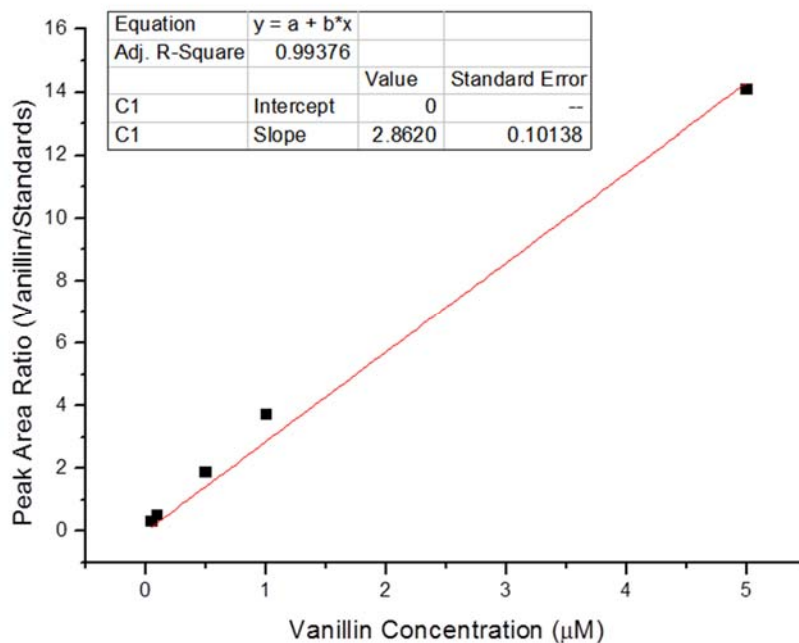


Figure 5.9 Calibration curve for vanillin concentration vs peak area ratio (vanillin / internal standard)

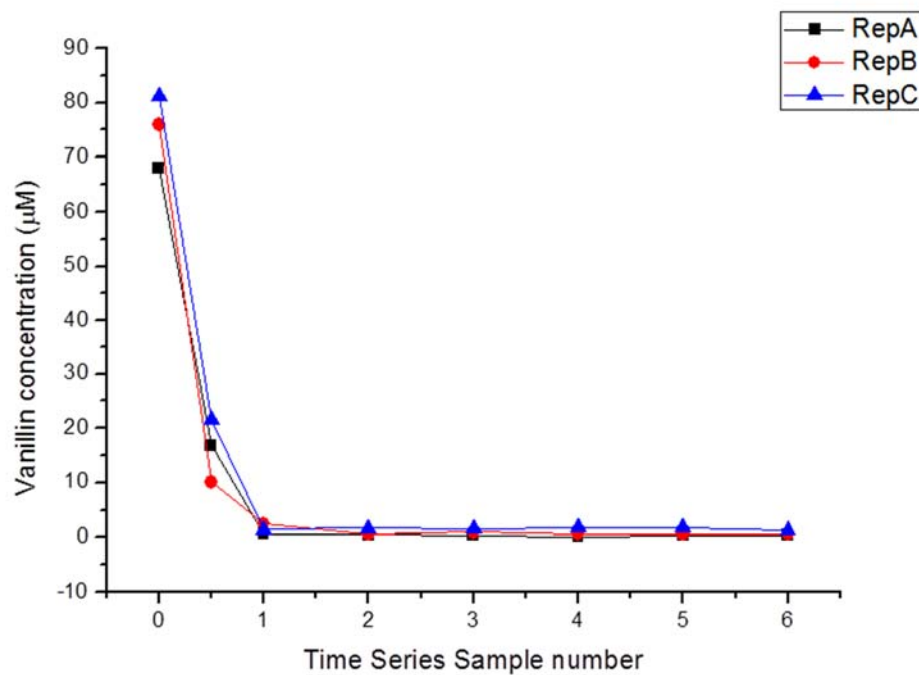


Figure 5.10 Vanillin concentration measured in samples T₀-T₆.

Above results showed that during incubation, the concentration of vanillin dropped drastically. This finding suggests that aromatic compounds are being consumed by the salt water bacteria. The most significant drop occurred between samples T₀ and T_{0.5}, which reduced vanillin concentration to almost 0.

5.3.4 HPLC-MS Analysis of Mimivirus Lignin Degradation Samples

A mimivirus enzyme R135 was incubated with a lignin β -O-4 dimer (guaiacyl glycerol- β -guaiacyl ether) in order to test its ability to break the β -O-4 linkage. This mimivirus requires phosphate buffer to maintain normal function. Therefore, SPE

experiments were employed to extract the sample of interest (lignin β -O-4 dimer and its possible degradation products) from the culture medium.

An artificial mixture of vanillin (model compound for the degradation product) and guaiacyl glycerol- β -guaiacyl ether was used to test the effectiveness of the SPE step. The artificial mixture was prepared using PBS buffer and subjected to SPE and subsequent HPLC-MS analysis. Results showed that both compounds were retained on the SPE cartridge and could be effectively separated and detected by HPLC-MS (Figure 5.11).

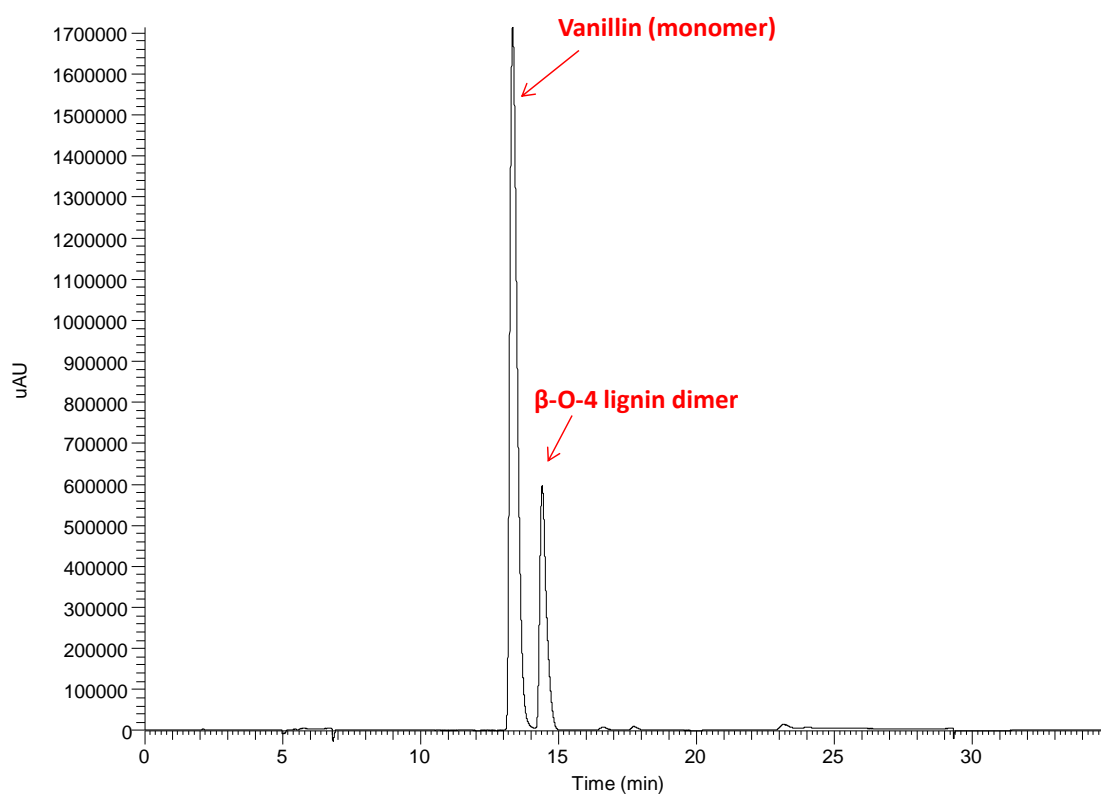


Figure 5.11 HPLC-MS analysis of an artificial mixture of vanillin and guaiacyl glycerol- β -guaiacyl ether after SPE.

One degradation sample (β -O-4 dimer incubated with mimivirus R135) and two control samples (β -O-4 dimer without virus and β -O-4 dimer incubated with a mutated mimivirus) were processed via solid phase extraction and subjected to HPLC-MS analysis. However, no significant differences were observed for these three samples (Figure 5.12). Only the lignin dimer was shown in high abundance and no monomers were observed. These results suggest that the mimivirus R135 does not specifically target the β -O-4 linkage within lignin.

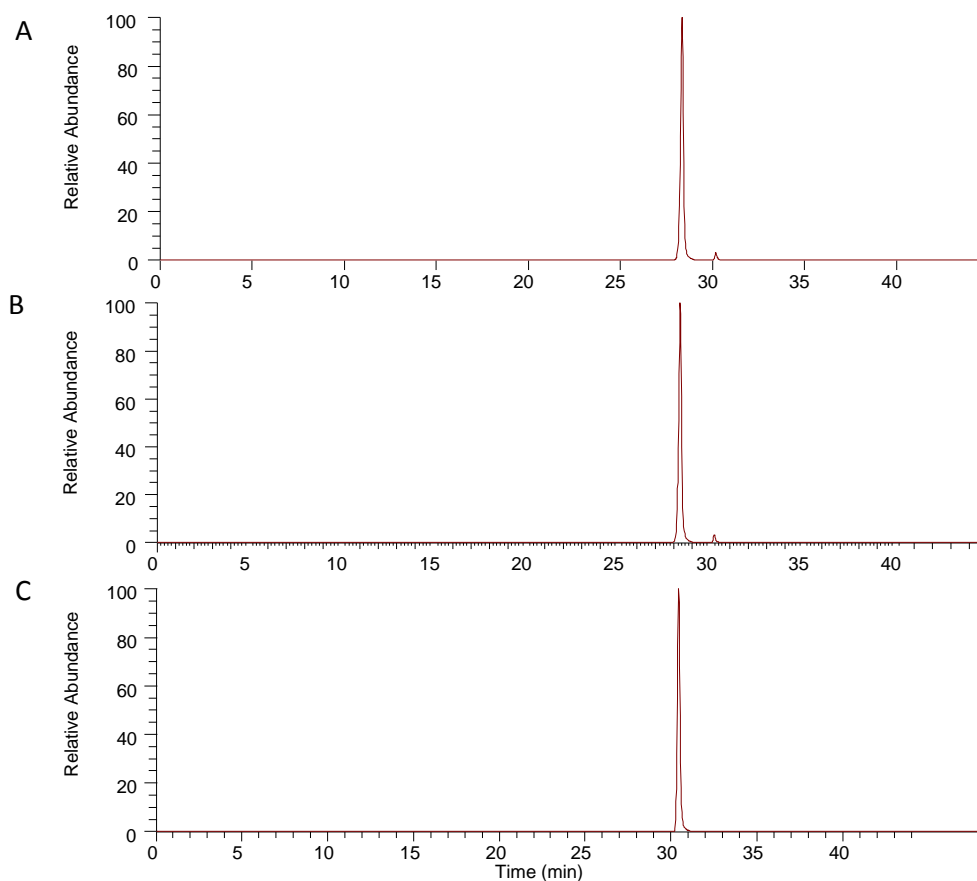


Figure 5.12 Selected ion chromatogram of the (A) experimental sample, (B) control sample with wildtype mimivirus, and (C) control sample with no added mimivirus.

5.4 Conclusions

Two different sample preparation techniques were developed for the analysis of lignin microbial degradation products. Preparative HPLC with a reverse phase column was used to desalt cordgrass samples while SPE was used to desalt mimivirus lignin degradation samples. These two methods allowed the characterization of salty samples that are not compatible with direct ESI analysis.

Vanillin, vanillic acid, and salicylic acid were found to be present in the fungal lignin degradation product samples. The structures of these molecules were proposed by comparing their CAD fragmentation data with literature database. Comparison of HPLC retention time with an artificial mixture was used to further confirm the structures. Quantification of the identified compounds was achieved using mass spectrometer to monitor extracted ion current of the compound of interest and showed superior sensitivity compared with UV detection.

For the mimivirus lignin degradation products, a desalting method based on solid phase extraction was developed. This method was validated via testing of an artificial mixture. However, no degradation products were observed for the sample containing both mimivirus and lignin β -O-4 dimer, suggesting that the mimivirus does not break down β -O-4 linkages.

5.5 References

- (1) Chang, M. C. Y. *Curr. Opin. Chem. Biol.* **2007**, *11* (6), 677–684.
- (2) Ragauskas, A. J.; Williams, C. K.; Davison, B. H.; Britovsek, G.; Cairney, J.; Eckert, C. A.; Frederick, W. J.; Hallett, J. P.; Leak, D. J.; Liotta, C. L.; Mielenz, J. R.; Murphy, R.; Templer, R.; Tschaplinski, T. *Science* **2006**, *311* (5760), 484–489.
- (3) Hamelinck, C. N.; Hooijdonk, G. van; Faaij, A. P. *Biomass Bioenergy* **2005**, *28* (4), 384–410.
- (4) Venkatakrisnan, V. K.; Degenstein, J. C.; Smeltz, A. D.; Delgass, W. N.; Agrawal, R.; Ribeiro, F. H. *Green Chem.* **2014**, *16* (2), 792–802.
- (5) Azadi, P.; Inderwildi, O. R.; Farnood, R.; King, D. A. *Renew. Sustain. Energy Rev.* **2013**, *21*, 506–523.
- (6) Calvo-Flores, F. G.; Dobado, J. A. *ChemSusChem* **2010**, *3* (11), 1227–1235.
- (7) Hisano, H.; Nandakumar, R.; Wang, Z.-Y. *Vitro Cell. Dev. Biol. Plant* **2009**, *45* (3), 306–313.
- (8) Zakzeski, J.; Bruijninx, P. C. A.; Jongerius, A. L.; Weckhuysen, B. M. *Chem. Rev.* **2010**, *110* (6), 3552–3599.
- (9) Weng, J.-K.; Li, X.; Bonawitz, N. D.; Chapple, C. *Curr. Opin. Biotechnol.* **2008**, *19* (2), 166–172.
- (10) Hauptert, L. J.; Owen, B. C.; Marcum, C. L.; Jarrell, T. M.; Pulliam, C. J.; Amundson, L. M.; Narra, P.; Aqueel, M. S.; Parsell, T. H.; Abu-Omar, M. M.; Kenttämaa, H. I. *Fuel* **2012**, *95*, 634–641.
- (11) Owen, B. C.; Hauptert, L. J.; Jarrell, T. M.; Marcum, C. L.; Parsell, T. H.; Abu-Omar, M. M.; Bozell, J. J.; Black, S. K.; Kenttämaa, H. I. *Anal. Chem.* **2012**, *84* (14), 6000–6007.
- (12) Jarrell, T. M.; Marcum, C. L.; Sheng, H.; Owen, B. C.; O’Lenick, C. J.; Maraun, H.; Bozell, J. J.; Kenttämaa, H. I. *Green Chem.* **2014**, *16* (5), 2713–2727.
- (13) Crawford, D. L.; Crawford, R. L. *Enzyme Microb. Technol.* **1980**, *2* (1), 11–22.
- (14) Ruiz□Dueñas, F. J.; Martínez, Á. T. *Microb. Biotechnol.* **2009**, *2* (2), 164–177.
- (15) Bugg, T. D. H.; Ahmad, M.; Hardiman, E. M.; Rahmanpour, R. *Nat. Prod. Rep.* **2011**, *28* (12), 1883–1896.

- (16) Klose, T.; Herbst, D. A.; Zhu, H.; Max, J. P.; Kenttämä, H. I.; Rossmann, M. G. *Structure* **2015**, *23* (6), 1058–1065.
- (17) Sterling, H. J.; Batchelor, J. D.; Wemmer, D. E.; Williams, E. R. *J. Am. Soc. Mass Spectrom.* **2010**, *21* (6), 1045–1049.
- (18) Marcum, C. L.; Jarrell, T. M.; Zhu, H.; Owen, B. C.; Hauptert, L. J.; Easton, M.; Hosseinaei, O.; Bozell, J.; Nash, J. J.; Kenttämä, H. I. *ChemSusChem* **2016**

CHAPTER 6. ANALYSIS OF ORGANOSOLV LIGNIN VIA HIGH PERFORMANCE LIQUID CHROMATOGRAPHY COUPLED WITH TANDEM MASS SPECTROMETRY

6.1 Introduction

As discussed in the previous chapters, many current efforts are focused on the conversion of lignocellulosic biomass into biofuels and other valuable chemicals.¹⁻³ Lignocellulosic biomass contains three primary components: cellulose, hemicellulose, and lignin.⁴ As no conversion process can efficiently convert all three components at once, biomass treatment often starts by separating it into individual components.⁵ These individual components are then subjected to the most suitable conversion processes. Therefore, efficient extraction of certain components from total biomass is desired.

Lignin is the second most abundant naturally occurring polymer and makes up to 25% in weight of total biomass.⁴ Due to its high aromatic content, it is viewed as ideal feedstock for conversion into valuable aromatic compounds currently derived from crude oil.⁶ Thus, multiple methods have been developed to extract lignin from biomass. One of these methods is organosolv, a process that uses organic solvents with heat and acid to selectively solubilize lignin and hemicellulose components of biomass feedstocks.⁷ The extracted lignin and hemicellulose are separated by adding brine into the organic solution. Lignin remains in the organic layer while hemicellulose is extracted into the aqueous layer. In this way, lignin can be extracted with high purity and efficiency.⁸

However, the chemical linkages within lignin can change under the conditions utilized in the organosolv process. Thus, chemical characterization of the lignin component extracted via organosolv is needed for the design and optimization of downstream conversion processes.

The major obstacle in organosolv lignin characterization lies in the complexity of lignin structure. Lignin contains a wide variety of structural motifs that can undergo various transformations upon the organosolv process.⁹ In addition, lignin has been shown to covalently crosslink with the hemicellulose within plants, further increasing its complexity.¹⁰ Commonly used analysis techniques, such as NMR, only provide bulk information and cannot identify individual components.

Mass spectrometry has been shown to be a powerful tool for the analysis of mixtures related to lignin.^{11,12} For instance, ESI with NaOH dopant has been reported to be a highly efficient ionization method for lignin related compounds.¹³ This chapter discusses the application of high-performance liquid chromatography coupled with multiple-stage tandem mass spectrometry (HPLC-MSⁿ) in organosolv lignin analysis. Chemical formulae of the molecules present in organosolv lignin were determined via high resolution mass measurements and structural information was obtained via CAD.

6.2 Experimental

6.2.1 Materials

Organosolv lignin was obtained by our collaborator, Dr. Joe Bozell, via a process reported previously.⁹ In short, milled switchgrass was treated with a 16: 34 : 50 wt% mixture of methyl isobutyl ketone, ethanol, and water in the presence of sulfuric acid (0.1 M) in a flow reactor at a temperature of 120 °C for 120 min. 100 g/mL NaCl solution was added to the organic solution produced from the reactor, separating it into the lignin containing organic layer and the hemicellulose containing aqueous later. The lignin containing organic layer was separated via a separation funnel and washed repeatedly with water before being dried. For HPLC-MS analysis, 10 mg of the obtained organosolv lignin dried powder was dissolved in 50/50 (v/v) THF/H₂O to a final concentration of 2 mg/mL.

6.2.2 Mass Spectrometry

All experiments were performed on a Thermo Scientific LTQ-Orbitrap XL mass spectrometer coupled with an ESI source operated under negative ion mode. For high resolution mass measurements, the resolution of the instrument was set at 100,000. For CAD experiments, the ion of interest was isolated with a m/z window of 1.5 and subjected to CAD at a collision energy of 25 (arbitrary units) and at a q value of 0.250.

6.2.3 High-performance Liquid Chromatography

HPLC separations were carried out on a Surveyor Plus HPLC system consisting of a quaternary pump, an autosampler, and a Zorbax SB-C18 column. A non-linear gradient of water (A) and acetonitrile (B) was used: 0.00 min, 80% A and 20% B; 35.00 min, 100% B; 40.00 min, 100% B; 41.00 min, 80% A and 20% B; 45.00 min, 80% A and 20% B. The flow rate of the mobile phase was kept at 500 $\mu\text{L}/\text{min}$. HPLC eluents were mixed via a T-connector with 1% NaOH solution at a flow rate of 0.1 $\mu\text{L}/\text{min}$ before being ionized in an ESI source operating under negative ion mode with the following conditions: 3.25 kV spray voltage; 50 (arbitrary units) sheath gas (N_2) flow and 20 (arbitrary units) auxiliary gas (N_2) flow.

6.3 Results and Discussion

Complex mixture analyses often produce large amount of data that is difficult to process. The HPLC data collected for the organosolv lignin was visualized via base peak mode to identify its major components. Structure of these major components were probed via high-resolution mass measurement and CAD experiments performed on the deprotonated molecules.

6.3.1 HPLC Data Visualization

Complex mixtures, such as organosolv lignin, typically contain hundreds of different compounds. HPLC analyses performed on complex mixtures often produce complex chromatograms that are difficult to process and analyze. Hence, data visualization is important to identify the primary components present in a mixture, which

contribute the most to the properties of the entire mixture. In HPLC analysis, major components of the analyzed mixture are identified by locating large HPLC peaks where the concentration of the eluted analyte first increases and then decreases. For most HPLC analyses with MS detection, eluates concentration is measured using the strength of the total ion current produced upon ionization. However, the total ion current is the sum of the abundances of all ions producing the mass spectrum. Hence, ions with lower abundances will interfere with the identification of major components. Base peak ion current is the ion current of the most abundant ion producing the mass spectrum. By plotting the base peak ion current instead of total ion current, interference of ions with lower abundances can be reduced.

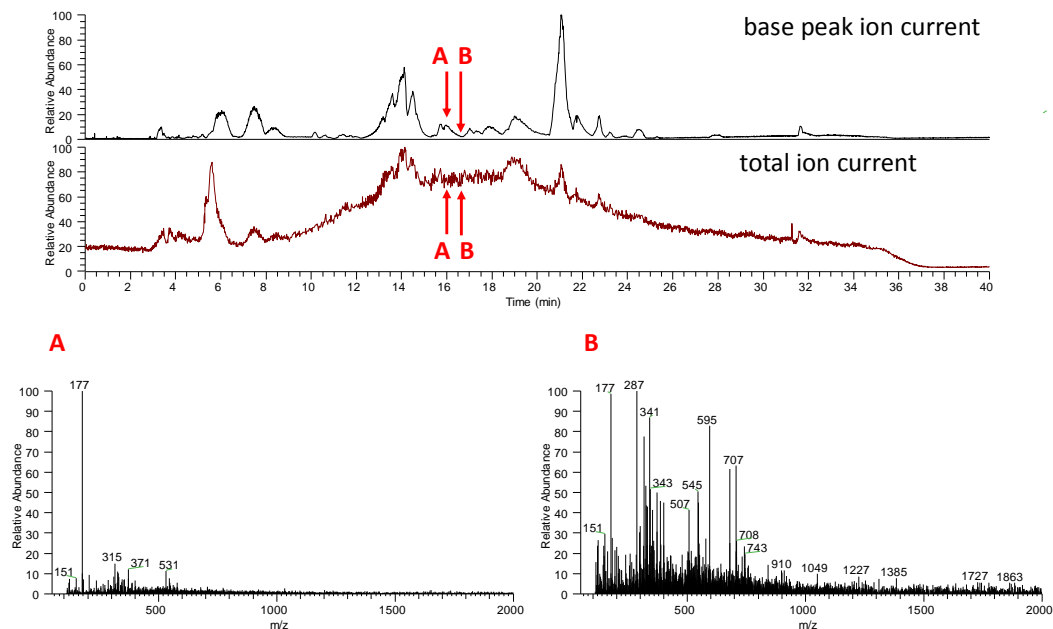


Figure 6.1 (Top) Comparison between HPLC chromatograms obtained by plotting base peak ion current versus time and total ion current versus time. (Bottom) Mass spectra measured at time A and time B.

As shown in Figure 6.1, HPLC peaks are better visualized in base peak ion current chromatogram compared to total ion current. For instance, a HPLC peak corresponding to ion of m/z 177 clearly exists at time point A. However, this peak is not visible in the total ion current chromatogram, which showed similar total ion current for time points A and B. This was because at time point A, the total ion current was primarily contributed by a single ion of m/z 177, while at time point B, multiple low abundance ions contributed to the total ion current. The above case clearly demonstrates that HPLC data visualization via base peak ion current chromatogram is makes peak identification easier for complex mixtures.

6.3.2 Elemental Composition Determination via High Resolution Mass Spectrometry

14 major peaks were identified in base peak ion current mode (Figure 6.2). The exact m/z values of the ions correlating with those peaks were measured at a resolution of 100,000. Based on the high-resolution data, chemical formulas for these ions were proposed assuming that they only contain carbon, oxygen, and hydrogen atoms (Table 5.1). Only one out of the 14 proposed elemental compositions had a relative error larger than 5 ppm (+7.5 ppm). Given the small relative errors, the proposed elemental compositions can be accepted with high confidence.

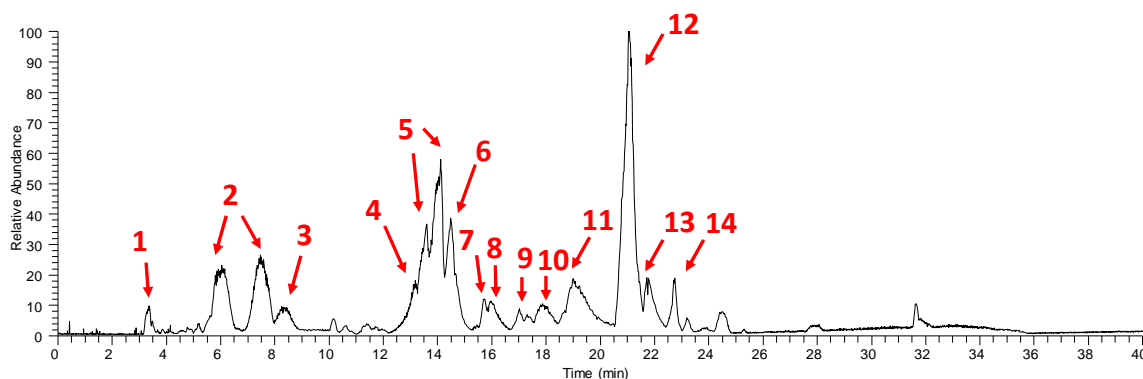


Figure 6.2 14 major components identified in organosolv lignin via base peak ion current chromatogram.

Table 6.1 Elemental compositions obtained for the major components in organosolv lignin via high resolution mass measurements.

Peak number	Elemental composition	m/z	Measured exact m/z (relative error)
1	C ₆ H ₅ O ₃	125	125.02412 (+3.2 ppm)
2	C ₉ H ₇ O ₃	163	163.03967 (+4.3 ppm)
3	C ₁₀ H ₉ O ₄	193	193.05002 (+2.5 ppm)
4	C ₇ H ₅ O ₂	121	121.02931 (+7.5 ppm)
5	C ₁₆ H ₁₉ O ₇	323	323.11261 (+0.2 ppm)
6	C ₁₇ H ₂₁ O ₈	353	353.12311 (+0.1 ppm)
7	C ₁₈ H ₁₉ O ₆	331	331.11768 (+0.2 ppm)
8	C ₁₀ H ₉ O ₃	177	177.05515 (+2.9 ppm)
9	C ₁₆ H ₁₅ O ₅	287	287.09158 (+0.6 ppm)
10	C ₁₀ H ₉ O ₄	193	193.05002 (+2.5 ppm)
11	C ₁₇ H ₁₃ O ₇	329	329.06552 (-0.2 ppm)
12	C ₁₁ H ₁₁ O ₃	191	191.07083 (+2.9 ppm)
13	C ₁₂ H ₁₃ O ₄	221	221.08131 (+2.1 ppm)
14	C ₁₆ H ₁₅ O ₂	239	239.10709 (+1.8 ppm)

6.3.3 Structural Elucidation via CAD

After obtaining the elemental compositions of the major ionized components, CAD experiments were performed to obtain structural information for these ions. Structures were proposed for 13 out of 14 major compounds based on the fragmentation patterns as well as elemental compositions of their ions (Table 6.2). Out of the 13 structures, 8 were monomeric lignin molecules that only contained one aromatic ring. Three were dimeric lignin compounds with two aromatic rings. Two were covalent complexes formed between a monomeric lignin compound and a C7 sugar. Lignin compounds with three or more aromatic rings were not observed. The above structural assignments suggested that the organosolv process breaks down the majority of the linkages between monomeric units within the lignin polymer.

Table 6.2 Proposed structures for the major components present in organosolv lignin based on CAD fragmentation data of the ionized compounds.

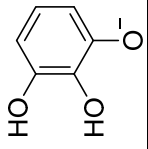
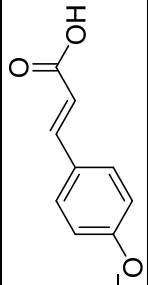
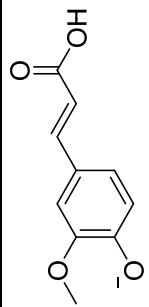
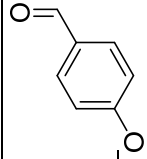
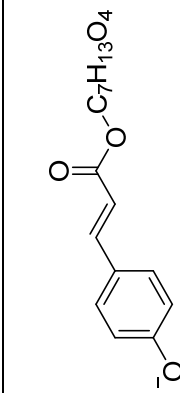
Proposed ion structure	m/z	MS ² product ions (m/z) and their relative abundance	MS ³ product ions (m/z) and their relative abundance	MS ⁴ product ions (m/z) and their relative abundance
	125	125 – CO (97) 100%	none	
	163	163 – CO ₂ (119) 100%	none	
	193	193 – CO ₂ – CH ₃ (134) 100% 193 – CO ₂ (149) 50% 193 – CH ₃ (178) 20%	none	
	121	121 – CO (93) 100% 121 – H ₂ O (103) 30% 121 – CHO (92) 10%	none	
	323	323 – C ₇ H ₁₄ O ₅ (145) 100% 323 – C ₇ H ₁₂ O ₄ (163) 25% 323 – CO – H ₂ O (277) 15%	145 – CO (117) 100%	none

Table 6.2, continued

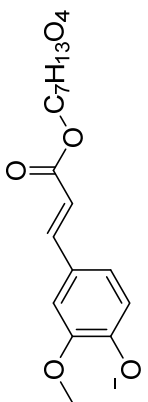
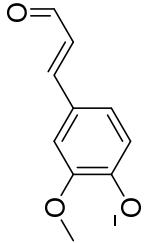
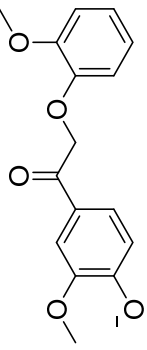
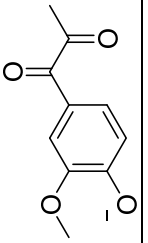
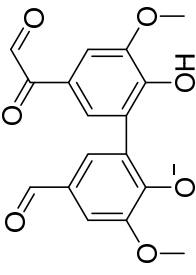
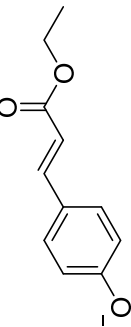
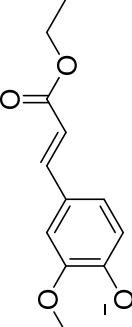
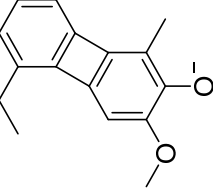
Proposed ion structure	m/z	MS ² product ions (m/z) and their relative abundance	MS ³ product ions (m/z) and their relative abundance	MS ⁴ product ions (m/z) and their relative abundance
	353	353 – C ₇ H ₁₄ O ₅ (175) 100% 353 – C ₈ H ₁₇ O ₅ (160) 20% 353 – CH ₃ (338) 20% 353 – C ₇ H ₁₂ O ₄ (193) 15%	175 – CH ₃ (160) 100%	160 – CO (132) 100%
Unidentified	331	331 – H ₂ O (313) 100%	313 – H ₂ O (295) 100%	295 – H ₂ O (277) 100% 295 – CH ₂ O (265) 20%
	177	177 – CH ₃ (162) 100%	162 – CO (134) 100% 162 – CHO (133) 40% 162 – C ₂ H ₂ O (120) 15% 162 – H ₂ O –CO (106) 20%	none
	287	287 – CH ₃ (272) 100% 287 – C ₈ H ₇ O ₃ (136) 20%	272 – C ₇ H ₆ O ₂ (150) 10% 272 – C ₇ H ₄ O ₃ (136) 100% 272 – C ₉ H ₈ O ₃ (108) 25%	136 – CO (108) 100%
	193	193 – CH ₃ (178) 100%	178 – C ₂ H ₂ O (136) 100%	136 – CO (108) 100%

Table 6.2, continued

Proposed ion structure	m/z	MS ² product ions (m/z) and their relative abundance	MS ³ product ions (m/z) and their relative abundance	MS ⁴ product ions (m/z) and their relative abundance
	329	329 – CH ₃ (314) 100%	314 – CH ₃ (299) 100%	299 – CO (271) 100% 299 – CO – CO ₂ (227) 15%
	191	191 – CO (163) 100% 191 – C ₂ H ₆ O (145) 20% 191 – C ₃ H ₄ O ₂ (119) 15%	163 – CO ₂ (119) 100%	none
	221	221 – CH ₃ (206) 100%	206 – CHO (177) 100% 206 – CO (178) 25% 206 – C ₃ H ₅ O ₂ (133) 40%	177 – CO ₂ (133) 100%
	239	239 – CH ₃ (224) 100%	224 – CH ₃ (209) 100% 224 – C ₃ H ₅ O ₂ (151) 50%	none

In order to confirm that the above 14 identified compounds are representative for the bulk of the mixture, an extracted ion current chromatogram that only showed the identified compounds was produced (Figure 5.2). The extracted ion current chromatogram was very similar to the base peak ion current chromatogram. This result suggested that the identified compounds were indeed the major components of the organosolv sample.

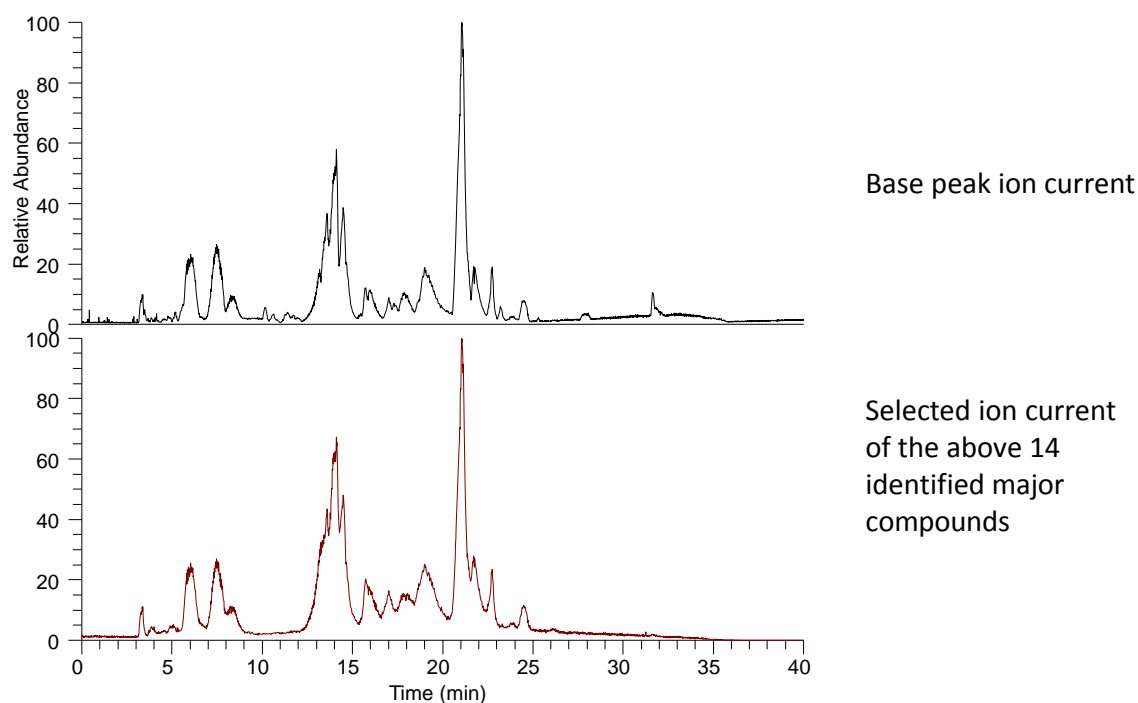


Figure 6.3 (Top) Base peak ion current chromatogram and (bottom) selected ion current chromatogram of the identified compounds for the organosolv lignin sample.

6.4 Conclusions

Swithgrass organosolv lignin was analyzed via HPLC-MSⁿ. Elemental compositions of the major components were determined based on the high resolution m/z measurements. Structural motifs present in the unknown compounds were identified via CAD experiments. Based on the above two pieces of information, structures were proposed for 13 out of 14 identified major unknown compounds. Out of the 13 proposed structures, 8 were monomeric compounds, 3 were dimeric compounds, and 2 were lignin-carbohydrate complexes. These results show that the organosolv process breaks lignin polymer into relatively small compounds.

6.5 References

- (1) Chang, M. C. Y. *Curr. Opin. Chem. Biol.* **2007**, *11* (6), 677–684.
- (2) Hamelinck, C. N.; Hooijdonk, G. van; Faaij, A. P. *Biomass Bioenergy* **2005**, *28* (4), 384–410.
- (3) Ragauskas, A. J.; Williams, C. K.; Davison, B. H.; Britovsek, G.; Cairney, J.; Eckert, C. A.; Frederick, W. J.; Hallett, J. P.; Leak, D. J.; Liotta, C. L.; Mielenz, J. R.; Murphy, R.; Templer, R.; Tschaplinski, T. *Science* **2006**, *311* (5760), 484–489.
- (4) Zakzeski, J.; Bruijninx, P. C. A.; Jongerius, A. L.; Weckhuysen, B. M. *Chem. Rev.* **2010**, *110* (6), 3552–3599.
- (5) Watkins, D.; Nuruddin, M.; Hosur, M.; Tcherbi-Narteh, A.; Jeelani, S. *J. Mater. Res. Technol.* **2015**, *4* (1), 26–32.
- (6) Luo, H.; Klein, I. M.; Jiang, Y.; Zhu, H.; Liu, B.; Kenttämä, H. I.; Abu-Omar, M. M. *ACS Sustain. Chem. Eng.* **2016**, *4* (4), 2316–2322.
- (7) de la Torre, M. J.; Moral, A.; Hernández, M. D.; Cabeza, E.; Tijero, A. *Ind. Crops Prod.* **2013**, *45*, 58–63.
- (8) El Hage, R.; Brosse, N.; Chrusciel, L.; Sanchez, C.; Sannigrahi, P.; Ragauskas, A. *Polym. Degrad. Stab.* **2009**, *94* (10), 1632–1638.
- (9) Bozell, J. J.; Black, S. K.; Myers, M.; Cahill, D.; Miller, W. P.; Park, S. *Biomass Bioenergy* **2011**, *35* (10), 4197–4208.
- (10) Gübitz, G. M.; Stebbing, D. W.; Johansson, C. I.; Saddler, J. N. *Appl. Microbiol. Biotechnol.* *50* (3), 390–395.
- (11) Cooks, R. G.; Jarmusch, A. K.; Wleklinski, M. *Int. J. Mass Spectrom.* **2015**, *377*, 709–718.
- (12) McLafferty, F. W. *Int. J. Mass Spectrom.* **2001**, *212* (1–3), 81–87.
- (13) Jarrell, T. M.; Marcum, C. L.; Sheng, H.; Owen, B. C.; O’Lenick, C. J.; Maraun, H.; Bozell, J. J.; Kenttämä, H. I. *Green Chem.* **2014**, *16* (5), 2713–2727.

VITA

VITA

In 2008, Hanyu entered Peking University as an undergraduate student majoring in Chemistry. With the passion in biomedical engineering, Hanyu joined Prof. Ying Luo's research group to study the application of chemically modification of biomacromolecules as drug delivery vehicles. After two years of research, a PAMAM based delivery system was developed. During this process, Hanyu found himself interested in analytical chemistry and decided to pursue a doctoral degree in United States.

In 2012, Hanyu joined the Ph.D program in Department of Chemistry at Purdue University with a major in the division of Analytical Chemistry. In Prof. Hilkka Kenttamaa's research group Hanyu developed various tandem mass spectrometric methods for structural elucidation of deprotonated analytes in biomass degradation products and drug metabolites.

PUBLICATION

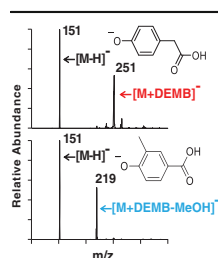


RESEARCH ARTICLE

Identification of the Phenol Functionality in Deprotonated Monomeric and Dimeric Lignin Degradation Products via Tandem Mass Spectrometry Based on Ion–Molecule Reactions with Diethylmethoxyborane

Hanyu Zhu, Joann P. Max, Christopher L. Marcum, Hao Luo, Mahdi M. Abu-Omar, Hilikka I. Kenttämaa

Department of Chemistry, Purdue University, West Lafayette, IN, USA



Abstract. Conversion of lignin into smaller molecules provides a promising alternate and sustainable source for the valuable chemicals currently derived from crude oil. Better understanding of the chemical composition of the resulting product mixtures is essential for the optimization of such conversion processes. However, these mixtures are complex and contain isomeric molecules with a wide variety of functionalities, which makes their characterization challenging. Tandem mass spectrometry based on ion–molecule reactions has proven to be a powerful tool in functional group identification and isomer differentiation for previously unknown compounds. This study demonstrates that the identification of the phenol functionality, the most commonly observed functionality in lignin degradation products, can be achieved via ion–

molecule reactions between diethylmethoxyborane (DEMB) and the deprotonated analyte in the absence of strongly electron-withdrawing substituents in the *ortho*- and *para*-positions. Either a stable DEMB adduct or an adduct that has lost a methanol molecule (DEMB adduct-MeOH) is formed for these ions. Deprotonated phenols with an adjacent phenol or hydroxymethyl functionality or a conjugated carboxylic acid functionality can be identified based on the formation of DEMB adduct-MeOH. Deprotonated compounds not containing the phenol functionality and phenols containing an electron-withdrawing *ortho*- or *para*-substituent were found to be unreactive toward diethylmethoxyborane. Hence, certain deprotonated isomeric compounds with phenol and carboxylic acid, aldehyde, carboxylic acid ester, or nitro functionalities can be differentiated via these reactions. The above mass spectrometry method was successfully coupled with high-performance liquid chromatography for the analysis of a complex biomass degradation mixture.

Keywords: Ion–molecule reactions, Lignin degradation products, Phenol functionality, Phenols

Received: 31 March 2016/Revised: 20 June 2016/Accepted: 21 June 2016/Published Online: 23 August 2016

Introduction

The pursuit of renewable and sustainable chemical resources for energy and chemicals currently derived from crude oil has motivated researchers in exploring the conversion of lignocellulosic biomass into fuels and chemicals [1–6]. An important component of lignocellulosic biomass is lignin, which can make up to 25% of whole lignocellulosic biomass [7].

Electronic supplementary material The online version of this article (doi:10.1007/s13361-016-1442-9) contains supplementary material, which is available to authorized users.

Correspondence to: Hilikka I. Kenttämaa; e-mail: hilikka@purdue.edu

Lignin is a heavily crosslinked biopolymer composed of phenolic units with diverse and complex structural motifs [8, 9]. Due to its high aromatic carbon content, researchers have focused on converting lignin into valuable aromatic chemicals [7–10]. However, the inherent complexity of lignin often leads to the production of very complex mixtures of molecules with a wide variety of functionalities. The analysis of such mixtures is a challenging task. Yet, chemical characterization of these product mixtures is essential for the optimization of the lignin degradation processes and further conversion of the products into valuable chemicals.

Tandem mass spectrometry has proven to be a powerful tool in the characterization of lignin degradation product mixtures. Negative ion mode electrospray ionization (ESI) with sodium

hydroxide dopant has been identified as the best ionization method for degraded lignin as it exclusively forms deprotonated molecules with no fragmentation for lignin model compounds [11]. Other ionization methods, such as positive ion mode ESI or atmospheric pressure chemical ionization (APCI), either cause extensive fragmentation or form multiple ion types for each compound [11]. When used in HPLC/tandem mass spectrometry experiments, negative ion mode ESI facilitates the analysis of complex lignin degradation product mixtures [12, 13]. Structural information for the ionized molecules can be obtained via multiple stages of ion isolation and collisionally activated dissociation (CAD) experiments [14]. However, isomeric ions can have similar CAD fragmentation patterns, making their differentiation challenging [12]. Therefore, new methods for structural elucidation of isomeric aromatic ions are needed.

Past studies have shown that ion–molecule reactions can be a powerful tool for structural elucidation of ionized analytes [15, 16]. Identification of functional groups can be achieved by using neutral reagents that exhibit specific reactivity towards ions with these functional groups [17–23]. However, most studies on functional group-specific ion–molecule reactions have focused on protonated analytes. Only in a few cases were deprotonated analytes examined [24–28], and to the best of our knowledge, no reagents have been developed for the identification of the phenol functionality. In this study, diethyl methoxyborane (DEMB) is explored as a reagent for the identification of the phenol functionality in deprotonated lignin-related analytes. DEMB is known to react with negative ions and has been shown to allow differentiation of isobaric ions (deprotonated phosphorus- and sulfocarbohydrates) [25].

Experimental

Chemicals

Diethylmethoxyborane (97%), phenol (99%), 2-ethoxyphenol (98%), 3-methoxyphenol (96%), 4-ethoxyphenol (99%), 2-methoxy-4-propylphenol (99%), isoeugenol (98%), methyl ferulate (99%), catechol (99%), resorcinol (99%), hydroquinone (99%), 2-hydroxybenzyl alcohol (99%), 3-hydroxybenzyl alcohol (99%), benzoic acid (99.5%), terephthalic acid (98%), phthalic acid (99.5%), 3-nitrophenol (99%), 4-nitrophenol (99%), 2-hydroxybenzaldehyde (98%), 3-hydroxybenzaldehyde (99%), 4-hydroxybenzaldehyde (98%), methyl 2-hydroxybenzoate (99%), methyl 3-hydroxybenzoate (99%), methyl 4-hydroxybenzoate (99%), 2-hydroxybenzoic acid (99%), 3-hydroxybenzoic acid (99%), 4-hydroxybenzoic acid (99%), 2-hydroxycinnamic acid (99%), 3-hydroxycinnamic acid (98%), 4-hydroxycinnamic acid (97%), 2-hydroxyphenacetic acid (97%), 3-hydroxyphenacetic acid (99%), 4-hydroxyphenacetic acid (98%), vanillic acid (97%), syringic acid (95%), sinapic acid (98%), 4-methoxybenzoic acid (99%), and 4-hydroxy-3-methylbenzoic acid (97%) were purchased from Sigma Aldrich (MO, USA) and used as received. Vanillin (99%) was purchased from

Fisher Scientific (MA, USA) and used as received. Guaiacylglycerol guaiacyl ether (97%) was purchased from TCI America (OR, USA) and used as received. Lignin β -5 dimer was synthesized via a previously reported method [29]. Converted *Miscanthus* biomass was obtained via a previously published procedure [30].

Mass Spectrometry

All experiments were performed on a Thermo Scientific (MA, USA) linear quadrupole ion trap (LQIT) mass spectrometer equipped with an electrospray ionization (ESI) source operated in the negative ion mode. Sample solutions were prepared at a concentration of 1 mmol in 50/50 water/methanol (v/v) solution. Ten μ L of 1 mM NaOH water solution were added into 5 mL of sample solution to facilitate the formation of deprotonated analyte molecules. The NaOH-doped sample solutions were injected into the ion source at a flow rate of 10 μ L/min. The injected solutions were mixed via a T-connector with 50/50 water/methanol (v/v) at a flow rate of 100 μ L/min to maintain stable spray current. Typical ESI conditions were: 3.5 kV spray voltage, 20 (arbitrary unit) sheath gas (N_2) flow, 10 (arbitrary unit) auxiliary gas (N_2) flow, and 2 (arbitrary unit) sweep gas (N_2) flow.

Ion–Molecule Reactions

Ion–molecule reactions between deprotonated analytes and DEMB were studied using an external reagent mixing manifold described previously [18, 31, 32]. DEMB was injected into the manifold by using a syringe drive at a flow rate of 10 μ L/min and then diluted with helium at a flow rate of 500 mL/min. The manifold was heated to 70 °C for efficient evaporation of DEMB into helium. The DEMB-helium mixture was then directed into a variable leak valve that allowed part of the mixture gas to enter the ion trap at a flow rate of 2 mL/min while the excess was directed into waste. Analyte ions were isolated using an isolation window of 2 m/z and a q value of 0.25. The isolated ions were allowed to react with DEMB for 30–500 ms before being ejected for detection.

High Performance Liquid Chromatography

All HPLC separations were performed on a Surveyor Plus HPLC system consisting of a dcolum. A nonlinear gradient of water (A) and acetonitrile (B) was used as follows: 0.00 min, 95% A and 5% B; 10.00 min, 95% A and 5% B; 30.00 min, 40% A and 60% B; 35.00 min, 5% A and 95%; 38.00 min, 5% A and 95% B; 38.50 min, 95% A and 5% B; 45.00 min, 95% A and 5% B. The flow rate of the mobile phase was kept at 500 μ L/min. PDA detector was set at the wavelength of 254 nm.

HPLC eluents were mixed via a T-connector with 1% sodium hydroxide solution at a flow rate of 0.1 μ L/min before entering the ESI source. ESI source conditions were set as: 3.5 kV spray voltage; 50 (arbitrary unit) sheath gas (N_2) flow, and 20 (arbitrary unit) auxiliary gas (N_2) flow.

Table 1. Ionic Products Formed Upon Reactions of Deprotonated Model Compounds with Diethylmethoxyborane (DEMB) for 200 ms

Analyte ion (m/z of [M-H] ⁻)	Ion structure	Products formed upon reactions with DEMB ^a (m/z)
phenol (91)		91+DEMB (191)
2-ethoxyphenol (137)		137+DEMB (237)
3-methoxyphenol (137)		123+DEMB (223)
4-ethoxyphenol (123)		137+DEMB (237)
2-methoxy-4-propylphenol (165)		165+DEMB (265)
isoeugenol (163)		163+DEMB (263)
methyl ferulate (207)		207+DEMB (307)
catechol (109)		109+DEMB-MeOH (177)
resorcinol (109)		109+DEMB (209)
hydroquinone (109)		109+DEMB (209)
2-hydroxybenzyl alcohol (123)		123+DEMB-MeOH (191)
3-hydroxybenzyl alcohol (123)		123+DEMB (223)
guaiacylglycerol guaiacyl ether (319)		319+DEMB (419)
lignin β-5 dimer (325)		325+DEMB (425)
benzoic acid (121)		No products observed
terephthalic acid (165)		No products observed

^a Only products with 5% or greater relative abundance reported. DEMB adduct are colored in red; DEMB adduct-MeOH are colored in blue

Computational Details

All density functional theory (DFT) calculations were performed using the Gaussian 09 software package [33]. Geometry optimizations were performed using the hybrid

functional M06-2X [34] with the 6-31+G(d,p) basis set for potential surface calculations. All other geometries were optimized using 6-311++G(2d,p) basis set. Enthalpy values were obtained by calculating vibrational frequencies at the same level of theory at which they were optimized. Natural

bond orbital (NBO) analyses were performed at the M06-2X/6-311++G(2d,p) level of theory.

phenols in a catalytically converted biomass sample containing multiple phenolic compounds.

Results and Discussion

Multiple model compounds containing phenol, carboxylic acid, and other functionalities (Tables 1, 2, and 3) were ionized via negative ion mode ESI with NaOH as dopant. These compounds formed exclusively $[M - H]^-$ upon ionization. The deprotonated analytes were allowed to react with diethylmethoxyborane (DEMB) in order to explore whether it provides a useful reagent for the identification of the phenol functionality in deprotonated lignin-related analytes. After obtaining promising results on model compounds, the method was used to identify

Formation of a DEMB Adduct for Deprotonated Phenols

Upon reactions with DEMB, deprotonated phenol and most deprotonated substituted phenols (Tables 1, 2, and 3) formed a DEMB adduct ion ($[M - H + DEMB]^-$) that has 100 units greater m/z -value than the analyte ion. The substituents include alkyl, alkenyl, hydroxymethyl, alkoxy, phenol (Table 1), nitro, aldehyde, carboxylic acid ester (Table 2), and carboxylic acid (Table 3). The boron-containing adduct can be easily identified by the characteristic boron isotope distribution (100% ^{11}B to 20% ^{10}B). Larger model compounds (i.e., two lignin dimers with β -O-

Table 2. Ionic Products Formed Upon Reactions of Deprotonated Phenol and Its Derivatives Containing Electron-Withdrawing Substituents with DEMB for 200 ms, Calculated NBO Charges of the Deprotonated Phenols at the Phenoxide Oxygen, and Calculated Energy Differences Between the Reactants and Their Products

Analyte ion (m/z of $[M-H]^-$)	Ion structure	Products formed upon reactions with DEMB ^a (m/z)	Calculated NBO charge ^b	Energy difference (kcal/mol) ^d
phenol (91)		91+DEMB (191)	-0.808 ^c	-34.2
vanillin (151)		No products observed	-0.721 ^c	-25.1
3-nitrophenol (138)		138+DEMB (238)	-0.782 ^c	-28.8
4-nitrophenol (138)		No products observed	-0.726 ^c	-23.4
2-hydroxybenzaldehyde (121)		121+DEMB (221) minor	-0.766 ^c	-27.3
3-hydroxybenzaldehyde (121)		121+DEMB (221)	-0.793 ^c	-31.0
4-hydroxybenzaldehyde (121)		No products observed	-0.743 ^c	-26.4
methyl 2-hydroxybenzoate (151)		151+DEMB (251) minor	-0.724 ^c	-27.6
methyl 3-hydroxybenzoate (151)		151+DEMB (251)	-0.798 ^c	-31.9
methyl 4-hydroxybenzoate (151)		151+DEMB (251) minor	-0.752 ^c	-27.2

^a Products with 5% or greater relative abundance are colored in red. Products with relative abundance between 0.1% and 5% are considered to be minor

^b NBO = natural bond orbital. Calculated at M06-2X/6-311G++(2d,p)

^c Charge on the phenoxide oxygen atom

^d Relative energy difference in enthalpy between product ion and separated reactants. Calculated at M06-2X/6-311G++(2d,p) level of theory

4 and β -5 linkages) also exclusively produced DEMB adducts (Table 1). However, deprotonated compounds not containing the phenol functionality, such as deprotonated benzoic acid, showed no reactivity towards DEMB (Table 1). Based on the above results and the results discussed below, the formation of a DEMB adduct is unique to deprotonated analytes with the phenol functionality. However, not all phenolic compounds form this adduct.

In contrast to the phenolic compounds discussed above, DEMB adduct formation was not observed for deprotonated

vanillin (Table 2) that contains a phenol functionality as well as an electron-withdrawing aldehyde functional group. This observation led to further examination of the effects of electron-withdrawing substituents (aldehyde, nitro, and carboxylic acid ester) in the analyte ion on its reactivity toward DEMB (Table 2). Deprotonated phenols with an electron-withdrawing substituent at the *ortho*- or *para*-position were found to exhibit no reactivity towards DEMB, whereas the *meta*-substituted isomers formed the DEMB adduct ion (Table 2). An explanation for this behavior was sought by quantum chemical calculations.

Table 3. Ionic Products Formed upon Reactions of Deprotonated Model Compounds Containing a Phenol and a Carboxylic Acid Functional Group with DEMB for 200 ms

Analyte ion (m/z of [M-H] ⁻)	Structure	Products formed upon reactions with DEMB ^a (m/z)
2-hydroxybenzoic acid (137)		No products observed
3-hydroxybenzoic acid (137)		137+DEMB (251)
4-hydroxybenzoic acid (137)		137+DEMB-MeOH (177)
2-hydroxycinnamic acid (137)		137+DEMB-MeOH (177)
3-hydroxycinnamic acid (137)		137+DEMB (251)
4-hydroxycinnamic acid (137)		137+DEMB-MeOH (177)
2-hydroxyphenacetic acid (151)		No products observed
3-hydroxyphenacetic acid (151)		151+DEMB (251)
4-hydroxyphenacetic acid (151)		151+DEMB (251)
vanillic acid (16)		167+DEMB-MeOH (235)
syringic acid (197)		197+DEMB-MeOH (265)
sinapic acid (223)		223+DEMB-MeOH (291)

^aOnly products with 5% or greater relative abundance are reported. DEMB adduct is colored in red, DEMB adduct-MeOH is colored in blue

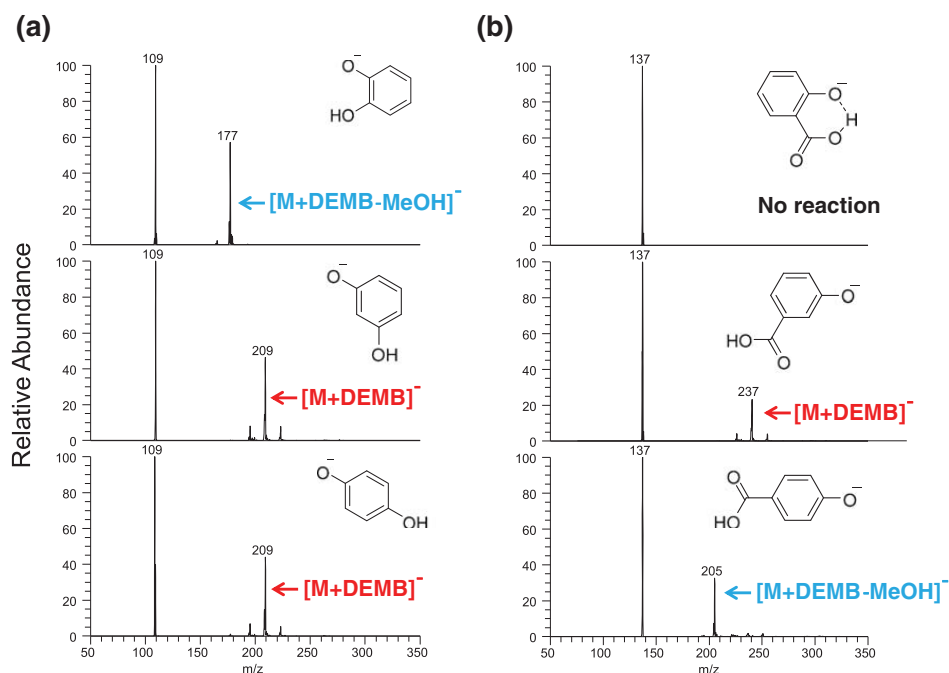


Figure 1. (a) Tandem mass spectra measured after reactions of (top) deprotonated catechol, (middle) deprotonated resorcinol, and (bottom) deprotonated hydroquinone with DEMB for 200 ms. (b) Tandem mass spectra measured after reactions of (top) deprotonated 2-hydroxybenzoic acid, (middle) deprotonated 3-hydroxybenzoic acid, and (bottom) deprotonated 4-hydroxybenzoic acid with DEMB for 200 ms

Calculations based on density functional theory showed that the NBO electron density on the phenoxide oxygen atom in deprotonated phenols is reduced in the presence of an *ortho*- or *para*-positioned electron-withdrawing substituent compared with *meta*-substituted phenols (Table 2), making them weaker nucleophiles. For example, the *meta*-substituted 3-hydroxybenzaldehyde

has a NBO charge density of -0.793 on its phenoxide oxygen (formation of a stable DEMB adduct was observed) whereas its isomer, the *para*-substituted 4-hydroxybenzaldehyde, has a lower NBO charge density of -0.743 (no reactivity toward DEMB was observed). The *ortho*-substituted 2-hydroxybenzaldehyde has a NBO charge of -0.766 that falls between 3-hydroxy

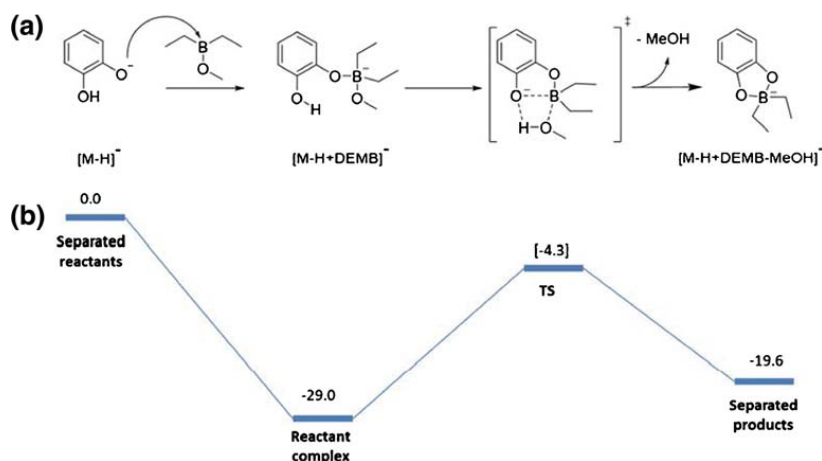


Figure 2. (a) Proposed mechanism and (b) calculated potential energy surface (enthalpy in kcal/mol) for the formation of a DEMB adduct that has lost methanol upon reactions between deprotonated catechol and DEMB (M06-2X/6-31+G(d,p) level of theory)

benzaldehyde and 4-hydroxybenzaldehyde (a minor DEMB adduct was observed). The above results show that a larger charge density on the phenoxide oxygen correlates with higher reactivity towards DEMB.

However, based on calculations, all the phenols form a low-energy covalently bound adduct with DEMB (Table 2). In the gas phase, these adducts are not stable toward dissociation back to reactants unless they are stabilized either by emission of IR light or by collisions with the helium buffer gas. The lower the energy of the adduct, the longer its lifetime, and the more likely it is that it gets stabilized via one of these processes. Indeed, the energy of the covalent DEMB adducts relative to the separated reactants (Table 2) was calculated to be greatest (from -29 down to -34 kcal/mol) for those ions that formed an abundant stable adduct as a final product, slightly less for those that formed a minor adduct (-27 kcal/mol) and even less for those that did not form a stable adduct (from -23 down to -26 kcal/mol). This

likely explains the selectivity for stable DEMB adduct formation for different deprotonated phenols.

Formation of DEMB Adduct-MeOH

When deprotonated catechol (containing two adjacent phenol functionalities) was allowed to react with DEMB, it did not form a stable DEMB adduct but instead a DEMB adduct that had lost methanol ($[M-H+DEMB-MeOH]^-$) with 68 units greater m/z -value than the analyte ion (Table 1, Figure 1a). Formation of this type of product ion was not observed for the isomeric resorcinol or hydroquinone, which both formed a stable DEMB adduct instead (Table 1; Figure 1a). Exclusive formation of DEMB adduct-MeOH was also observed for deprotonated 2-hydroxybenzyl alcohol but not for the isomeric deprotonated 3-hydroxybenzyl alcohol, the hydroxyl and phenol groups of which are further away from each other (Table 1). These observations suggest that an additional phenol or hydroxyl functionality in close proximity to the deprotonated

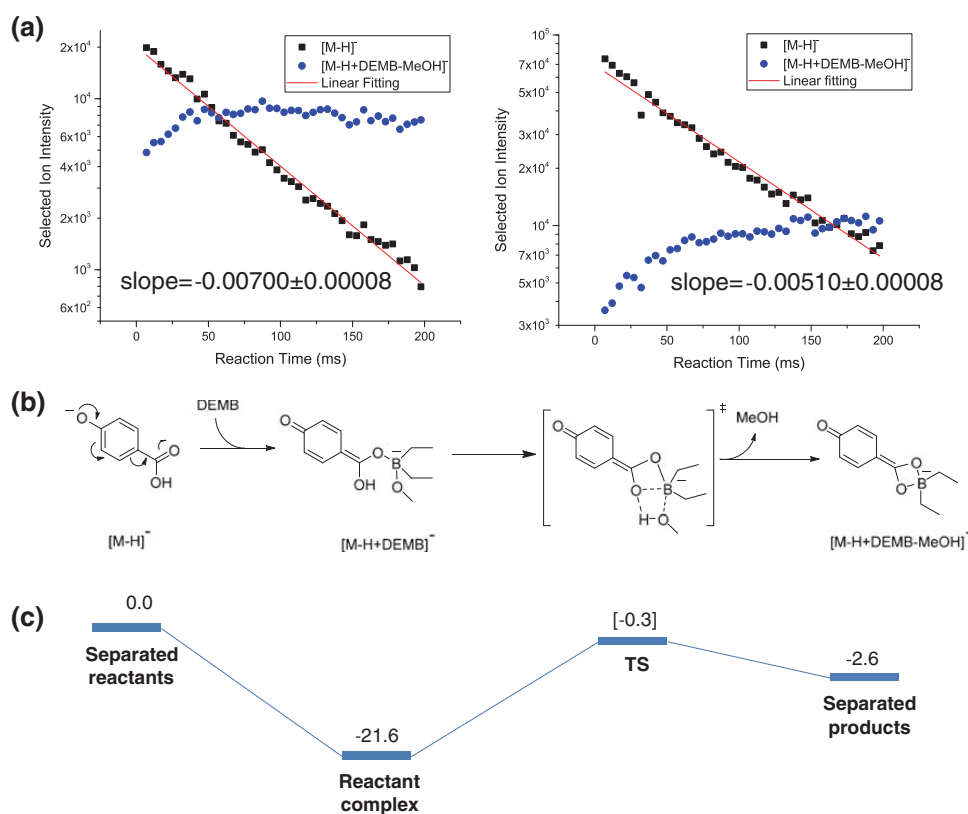


Figure 3. (a) Logarithm of the abundances of deprotonated 4-hydroxybenzoic acid (black symbols) and DEMB adduct-MeOH product ion (blue symbols) plotted as a function of reaction time for the reaction between DEMB and deprotonated 4-hydroxybenzoic acid generated using NaOH doped water solution (left) and acetonitrile solution (right). (b) Mechanism proposed for the formation of DEMB adduct that has lost methanol. (c) Calculated potential energy surface (enthalpies in kcal/mol) for the formation of DEMB adduct-MeOH (M06-2X/6-31+G(d,p) level of theory)

phenol group is critical for the formation of DEMB adduct-MeOH. The potential energy surface for the proposed mechanism, calculated via density functional theory, is shown in Figure 2 for catechol (CAD mass spectrum of the product ion is shown in Supplementary Table S1, Supporting Information).

Formation of DEMB adduct-MeOH was also observed for certain deprotonated phenols with carboxylic acid functionalities. When regioisomers of deprotonated hydroxycinnamic acid, hydroxyphenylacetic acid, and hydroxybenzoic acid were allowed to react with DEMB (Table 3), DEMB adduct-MeOH was observed for 4-hydroxybenzoic acid, 2-hydroxycinnamic acid, and 4-hydroxycinnamic acid, the phenol and carboxylic acid functionalities of which are conjugated. All other ions either only formed a DEMB adduct or were unreactive. The lack of products for 2-hydroxyphenylacetic acid and 2-hydroxybenzoic acid can be explained by the presence of strong intramolecular hydrogen bonding in their deprotonated forms (Figure 1b), which reduces their nucleophilicity. For the ions that formed DEMB adduct-MeOH, such as 4-hydroxybenzoic acid, the originally proposed mechanism (Figure 2) is no longer applicable since the distance between the carboxylic acid and phenol functionalities is too great. Therefore, a different mechanism must be involved.

One issue that must be considered here is that hydroxybenzoic acids have two possible deprotonation sites. If the benzoic acid moiety is exclusively deprotonated in some of them, one would expect no reactivity toward DEMB, based on the above results. Literature studies have shown that experimental conditions can influence the site of deprotonation of 4-hydroxybenzoic acid upon ESI [35, 36]. After some controversy on which is the preferred site of deprotonation in different solvent systems, the generally agreed upon conclusion appears to be that the phenoxide anion greatly dominates when using aprotic solvents (such as acetonitrile) while the carboxylate tautomer is also formed when using protic solvents (such as water) [35, 36]. In order to establish whether this applies to the present experiments utilizing ESI and protic solvents, the reactivity of DEMB toward 4-hydroxybenzoic acid deprotonated using different solvents was studied.

The abundances of 4-hydroxybenzoic acid deprotonated using an aprotic (acetonitrile) and protic solvent (water with 0.1% NaOH) and its DEMB adduct-MeOH product were measured as a function of reaction time. Ion–molecule reactions studied under the conditions utilized here follow pseudo-first order kinetics. Hence, a plot of the logarithm of the reactant ion's relative abundance versus reaction time is a straight line with a negative slope equal to the rate constant multiplied by

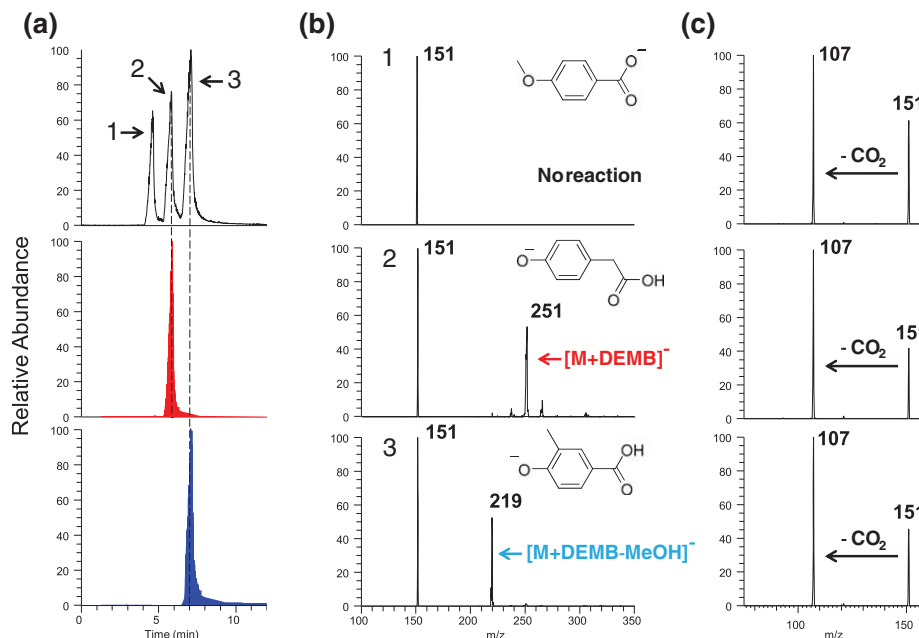


Figure 4. (a) (top) Total ion HPLC chromatogram measured for an equimolar mixture of 4-methoxybenzoic acid (1), 4-hydroxyphenylacetic acid (2), and 4-hydroxy-3-methylbenzoic acid (3). Selected ion HPLC chromatograms measured for all ions that formed DEMB adduct (middle), and DEMB adduct-MeOH (bottom) upon reaction with DEMB. (b) MS² spectra measured after reaction of deprotonated 4-methoxybenzoic acid (top), deprotonated 4-hydroxyphenylacetic acid (middle), and deprotonated 4-hydroxy-3-methylbenzoic acid (bottom) with DEMB for 200 ms. (c) CAD MS² spectra measured for deprotonated 4-methoxybenzoic acid (top), deprotonated 4-hydroxyphenylacetic acid (middle), and deprotonated 4-hydroxy-3-methylbenzoic acid (bottom) after a separate HPLC run followed by ionization, ion isolation and CAD

DEMB concentration. With the concentration of DEMB staying constant under the conditions employed here (the concentration of reactant ions is substantially smaller than the concentration of the reagent molecules), the rate constant is proportional to the value of the negative slope, which is larger (0.007 versus 0.005) when the reactant ions were generated using acetonitrile (Figure 3a). This finding is in agreement with the literature results discussed above that acetonitrile is expected to produce more phenoxide ions, whereas water doped with NaOH should produce more carboxylate anions (about 40% relative to the phenoxide ions) [35]. However, since both ion populations are reactive toward DEMB, phenoxide ions exist in both. Hence, exclusive deprotonation of the carboxylic acid moiety is unlikely. This finding is in agreement with the CAD mass spectra measured for 4-hydroxybenzoic acid deprotonated using the aprotic and protic solvent systems and the potential energy surfaces calculated for these reactions (Supplementary Figures S1 and S2). CO₂ loss from the phenoxide ion is calculated to be more energetically favorable than from the carboxylate ion (Supplementary Figure S1). Indeed, the ions generated from acetonitrile solution fragment more readily by CO₂ loss than the ions generated from water/NaOH solution (Supplementary Figure S2), suggesting that more phenoxide ions had been formed in the acetonitrile solution.

Based on the findings above, a new mechanism is proposed for the formation of DEMB adduct-MeOH (Figure 3b) for compounds with conjugated carboxylic acid and phenol functionalities, such as 4-hydroxybenzoic acid. In these deprotonated molecules, the charge on the deprotonated phenol moiety can resonate onto the carboxylic acid oxygen, which enables nucleophilic attack by the carboxylic acid moiety at the boron atom in DEMB. After addition, the carboxylic acid moiety can donate a proton to a methoxy group to eliminate methanol. Potential energy surface calculated for the proposed mechanism shows a low barrier of -0.3 kcal/mol for DEMB adduct-MeOH formation for the reaction between deprotonated 4-hydroxybenzoic acid and DEMB (Figure 3c; CAD mass spectrum of the product ion is shown in Supplementary Table S1 and proposed fragmentation mechanism in Supplementary Scheme S1).

DEMB Ion–Molecule Reactions Coupled with HPLC

The formation of a DEMB adduct or DEMB adduct-MeOH is fast. At 200 ms reaction time, the relative abundances of DEMB adduct ions with respect to analyte ions are greater than 20% for all model compounds that exhibit reactivity towards

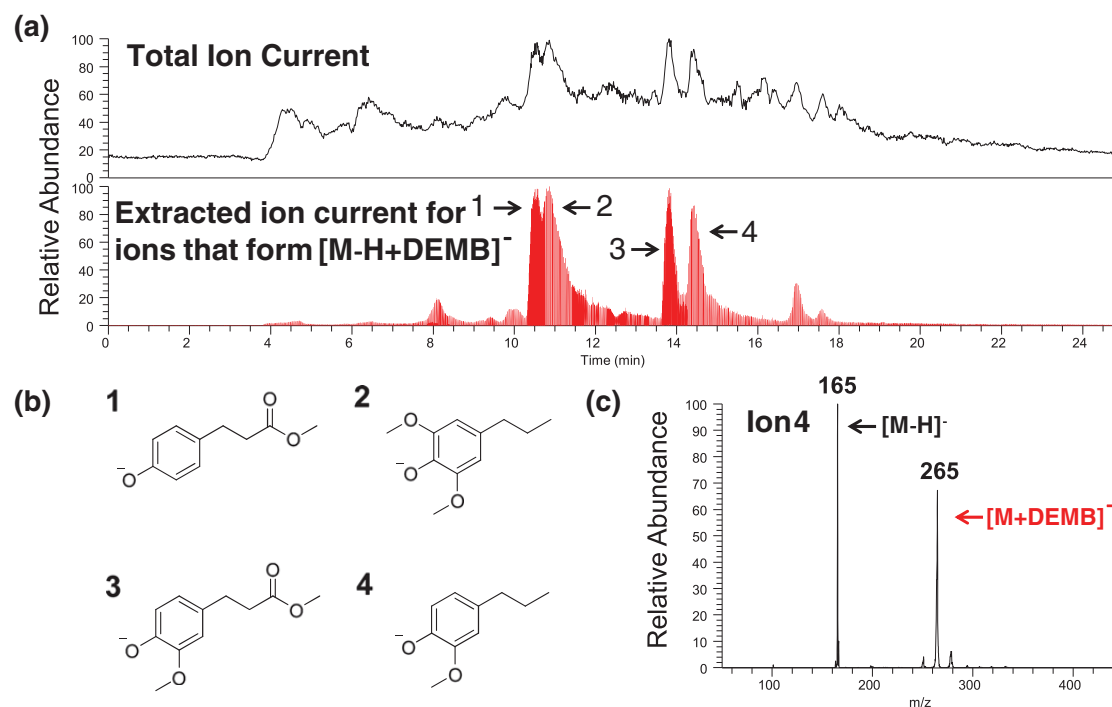


Figure 5. (a) (top) Total ion current HPLC chromatogram for a mixture obtained via catalytic conversion of *Miscanthus* biomass. (bottom) Selected ion HPLC chromatogram for all ions that form a DEMB adduct. (b) Structures of the four major phenols that were identified in the mixture. (c) MS² spectrum measured after isolation of ion 4 (m/z 165) and reaction with DEMB for 200 ms

DEMB. Thus, this reaction should be compatible with chromatographic time scale. In order to test this hypothesis, an equimolar mixture of three isomers, 4-methoxybenzoic acid, 4-hydroxyphenylacetic acid, and 4-hydroxy-3-methylbenzoic acid, was subjected to HPLC/tandem mass spectrometric analysis (Figure 4a). The compounds were eluted using a gradient consisting of water and acetonitrile, deprotonated via ESI as they eluted from the column, and allowed to react with DEMB for 200 ms in the ion trap. Typically, about 40 such MS experiments were performed for each HPLC peak. Due to the lack of a phenol functional group, deprotonated 4-methoxybenzoic acid showed no reactivity toward DEMB (Figure 4b). Deprotonated 4-hydroxy-3-methylbenzoic acid that contains both a phenol functional group and a conjugated carboxylic acid functional group formed DEMB adduct–MeOH, whereas deprotonated 4-hydroxyphenylacetic acid formed DEMB adduct (Figure 4b). Hence, these three isomers can be differentiated using this approach. It is notable that these isomers cannot be differentiated when using conventional HPLC/MS² analysis based on CAD, as all three ionized isomeric compounds undergo the same fragmentations upon CAD (Figure 4c).

Once coupled with HPLC, the above approach can be used for rapid screening of mixtures for the presence of phenol-containing compound. This was demonstrated by the analysis of a product mixture obtained by catalytic conversion of *Miscanthus* biomass (Figure 5). Using the same water/acetonitrile gradient, HPLC eluates were ionized by negative ion mode ESI and the most abundant ion formed for each eluate was isolated and allowed to react with DEMB for 200 ms in the ion trap. The complexity of the product mixture is demonstrated by the total ion current chromatograph shown in Figure 5a. However, by monitoring ions that produce an ion with 100 units greater *m/z* value, an extracted ion chromatogram can be obtained that represents compounds with the phenol functionality (Figure 5a). No DEMB adduct–MeOH product ions were observed, indicating the absence of phenols with adjacent hydroxyl or conjugated carboxylic acid functionalities. For the product mixture studied, four major phenols were identified. Their structures were elucidated via CAD of their deprotonated forms and comparison to CAD of model compounds (Figure 5b) [30].

Conclusions

A tandem mass spectrometry method is presented for the selective detection of the phenol functionality in di- and polyfunctional analytes related to lignin. The method is based on gas-phase ion–molecule reactions of the deprotonated analytes with DEMB. All deprotonated phenol model compounds form stable DEMB adduct ions ($[M - H + DEMB]^-$) or DEMB adduct ions that have lost a methanol molecule ($[M - H + DEMB - MeOH]^-$) except for the ones with a strong electron withdrawing substituent in the *ortho*- or *para*-position. Deprotonated phenols with an adjacent phenol or

hydroxymethyl group and those with a conjugated carboxylic acid group can be identified based on the formation of DEMB adduct–MeOH, although this product ion is formed via different mechanisms for these two types of analytes. Deprotonated compounds with no phenol functionalities and phenols with an electron-withdrawing substituent in the *ortho*- or *para*-position were unreactive toward DEMB. By coupling the above technique with HPLC, an entire class of analytes can be identified in complex mixtures by using a single HPLC run. A catalytically converted *Miscanthus* biomass sample was analyzed to demonstrate the potential of tandem mass spectrometry based on ion–molecule reactions as a high-throughput screening tool for lignin degradation product mixtures.

Acknowledgments

This material is based upon work supported as part of the Center for Direct Catalytic Conversion of Biomass to Biofuels (C3Bio), an Energy Frontier Research Center funded by the U.S. Department of Energy, Office of Basic Energy Sciences, award number DE-SC0000997.

References

- Service, R.F.: Battle for the barrel. *Science* **339**, 1374–1379 (2013)
- Hamelinck, C.N., van Hooijdonk, G., Faaij, A.P.: Ethanol from lignocellulosic biomass: techno-economic performance in short-, middle- and long-term. *Biomass Bioenerg.* **28**, 384–410 (2005)
- Hisano, H., Nandakumar, R., Wang, Z.-Y.: Genetic modification of lignin biosynthesis for improved biofuel production. *Vitro Cell. Dev. Biol. Plant* **45**, 306–313 (2009)
- Chang, M.C.Y.: Harnessing energy from plant biomass. *Curr. Opin. Chem. Biol.* **11**, 677–684 (2007)
- Ragauskas, A.J., Williams, C.K., Davison, B.H., Britovsek, G., Cairney, J., Eckert, C.A., Frederick, W.J., Hallett, J.P., Leak, D.J., Liotta, C.L., Mielenz, J.R., Murphy, R., Templer, R., Tschaplinski, T.: The path forward for biofuels and biomaterials. *Science* **311**, 484–489 (2006)
- Weng, J.-K., Li, X., Bonawitz, N.D., Chapple, C.: Emerging strategies of lignin engineering and degradation for cellulosic biofuel production. *Curr. Opin. Biotechnol.* **19**, 166–172 (2008)
- Calvo-Flores, F.G., Dobado, J.A.: Lignin as renewable raw material. *ChemSusChem* **3**, 1227–1235 (2010)
- Azadi, P., Inderwildi, O.R., Farnood, R., King, D.A.: Liquid fuels, hydrogen, and chemicals from lignin: a critical review. *Renew. Sustain. Energy Rev.* **21**, 506–523 (2013)
- Zakzeski, J., Bruijninx, P.C.A., Jongerijs, A.L., Weckhuysen, B.M.: The catalytic valorization of lignin for the production of renewable chemicals. *Chem. Rev.* **110**, 3552–3599 (2010)
- Parsell, T., Yohe, S., Degenstein, J., Jarrell, T., Klein, I., Gencer, E., Hewetson, B., Hurt, M., Kim, J.I., Choudhari, H., Saha, B., Meilan, R., Mosier, N., Ribeiro, F., Delgass, W.N., Chapple, C., Kenttämää, H.I., Agrawal, R., Abu-Omar, M.M.: A synergistic biorefinery based on catalytic conversion of lignin prior to cellulose starting from lignocellulosic biomass. *Green Chem.* **17**, 1492–1499 (2015)
- Hauptert, L.J., Owen, B.C., Marcum, C.L., Jarrell, T.M., Pulliam, C.J., Amundson, L.M., Narra, P., Aqueel, M.S., Parsell, T.H., Abu-Omar, M.M., Kenttämää, H.I.: Characterization of model compounds of processed lignin and the lignome by using atmospheric pressure ionization tandem mass spectrometry. *Fuel* **95**, 634–641 (2012)
- Jarrell, T.M., Marcum, C.L., Sheng, H., Owen, B.C., O'Lenick, C.J., Maraun, H., Bozell, J.J., Kenttämää, H.I.: Characterization of organosolv switchgrass lignin by using high performance liquid chromatography/high resolution tandem mass spectrometry using hydroxide-doped negative-ion mode electrospray ionization. *Green Chem.* **16**, 2713–2727 (2014)
- Owen, B.C., Hauptert, L.J., Jarrell, T.M., Marcum, C.L., Parsell, T.H., Abu-Omar, M.M., Bozell, J.J., Black, S.K., Kenttämää, H.I.: High-performance

- liquid chromatography/high-resolution multiple stage tandem mass spectrometry using negative-ion-mode hydroxide-doped electrospray ionization for the characterization of lignin degradation products. *Anal. Chem.* **84**, 6000–6007 (2012)
14. Amundson, L.M., Eismín, R.J., Reece, J.N., Fu, M., Habicht, S.C., Mossman, A.B., Shea, R.C., Kenttämäa, H.I.: Identification and counting of oxygen functionalities in aromatic analytes related to lignin by using negative-mode electrospray ionization and multiple collision-activated dissociation steps. *Energy Fuels* **25**, 3212–3222 (2011)
 15. Brodbelt, J.S.: Analytical applications of ion–molecule reactions. *Mass Spectrom. Rev.* **16**, 91–110 (1997)
 16. Eberlin, M.N.: Structurally diagnostic ion/molecule reactions: class and functional-group identification by mass spectrometry. *J. Mass Spectrom.* **41**, 141–156 (2006)
 17. Somuramasami, J., Winger, B.E., Gillespie, T.A., Kenttämäa, H.I.: Identification and counting of carbonyl and hydroxyl functionalities in protonated bifunctional analytes by using solution derivatization prior to mass spectrometric analysis via ion–molecule reactions. *J. Am. Soc. Mass Spectrom.* **21**, 773–784 (2010)
 18. Habicht, S.C., Vinueza, N.R., Archibold, E.F., Duan, P., Kenttämäa, H.I.: Identification of the carboxylic acid functionality by using electrospray ionization and ion–molecule reactions in a modified linear quadrupole ion trap mass spectrometer. *Anal. Chem.* **80**, 3416–3421 (2008)
 19. Sheng, H., Williams, P.E., Tang, W., Riedeman, J.S., Zhang, M., Kenttämäa, H.I.: Identification of the sulfone functionality in protonated analytes via ion/molecule reactions in a linear quadrupole ion trap mass spectrometer. *J. Org. Chem.* **79**, 2883–2889 (2014)
 20. Watkins, M.A., Winger, B.E., Shea, R.C., Kenttämäa, H.I.: Ion–molecule reactions for the characterization of polyols and polyol mixtures by ESI/FT-ICR mass spectrometry. *Anal. Chem.* **77**, 1385–1392 (2005)
 21. Fu, M., Duan, P., Gao, J., Kenttämäa, H.I.: Ion–molecule reactions for the differentiation of primary, secondary and tertiary hydroxyl functionalities in protonated analytes in a tandem mass spectrometer. *Analyst* **137**, 5720 (2012)
 22. Sheng, H., Tang, W., Yerabolu, R., Kong, J.Y., Williams, P.E., Zhang, M., Kenttämäa, H.I.: Mass spectrometric identification of the N-monosubstituted N-hydroxylamino functionality in protonated analytes via ion/molecule reactions in tandem mass spectrometry. *Rapid Commun. Mass Spectrom.* **29**, 730–734 (2015)
 23. Fu, M., Duan, P., Li, S., Habicht, S.C., Pinkston, D.S., Vinueza, N.R., Kenttämäa, H.I.: Regioselective ion–molecule reactions for the mass spectrometric differentiation of protonated isomeric aromatic diamines. *Analyst* **133**, 452 (2008)
 24. Piatkivskiy, A., Pyatkivskyy, Y., Ryzhov, V.: Evaluation of various silicon- and boron-containing compounds for the detection of phosphorylation in peptides via gas-phase ion–molecule reactions. *Eur. J. Mass Spectrom. Chichester Engl.* **20**, 337–344 (2014)
 25. Piatkivskiy, A., Pyatkivskyy, Y., Hurt, M., Ryzhov, V.: Utilization of gas-phase ion–molecule reactions for differentiation between phospho- and sulfocarbohydrates. *Eur. J. Mass Spectrom.* **20**, 177 (2014)
 26. Gronert, S., O’Hair, R.A.J.: Gas phase reactions of trimethyl borate with phosphates and their non-covalent complexes†. *J. Am. Soc. Mass Spectrom.* **13**, 1088–1098 (2002)
 27. Gao, H., Petzold, C.J., Leavell, M.D., Leary, J.A.: Investigation of ion/molecule reactions as a quantification method for phosphorylated positional isomers: an FT-ICR approach. *J. Am. Soc. Mass Spectrom.* **14**, 916–924 (2003)
 28. Leavell, M.D., Kruppa, G.H., Leary, J.A.: Analysis of phosphate position in hexose monosaccharides using ion–molecule reactions and SORI-CID on an FT-ICR mass spectrometer. *Anal. Chem.* **74**, 2608–2611 (2002)
 29. Forsythe, W.G., Garrett, M.D., Hardacre, C., Nieuwenhuyzen, M., Sheldrake, G.N.: An efficient and flexible synthesis of model lignin oligomers. *Green Chem.* **15**, 3031–3038 (2013)
 30. Luo, H., Klein, I.M., Jiang, Y., Zhu, H., Liu, B., Kenttämäa, H.I., Abu-Omar, M.M.: Total utilization of *Miscanthus* biomass, lignin and carbohydrates, using earth abundant nickel catalyst. *ACS Sustain. Chem. Eng.* (2016)
 31. Gronert, S.: Quadrupole ion trap studies of fundamental organic reactions. *Mass Spectrom. Rev.* **24**, 100–120 (2005)
 32. Gronert, S.: Estimation of effective ion temperatures in a quadrupole ion trap. *J. Am. Soc. Mass Spectrom.* **9**, 845–848 (1998)
 33. Frisch, M.J., Trucks, G.W., Schlegel, H.B., Scuseria, G.E., Robb, M.A., Cheeseman, J.R., Scalmani, G., Barone, V., Mennucci, B., Petersson, G.A., Nakatsuji, H., Caricato, M., Li, X., Hratchian, H.P., Izmaylov, A.F., Bloino, J., Zheng, G., Sonnenberg, J.L., Hada, M., Ehara, M., Toyota, K., Fukuda, R., Hasegawa, J., Ishida, M., Nakajima, T., Honda, Y., Kitao, O., Nakai, H., Vreven, T., Montgomery Jr., J.A., Peralta, J.E., Ogliaro, F., Bearpark, M.J., Heyd, J., Brothers, E.N., Kudin, K.N., Staroverov, V.N., Kobayashi, R., Normand, J., Raghavachari, K., Rendell, A.P., Burant, J.C., Iyengar, S.S., Tomasi, J., Cossi, M., Rega, N., Millam, N.J., Klene, M., Knox, J.E., Cross, J.B., Bakken, V., Adamo, C., Jaramillo, J., Gomperts, R., Stratmann, R.E., Yazyev, O., Austin, A.J., Cammi, R., Pomelli, C., Ochterski, J.W., Martin, R.L., Morokuma, K., Zakrzewski, V.G., Voth, G.A., Salvador, P., Dannenberg, J.J., Dapprich, S., Daniels, A.D., Farkas, Ö., Foresman, J.B., Ortiz, J.V., Cioslowski, J., Fox, D.J.: *Gaussian 09*. Gaussian, Inc.: Wallingford, CT, USA (2009)
 34. Zhao, Y., Truhlar, D.G.: The M06 suite of density functionals for main group thermochemistry, thermochemical kinetics, noncovalent interactions, excited states, and transition elements: two new functionals and systematic testing of four M06-class functionals and 12 other functionals. *Theor. Chem. Acc.* **120**, 215–241 (2007)
 35. Schröder, D., Buděšínský, M., Roithová, J.: Deprotonation of p-hydroxybenzoic acid: does electrospray ionization sample solution or gas-phase structures? *J. Am. Chem. Soc.* **134**, 15897–15905 (2012). **and references therein**
 36. Steill, J.D., Oomens, J.: Gas-phase deprotonation of p-hydroxybenzoic acid investigated by IR spectroscopy: solution-phase structure is retained upon ESI. *J. Am. Chem. Soc.* **131**, 13570–13571 (2009). **and references therein**